Influence of Metal Ions on Coordination Linkages of Epoxidized Natural Rubber

Kriengsak Damampai

A Thesis Submitted in Partial Fulfillment of the Requirement for the Degree
of Doctor of Philosophy in Rubber Technology
Prince of Songkla University
2566

Thesis Title   Influence of Metal Ions on Coordination Linkages of Epoxidized

Natural Rubber

Author   Mister Kriengsak Damampai

Major Program   Rubber Technology

_____

Major Advisor   **Examining Committee:**

…………………………………   ……………………………… Chairperson

(Assoc. Prof. Dr. Charoen Nakason)   (Prof. Dr. Suda Kiatkamjornwong)

                                                        ……………………………… Committee

Co-advisors   (Assoc. Prof. Dr. Charoen Nakason)

…………………………………   ……………………………… Committee

(Asst. Prof. Dr. Skulrat Pichaiyut)   (Asst. Prof. Dr. Skulrat Pichaiyut)

………………………………   ……………………………… Committee

(Dr. Amit Das)   (Dr. Amit Das)

                                                        ……………………………… Committee

                                                        (Assoc. Prof. Dr. Wannarat Chueangchayaphan)

The Graduate School, Prince of Songkla University, has approved this thesis as partial fulfillment of the requirement for the Doctor of Philosophy Degree in Rubber Technology

                                        ……………………………………….

                                        (Asst. Prof. Dr. Thakerng Wongsirichot)

                                        Dean of Graduate School

This is to certify that the work here submitted is the result of the candidate's own investigations. Due acknowledgement has been made of any assistance received.

.... Signature

(Assoc. Prof. Dr. Charoen Nakason)

Major Advisor

.... Signature

(Mister Kriengsak Damampai)

Candidate

I hereby certify that this work has not been accepted in substance for any degree, and is not being currently submitted in candidature for any degree.

.... Signature

(Mister Kriengsak Damampai)

Candidate

ชื่อวิทยานิพนธ์ อิทธิพลของโลหะไอออนต่อการเชื่อมขวางแบบโคออดิเนชั่นของยางธรรมชาติอิพอก
ไซด์

ผู้เขียน นาย เกรียงศักดิ์ ดำอำไพ

สาขาวิชา เทคโนโลยียาง

ปีการศึกษา 2565

<div align="center">

บทคัดย่อ

</div>

งานวิจัยนี้ได้ทำการเชื่อมขวางยางธรรมชาติอิพอกไซด์ (ENR) โดยใช้ไอออนโลหะเหล็กหรือไอออน
เฟอร์ริกที่ได้จากสารประกอบเฟอร์ริกคลอไรด์ (ferric chloride, $FeCl_3$) โดยใช้ยางธรรมชาติอิพอก
ไซด์ที่มีปริมาณหมู่อิพอกไซด์ 2 ระดับ คือ 25 และ 50% โมล (ENR-25 และ ENR-50) เปรียบเทียบ
กับการใช้ยางธรรมชาติที่ไม่ดัดแปรโมเลกุล ชนิดยางแผ่นผึ่งแห้ง (ADS) บดผสมในเครื่องผสมแบบปิด
ที่อุณหภูมิ 60°C และความเร็วโรเตอร์ 60 รอบต่อนาที จากการทดลองพบว่าเฟอร์ริกคลอไรด์สามารถ
เกิดปฏิกิริยาการเชื่อมขวางกับสายโซ่โมเลกุลยางธรรมชาติอิพอกไซด์ได้แต่ไม่เกิดปฏิกิริยากับยาง
ธรรมชาติที่ไม่ได้ดัดแปรโมเลกุล โดยพบว่าการเชื่อมขวางโมเลกุลยาง ENR ด้วยเฟอร์ริกคลอไรด์ให้
เส้นกราฟการวัลคาไนส์เป็นแบบมาชชิง (Marching curve) กล่าวคือ มีแนวโน้มค่าทอร์คเพิ่มขึ้นตาม
การเพิ่มเวลาการวัลคาไนส์ แสดงว่าเกิดปฏิกิริยาการเชื่อมขวางของสายโซ่โมเลกุลยาง ENR ด้วย
ปฏิกิริยาการเชื่อมขวางแบบโคออดิเนชัน โดยการเปิดวงแหวนอิพอกไซด์แล้วเกิดพันธะเคมี -Fe-O-
ซึ่งสามารถพิสูจน์จากการมีแถบการดูดกลืนรังสีอินฟราเรดที่เลขคลื่น 565 cm^{-1} นอกจากนี้ยังพบการ
เพิ่มปริมาณ $FeCl_3$ ในช่วงปริมาณ 1-10 มิลลิโมล ส่งผลต่อการเพิ่มค่าทอร์กซึ่งบ่งชี้ถึงปฏิกิริยาการ
เชื่อมขวางในโมเลกุลยาง ENR ตามการเพิ่มปริมาณเฟอร์ริกคลอไรด์ นอกจากเกิดการเชื่อมขวางโดย
ปฏิกิริยาโคออดิเนชันแล้วยังเกิดปฏิกิริยาการพอลิเมอไรเซชันภายใน (Internal polymerization)
โมเลกุลยาง ENR โดยพบว่าการใช้ $FeCl_3$ ในปริมาณสูงกว่า 7 มิลลิโมล ให้ยางวัลคาไนส์ที่มีสมบัติ
เชิงกลเหนือกว่ายางธรรมชาติอิพอกไซด์ที่เชื่อมขวางด้วยระบบกำมะถันแบบปกติ เนื่องมาจากมี
ปริมาณความหนาแน่นของพันธะการเชื่อมขวางที่สูงกว่า นอกจากนี้นำยาง ENR ที่เชื่อมขวางด้วย
เฟอร์ริกคลอไรด์ที่ปริมาณ 7 มิลลิโมล มาผสมกับสารตัวเติมท่อคาร์บอนนาโน (CNTs) โดยการแปร
ปริมาณท่อคาร์บอนนาโนเป็น 1, 3, 5, 7 และ 10 phr พบว่าหมู่ฟังก์ชันที่มีสภาพขั้วบนผิวของท่อ
คาร์บอนนาโนสามารถเกิดปฏิกิริยาและอันตรกิริยากับไอออนเฟอร์ริกและหมู่ฟังก์ชันที่มีสภาพขั้วใน
โมเลกุลยางธรรมชาติอิพอกไซด์ได้ดี ทำให้เกิดการเร่งปฏิกิริยาการวัลคาไนส์ให้เร็วขึ้น โดยสังเกตจาก
การลดเวลาสกอร์ช (scorch time) และเวลาการวัลคาไนส์ (cure time) ให้สั้นลง และพบว่ายาง
ENR ที่เชื่อมขวางด้วยไอออนเฟอร์ริกผสมท่อคาร์บอนนาโนเกิดการกระจายตัวได้ดีในเมทริกซ์ยาง
ENR ส่งผลให้มีสมบัติเชิงกล สมบัติเชิงพลวัต ความเสถียรต่อความร้อน รวมถึงค่าการนำไฟฟ้าสูงกว่า

ยาง ENR-FeCl$_3$ ที่ไม่มีการเติมท่อคาร์บอนนาโน เนื่องจากอันตรกิริยาทางเคมีระหว่างหมู่อิพอกไซด์
ของยาง ENR กับหมู่ฟังก์ชันที่มีขั้วบนพื้นผิวของท่อคาร์บอนนาโน นอกจากนี้วัสดุเชิงประกอบของ
ENR-FeCl$_3$ ที่เติมท่อคาร์บอนนาโนแสดงการกระจายตัวของท่อคาร์บอนนาโนได้ดีในยาง ENR ทำให้
มีสมบัติเด่น คือ สมบัติเชิงกล สมบัติเชิงพลวัต ความเสถียรต่อความร้อน และค่าการนำไฟฟ้า
นอกจากนี้พบว่าปริมาณท่อคาร์บอนนาโนที่ทำให้ยางนำไฟฟ้าแบบเฉียบพลันได้ (Percolation
threshold concentration) คือ ปริมาณ 7 phr จึงทดลองใช้ CNT ที่ปริมาณนี้เตรียมตัวเติมผสม
(Hybrid filler) โดยผสม CNTs กับคาร์บอนแบล็กชนิดนำไฟฟ้า (Conductive carbon black, CCB)
โดยแปรปริมาณของ CCB ที่ 2.5, 5.0, 7.0, 10.0 และ 15.0 phr พบว่าได้วัสดุเชิงประกอบนาโนที่มี
สมบัติเชิงกล สมบัติเชิงพลวัต และสมบัติการนำไฟฟ้าโดดเด่น เนื่องมาจากการเกิดอันตรกิริยาเคมี
ระหว่างหมู่ฟังก์ชันที่มีสภาพขั้วในโมเลกุลของยางธรรมชาติอิพอกไซด์ กับหมู่ฟังก์ชันที่มีสภาพขั้วที่
เกาะอยู่ที่ผิวของท่อคาร์บอนนาโน และคาร์บอนแบล็กชนิดนำไฟฟ้า นอกจากนี้ยังพบว่าการใช้ตัวเติม
ผสมทำให้ได้วัสดุเชิงประกอบนาโนที่มีสมบัติเด่น เมื่อเทียบกับการใช้ตัวเติมท่อคาร์บอนนาโนเพียง
อย่างเดียว เนื่องจากคาร์บอนแบล็กชนิดนำไฟฟ้าช่วยให้ท่อคาร์บอนนาโนเกิดการกระจายตัวในยาง
ธรรมชาติอิพอกไซด์ได้ดี เนื่องจากคาร์บอนแบล็กชนิดนำไฟฟ้า ขัดขวางการเกาะกลุ่มก้อนของท่อ
คาร์บอนนาโนในเมทริกซ์ยาง ENR

Keyword: ยางธรรมชาติอิพอกไซด์; เฟอร์ริกคลอไรด์; พันธะโคออดิเนชัน; ท่อคาร์บอนนาโน;
คาร์บอนแบล็กชนิดนำไฟฟ้า

Thesis Title   Influence of Metal Ions on Coordination Linkages of Epoxidized
                     Natural Rubber

Author   Mister Kriengsak Damampai

Major Program   Rubber Technology

Academic Year   2022

ABSTRACT

The crosslinking reaction of epoxidized natural rubber (ENR) with ferric ion (Fe^{3+}) from ferric chloride ($FeCl_3$) was investigated using ENR with two different levels of epoxide groups: 25 and 50 mol% (ENR-25 and ENR-50) and compared with unmodified natural rubber, air dry sheet (ADS). Mixing was performed in an internal mixer at 60°C and a rotor speed of 60 rpm. The results showed that the ENR-$FeCl_3$ compound exhibited an increased torque response with time (or marching cure curve), while unmodified natural rubber (ADS) did not have any torque response. The observed increased torque during the curing process can be attributed to a chemical reaction between the oxirane rings of ENR molecules and Fe^{3+} ions. This results in the formation of coordination -O-Fe-O- linkages, which is supported by the detection of the Fe-O absorption peak at the wavenumber 565 cm^{-1} in the infrared spectrum. Furthermore, the extent of coordination crosslinking reaction in ENR molecules was found to increase with increasing concentrations of $FeCl_3$ from 1 to 10 mmol. This leads to a more pronounced internal polymerization of the epoxy groups in the ENR molecular chains and an increased content of crosslinking networks. The results also indicated that the ENR-50 compound with $FeCl_3$ concentrations greater than 7 mmol exhibited the superior mechanical properties compared to those ENR cured with the conventional sulfur vulcanization. This is likely due to the higher crosslink density achieved through coordination crosslinking between epoxide groups and Fe^{3+} ions. Next, the ENR-$FeCl_3$ compound with a 7 mmol $FeCl_3$ concentration was filled with varying amounts of carbon nanotubes (CNTs) at 1, 3, 5, 7, and 10 phr. The addition of CNTs was found to accelerate the vulcanization reactions by reducing the scorch time and cure time. Furthermore, ENR-$FeCl_3$-CNTs nanocomposites exhibited higher mechanical, and dynamic properties, thermal resistance, and electrical conductivity than the compound

without CNTs. This is due to chemical interactions between the epoxy groups of ENR and polar functional groups on the CNTs' surface. Additionally, the ENR-FeCl$_3$-CNTs nanocomposites showed a finer dispersion of CNTs in the ENR matrix, resulting in outstanding mechanical, dynamic mechanical properties, thermal stabilities, and electrical conductivity. The percolation threshold concentration of ENR-FeCl$_3$-CNTs nanocomposites was determined to be about 7 phr of CNTs. Therefore, this content of CNTs (7 phr) was selected to prepare the ENR-FeCl$_3$ filled hybrid filler between CNTs and conductive carbon black (CCB) by varying CCB loadings at 2.5, 5.0, 7.0, 10.0, and 15.0 phr. The results indicated that the mechanical, dynamic, and electrical properties of ENR-FeCl$_3$/CNTs/CCB nanocomposites were further enhanced due to the chemical interactions between the polar functional groups in ENR molecules, CNT surfaces, CNT bundles, and CCB particles. Moreover, the ENR-FeCl$_3$/CNTs/CCB nanocomposites showed higher electrical conductivities than ENR-FeCl$_3$/CNTs without CCB, and a finer dispersion of CNTs in the ENR matrix was observed due to the CCB hindering the agglomeration of CNTs in the ENR matrix.

Keyword: Epoxidized natural rubber (ENR); ferric chloride (FeCl$_3$); coordination linkage; carbon nanotube (CNT); conductive carbon black (CCB)

ACKNOWLEDGEMENTS

CONTENTS

CONTENTS (CONTINUED)

CONTENTS (CONTINUED)

CONTENTS (CONTINUED)

LIST OF TABLES

LIST OF TABLES (CONTINUED)

LIST OF TABLES (CONTINUED)

LIST OF FIGURES

LIST OF FIGURES (CONTINUED)

LIST OF FIGURES (CONTINUED)

Page

LIST OF FIGURES (CONTINUED)

Page

LIST OF FIGURES (CONTINUED)

1

LIST OF FIGURES (CONTINUED)

LIST OF FIGURES (CONTINUED)

LIST OF FIGURES (CONTINUED)

LIST OF FIGURES (CONTINUED)

Page

LIST OF FIGURES (CONTINUED)

LIST OF FIGURES (CONTINUED)

LIST OF ABBREVIATIONS AND SYMBOLS

A	Area of an electrode
AcAc	Acetylacetonate
ADS	Air dried sheet
AgNP	Silver nanoparticle
AR	Acrylate rubber
$BaTiO_3$	Barium titanate
BMI	1-butyl-3-methyl-imidazolium-bis (trifluoromethylsulfonyl) imide
BPO	Benzoyl peroxide
BR	Butadiene rubber
C	Capacitance
CB	Carbon black
CCB	Conductive carbon black
ChCl	Choline chloride
cm^{-1}	Reciprocal centimeter
CNT	Carbon nanotube
CO_2	Carbon atmosphere
CR	Chloroprene rubber
$CuSO_4$	Copper(II) sulfate
CV	Conventional vulcanization
D	Dissipation factor
DAP	2,6-diaminopyridine
DCP	Di-cumyl peroxide
DDM	Diaminodiphenyl methane
DDS	Diaminodiphenyl sulphone
DMA	Dynamic mechanical analyzer
dNm	Deci newton meter
E(T)	Non-isothermal relaxation

E'	Storage modulus
E''	Loss modulus
ECF	Extra conductive furnace
EDX	Energy dispersive x-ray spectroscopy
E_g	Gap energy
EMA	Ethylene-methacrylic acid
ENR	Epoxidized natural rubber
ENR-25	Epoxidized natural rubber with 25 mol% epoxide
ENR-50	Epoxidized natural rubber with 50 mol% epoxide
EPDM	Ethylene propylene diene monomer rubber
EV	Efficient vulcanization
F	Force
$FeCl_3$	Ferric chloride
FTIR	Fourier transform infrared spectrophotometry
g/cm^3	Gram per cubic centimeter
g/mol	Gram per mole
GNTs	Graphene nanotubes
GPa	Giga-pascal
$H(T)$	Relaxation spectra
HA	High ammonium concentrated latex
HAF	High abrasive furnace black
Hz	Herz
IIR	Isobutylene isoprene rubber
IM	Imidazole
ISO	International organization for standardization
L	Inductance
L_0	Initial length
LiTFSI	Lithium bis(trifluoromethanesulfonyl) imide
MA	Maleic anhydride

MBTs	2,2'-dithiobis-(benzothaiazole)
MDR	Moving die rheometer
MgO	Magnesium oxide
M_H	Maximum torque
M_H-M_L	Torque difference
M_L	Minimum torque
mm	Millimeter
mmol	Millimole
MNR	Maleated natural rubber
MPa	Megapascal
MWCNTs	Multi-walled carbon nanotubes
Na-MMT	Sodium montmorillonite
NBR	Acrylonitrile rubber
NMCs	Natural rubber matrix composites
NMR	Nuclear magnetic resonance
NR	Natural rubber
NR-g-MA	Natural rubber-graft-maleic anhydride
NR-g-PDA	Natural rubber-graft-1, 2-phenylenediamin
NR-g-PMMA	Natural rubber-graft-poly(methyl methacrylate)
NR-g-SAN	Natural rubber-graft styrene and acrylonitrile
O_2	Oxygen atmosphere
OPD	Ortho-phenylene diamine
$PbTiO_3$	Lead titanate
PDA	1, 2-phenylenediamin
phr	Part per hundred rubbers
PMMA	Poly(methyl methacrylate)
PPD	Para-phenylene diamine
R	Resistance
RPA	Rubber process analyzer
rpm	Round per minute
SAN	Styrene and acrylonitrile

SEM	Scanning electron microscopy
Semi-EV	Semi-efficient vulcanization
$SnCl_2$	Stannous chloride
SWCNTs	Single-walled carbon nanotubes
$\tan \delta$	Loss tangent
t_{c90}	Cure time
TEM	Transmission electron microscopy
TESPT	Bis(trietoxysilyl propyl) tetrasulfide
TGA	Thermogravimetric analysis
t_{s1}	Scorch time
TSSR	Temperature scanning stress relaxation
V_c	Critical volumetric
V_L	Molar volume of toluene
XNBR	Carboxylate nitrile rubber
Z	Impedance
ZnO	Zinc oxide
α	Alpha
β	Beta
χ	interaction parameter of polymer and solvent
$\varnothing_p$	Volume fraction of rubber in the swollen network
G'_0	Minimum moduli
G'_{100}	Maximum moduli
[EMIM]Cl	1-ethyl-3-methylimidazolium chloride
ΔL	Changing in length
°C	Degree celsius
μm	Micrometer
1D	One-dimensional CNT network

CHAPTER 1

INTRODUCTION

1.1   Background and rationale

Natural rubber (NR) is an agricultural product with green, renewable resources and has high degree of biodegradation. NR has attracted both scientific and industrial interests due to its superior properties, including high elasticity, flexibility, mechanical strength and biodegradability. However, NR has some drawbacks including poor aging, weathering, oil resistance, and electrical conductivity. This causes limitation to use NR in some industrial applications. However, modification of NR molecules to be various forms could extend the application of NR. One of the popular chemical modified routes is to synthesize epoxidized natural rubber (ENR). It has been well established that ENRs enhance some properties for example weathering, gas permeation, oil resistance and high polarity (Baker and Gelling., 1985). In addition, applications of NR and ENR can be extended by incorporation of different types of polar fillers such as silica, clay, carbon black, conductive carbon black (CCB) and carbon nanotubes (CNTs), etc. These fillers are typically used to reinforce or enhance NR properties in particularly strength, stiffness, oil resistance, electrical properties, and weathering resistance. Moreover, cure or vulcanization systems are also one of the most important parameter to fabricate the un-vulcanized material to strong rubber vulcanizate. Normally, different cure systems have been used in the rubber formulation including sulfur, peroxide, phenolic, metal oxide and radiation vulcanization systems.

In polymers contain epoxirane rings, such as epoxy resin, curing could be possibly performed by using metal complex in order to improve mechanical, electrical and other related properties. For instance, the epoxy resin was cured by copper (II) chloride complexes of *ortho-phenylene* diamine (OPD) and found that the strong network formation was taken place from the reaction of the epoxy and metal complex (Hamerton *et al.*, 1995). In addition, the metal ions have also been used as a special type additive that can be used to tailor polymer and rubber properties. Also, some divalent transition metal ions (i.e., Mn^{2+}, Cu^{2+} and Fe^{2+}) were found to cause

acceleration of the oxidative degradation of solid rubber by fragmentation of the poly(isoprene) chains (Rippel *et al.*, 2002). In addition, the metal ions had a direct effect on molecular weight, branching and gel contents, especially on storage characteristics of natural rubber (Kurian and Mathew., 2011). Therefore, the introduction a certain amount of metal ions into polymers which contain ionic groups or epoxirane rings may exert an important role on their mechanical properties (Kurian and Mathew., 2011). Also, it has been well recognized that the elements that commonly found in NR latex are Ca, K, Al, Na, Mg, Mn, Fe, Si, Rb, P, N, S and O (Rippel *et al.*, 2002). It has been confirmed that mono-, di- and multivalent metal ions affect the NR properties (Gan *et al.*, 1993). That is, Na^+ and K^+ ions do not cause storage hardening phenomena of NR molecules, while Ca^{2+} and Mg^{2+} ions have high influence on reduction of storage hardening phenomenon in NR (Gan *et al.*, 1993).

Epoxy/anhydride/metal acetylacetonates (AcAcs) system has been investigated by using a number of different metal ions (Smith, 1981). It was found that the metal complexes had potentially acted as the curing agents in the malemide epoxy resins. A novel malemide epoxy containing Co(II), Ni(II) and Cu(II) ions have been synthesized by curing malemide epoxy resin and Co(II), Ni(II) and Cu(II) complexes of macrocyclic bis-hydrazone Schiff base (Lakshmi *et al.*, 2011). It was found that the cured systems exhibited excellent thermal stability and good chemical (acid/alkaline/solvent) and water absorption resistance. Additionally, coordinating metal ions can be altered by using suitable electrical potential but enhance of the electrical properties of rubber, conducting carbon nanotubes and/or conductive carbon black could also be also used (Krainoi *et al.*, 2018).

Carbon nanotubes (CNTs) are a new filler material with long, slender fullerene structures where the walls of the tubes are hexagonal carbons (i.e., graphite structure) with sp^2 hybridization and are often capped at each end. These cage-like forms of carbon have promoted exceptional material properties because of their symmetric structure. A number of works have claimed that the CNTs had mechanical properties exceed those of polymer composites (Ajayan *et al.*, 2000). That is, the carbon nanotubes have shown extremely high elastic modulus, greater than 1 TPa (the elastic modulus of diamond is 1.2 TPa) and strengths of 10–100 times higher than the

strongest steel on the weight basis (Ajayan *et al.*, 2000). Also, the CNTs have low density, high specific surface area and especially high aspect ratio, leading to high interaction with polymers. This makes the CNTs are more interesting to be used to reinforce the polymer matrix in particular NR. Also, incorporation of CNTs in NR could transform insulated NR material to be a more conductive one (Ajayan *et al.*, 2000). Electrical conductivity performance of NR/CNTs nanocomposites is recognized by observing the percolation threshold concentration that indicates the critical concentration of CNTs to form infinite CNTs dimensional network in polymer matrix. Generally, strong CNT agglomerations are formed due to its high aspect ratio, strong Van-der Waals attractions and π-π interaction between the CNT bundles or particles. Consequently, poor electrical conductivity and mechanical properties of the NR/CNTs vulcanizates are encountered. The challenge to prepare the NR/CNTs composites with very low percolation threshold concentration is to finely disperse CNTs in the NR matrix. and to maintain the overall properties of the rubber, especially the rubber elasticity that should not be deteriorated over the usage limit. For example, carbon nanotube (CNT) filled epoxidized natural rubber (ENR) caused improve mechanical and electrical properties (Krainoi *et al.*, 2018).

Conductive carbon black (CCB) becomes more popular filler in the conductive natural rubber nanocomposites (Nakaramontri *et al.*, 2017) and epoxidized natural rubber nanocomposites (Matchawet *et al.*, 2015). It was found the CCB filled NR and ENR composites had high mechanical, dynamic, and electrical properties together with very low percolation threshold concentration. This is due to the CCB has high structure, surface areas, and also high degree of porosity. These are significant characteristics that cause improvement of electrical properties at very low loadings or at low percolation threshold concentration (Matchawet *et al.*, 2016). That is, the ENR/S-MWCNTs composites had the lowest percolation threshold concentration at 3 phr (Matchawet *et al.*, 2015). In addition, the CCB/CNTs hybrid filler was studied to improve dispersion degree of filler in rubber matrix (Nakaramontri *et al.,* 2017). It was found that CCB particles could reduce the Van-der Waals attraction among CNTs particles, leading to

finer and better dispersion of CNTs in the NR matrix. Therefore, the secondary filler (i.e., CCB) contributes to improve the CNTs dispersion in ENR matrix.

The main aim of the present research work was to investigate the alternative route to vulcanize epoxidized natural rubber (ENR) by using metal ions (ferric chloride, Fe^{3+}, $FeCl_3$) based on coordination linkages of epoxidized natural rubber molecules. Furthermore, various properties of ENR cured with metal ions ($FeCl_3$) and its filled composites with CNTs and CNTs/CCB hybrid filler with various CCB loadings were investigated. The investigated properties include cure characteristic, mechanical, thermal, dynamic, morphological properties and electrical conductivity.

1.2   Scope of thesis

1.2.1   To prepare and characterize ENR compounded with metal ions (Fe^{3+}, $FeCl_3$) by melt mixing methods.

1.2.2   To investigate the network formation by observing the crosslink structure and other characterization methods (i.e., cure characteristics, mechanical, thermal, dynamic properties, morphology, stress relaxation, electrical conductivity) of epoxidized natural rubber vulcanized by metal ions.

1.2.3   To investigate effect of carbon nanotubes (CNTs) in metal ions cured ENR based nanocomposites on mechanical, dynamic, morphology, stress relaxation and thermal properties, together with electrical conductivity and other related properties.

1.2.4   To investigate the effect of CNTs hybrid filler with conductive carbon black (CCB) in ENR compounded with metal ions. The main aim was to improve electrical conductivity and other related properties.

1.3 Aim of thesis

1.3.1   To study influence of metal ions (Fe^{3+}, $FeCl_3$) on properties of ENR compounds by dry mixing methods.

1.3.2   To study the network formation of the metal ions cured ENR by observing the crosslink density and other related properties (i.e, cure characteristics, mechanical, thermal, dynamic properties, morphological, stress relaxation, electrical conductivity)

1.3.3   To study effect of carbon nanotubes (CNTs) on properties of the metal ions cured ENR nanocomposites by investigating electrical conductivity and other related properties (i.e, cure characteristics, mechanical, dynamic properties, morphological, stress relaxation and thermal properties).

1.3.4   To study effect of CNTs/CCB hybrid filler on properties of the metal ions cured ENR nanocomposites by investigating electrical conductivity and other related properties (i.e., cure characteristics, mechanical, dynamic properties, morphological, stress relaxation and thermal properties).

1.4 Novelty of the work

There are new findings that generate from this research work, as indicated below:

1.4.1   Epoxidized natural rubber (ENR) was successfully crosslinked by Fe^{3+} ions (from $FeCl_3$) to form the coordination crosslinks (–O–Fe–O– linkages) between ENR molecules and to form internal polymerized products from oxirane groups of ENR molecules. (Damampai *et al.,* 2021; Damampai *et al.,* 2022).

1.4.2   Epoxidized natural rubber (ENR) with 50% mol epoxide (ENR-50) cured with the optimum dose of 7 mmol $FeCl_3$ displays superior properties (i.e., mechanical and dynamic properties) than the ENR-50 cured with the conventional sulfur cured system (Damampai *et al.,* 2021).

1.4.3   Epoxidized natural rubber (ENR) with 50% mol epoxide (ENR-50) cured with Fe^{3+} ions ($FeCl_3$) and filled with CNTs has higher electrical conductivity than the ENR without CNTs (Damampai *et al.,* 2022).

1.4.4   Epoxidized natural rubber (ENR) with 50% mol epoxide (ENR-50) cured with Fe^{3+} ions ($FeCl_3$) and filled with CNTs/CCB hybrid filler caused improvement of mechanical, dynamic, thermal and electrical properties (Damampai *et al.,* 2022).

1.5   Thesis outline

This thesis involves preparation of ENR compounded with metal ions and filled with CNTs and CNT/CCB hybrid filler. It can be divided into eight chapters, as follows:

Chapter 1 introduction of thesis research work

Chapter 2 background and literature review

Chapter 3 materials and experimental methodology

Chapter 4 ferric chloride cross-linked epoxidized natural rubber with 25 mol% epoxide (ENR-25)

Chapter 5 cross-linking of epoxidized natural rubber with 50 mol% epoxide (ENR-50) by ferric chloride

Chapter 6 crosslinked epoxidized natural rubber by ferric chloride filled with carbon nanotubes

Chapter 7 crosslinked epoxidized natural rubber by ferric chloride filled with carbon nanotubes and conductive carbon black hybrid filler

Chapter 8 conclusions

CHAPTER 2

BACKGROUND AND LITERATURE REVIEW

2.1 Natural rubber (NR) and its derivatives

Natural rubber (NR) is derived from the latex of the rubber tree, *Hevea brasiliensis*. Natural rubber has attracted both scientific and industrial interests including automotive and rubber parts, truck and airplane tires due to its superior properties including high elasticity, flexibility, low-heat buildup and high resilience. In addition, NR has high stress relaxation resistance and good creep resistant properties. NR is often used as a matrix of rubber composites which have been widely studied and applied in high performance smart materials. However, NR has some drawbacks including poor aging, weathering, oil resistant properties, and poor electrical conductivity. This limits application of NR in some industries. However, this limitation can be revamped by modification of natural rubber molecules to form NR derivatives, such as epoxidized natural rubber (ENR), maleated natural rubber (MNR), and graft copolymers of NR with various polymers. These modified NRs are typically extended the intrinsic properties of NR to gain more strength, stiffness, oil resistance, air permeation, and weathering resistance.

2.1.1 Epoxidized natural rubber (ENR)

Epoxidized natural rubber (ENR) is a modified form of NR material that possesses higher toughness, polarity and electrical conductivity relative to original natural rubber (NR) with a nominal reduction in mechanical properties and thermal stability due to the presence of epoxy groups along the NR backbone chains. However, ENR gains higher solvent resistance, polarity and gas impermeability. ENR with different epoxide levels from 1 to 75 mol % can be readily prepared by peracid (such as, peacetic or perfomic acid) epoxidation in solution or latex states (Ruksakulpiwat *et al.*, 2008). It was found that a systematic change in properties of ENR was observed with the variation of the epoxidation levels (Ruksakulpiwat *et al.*, 2008). That is, ENR has dramatically improved heat and chemical resistance due to oxirane rings increase the

hydrophilicity and reduce the number of double bonds in the NR backbone. Likewise, ENR has high compatibility with polar polymers and high thermal resistance (Wei *et al.*, 2019). Moreover, ENR has considerable contents of epoxirane rings and reactive carbon-carbon double bonds in their molecular structures, which have high capability to interact with other polar materials and also some metal oxide (Yangthong *et al.*, 2018). These characteristics lead to a possibility to introduce some functional groups and/or new formed linkages among ENR molecules, which could improve some important properties of ENR vulcanizates including dynamic and mechanical properties together with electrical conductivity. In commercial manufacturing of ENR, two levels of epoxide levels at 25 and 50 mol% (i.e., ENR-25 and ENR-50) have been produced and used in research and industrial applications. Figure 2.1 shows a synthesis route of ENR by reacting formic acid and hydrogen peroxide to form peroxy formic acid or performic acid which subsequently reacts with NR molecules to form ENR molecule with formic acid by product. This represents a cycle for synthesis of ENR via an *in-situ* performic (or peroxy formic acid) epoxidation by in a latex state.
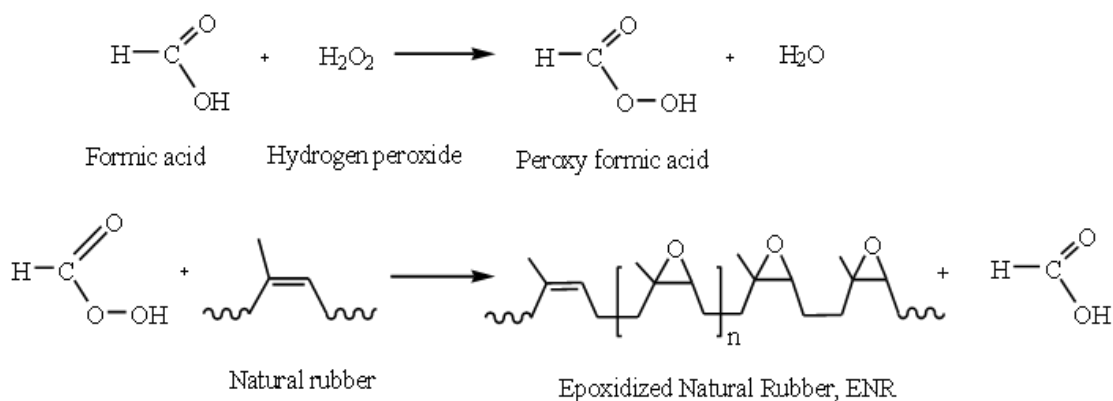
Figure 2.1 Synthesis of ENR by an *in-situ* performic epoxidation (Ruksakulpiwat *et al.*, 2008).

2.1.2.   Maleated natural rubber (MNR)

Maleated natural rubber (MNR) has been prepared by reacting maleic anhydride (MA) and NR molecules to gain succinic anhydride grafted onto natural rubber backbone chain, or NR-g-MA (Nakason *et al*., 2004). MNR has high compatibility with polar polymers due to the presence of succinic anhydride moieties on rubber molecules (Nakason *et al*., 2006). Also, MNR has high thermal resistance (Wei *et al*., 2019). In addition, MNR has been used to prepare rubber nanocomposites with various nanofillers. These include NR/organoclay nanocomposites with maleated natural rubber as a blend compatibilizer (Hakim and Ismail., 2009). It was found that shorter scorch and cure times were observed due to the reaction between accelerator and free maleic anhydride and/or succinic acid from a ring-opening reaction of maleated natural rubber (Nakason *et al*., 2001, Hakim and Ismail., 2009). Figure 2.2 shows a chemical reaction used to prepare MNR or NR-g-MA by reacting natural rubber molecules and maleic anhydride in the presence of benzoyl peroxide (BPO) initiator in toluene solution.
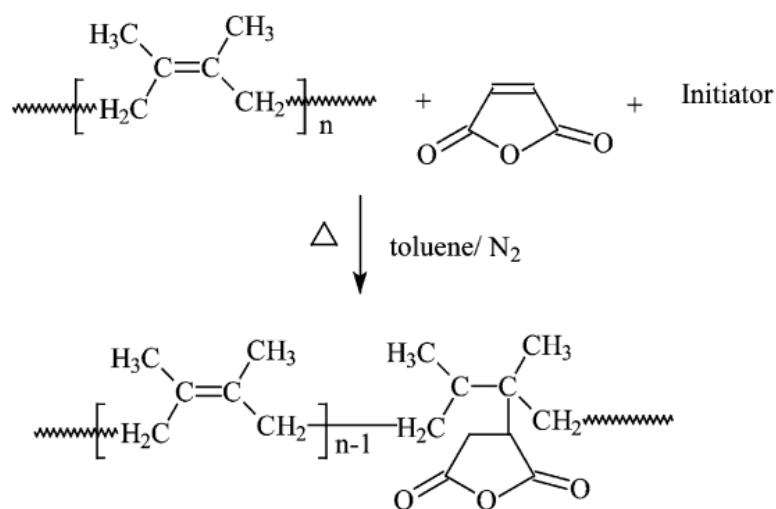
Figure 2.2 Chemical reaction between NR molecule and maleic anhydride in toluene solution with benzoyl peroxide initiator (Nakason *et al*., 2004).

2.1.3 Graft copolymer of natural rubber

Chemical modification of NR molecules via graft copolymerization is one of the most common method used to prepare a product that has some prominent properties than those of the neat unmodified NR. Graft copolymerization of NR has been prepared by using vinyl monomers. including styrene (Asaletha *et al.,* 1998), acrylonitrile (Okieimen *et al.*, 1996) and methyl methacrylate (Nakason *et al.,* 2004, Salim *et al.*, 2014). It was found that the ultimate tensile strength of the NR-g-PMMA increased with an increase in molar ratios of MMA monomers in the grafting reaction. This is attributed to increasing trend of the grafted PMMA onto the NR molecules, causing an increasing trend of stiffness (Nakason *et al.*, 2004). In addition, the natural rubber grafted with 1, 2-phenylenediamin (NR-g-PDA) could enhance the mechanical properties and oxidation resistance of the NR vulcanizates (El-Wakil., 2007). Graft copolymers of NR could be normally used as a compatibilizer in rubber blends. For instance, graft copolymer of styrene and acrylonitrile copolymer onto NR (NR-g-SAN) was used as a compatibilizer for NR/NBR blends (Angnanon *et al.*, 2011). It was claimed that improvement of mechanical properties and oil resistance of NR/NBR vulcanizates was gained due to the higher compatibility and interfacial adhesion between the rubber components. (Angnanon *et al.*, 2011). Figure 2.3 shows a representative molecular structure of NR-g-PMMA.
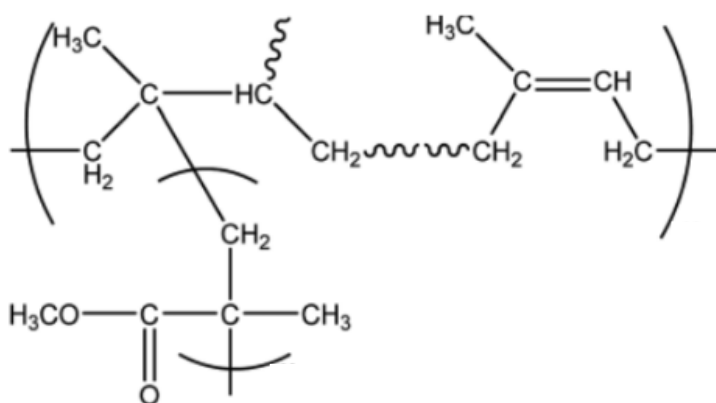
Figure 2.3 Molecular structure of NR-g-PMMA (Salim *et al.*, 2014).

2.2 Vulcanization system

Raw and uncured natural rubber has intrinsically poor strength, elasticity and dimensional stability. Enhancement of rubber elasticity, strength and other related properties can be done by introducing linkages or crosslinks between rubber chains to form three-dimensional networks. This crosslinking process is typically known as vulcanization or curing of rubber. They are usually formed by means of curing agents that are able to create and form covalent, coordination and other types of chemical bonds between the rubber chains. Various vulcanization systems have been extensively exploited to cure of rubber material. These include sulfur cured system (Cunneen and Russell, 1970), peroxide (Henning, 2008), phenolic (Imanifar, 2018), metal oxide (Mallon *et al.*, 1995) and coordination vulcanization system (Kasyanenko *et al.*, 2009).

2.2.1 Sulfur vulcanization system

Sulfur vulcanization has been widely applied in various types of diene rubbers with unsaturation in the molecular chains or in rubber with unsaturated side groups in their molecules (such as, ethylene propylene diene monomer rubber (EPDM)). It is noted that types and contents of crosslinks or crosslink density are largely depended on ratio of accelerator to sulfur (A/S ratio). They can be categorized into three different types of sulfur vulcanization systems: conventional vulcanization (CV), semi-efficient vulcanization (semi-EV) and efficient vulcanization (EV), as contents of sulfur, accelerator and A/S ratios in Table 2.1 (Akiba and Hashim, 1997).

Table 2.1 Composition of sulfur and accelerator in conventional, semi-EV and EV vulcanization systems (Akiba and Hashim, 1997).

vulcanization system	Sulfur (S, phr)	Accelerator (A, phr)	A/S ratio
Conventional (CV)	2.0-3.5	0.4-1.2	0.1-0.6
Semi-efficient (Semi-EV)	1.0-1.7	1.2-2.5	0.7-2.5
Efficient (EV)	0.4-0.8	2.0-5.0	2.5-12

When the sulfur vulcanization system is employed, there are possibly three different kinds of covalent bonds or chemical linkages: mono-sulfidic (–C–S–), disulfidic (–C–S–S–C–) or polysulfidic linkages (–C–S_x–C–), where x is greater than 3 (Cunneen and Russell, 1970; Coran, 2003). Different types of sulfidic linkages are as schematically shown in Figure 2.4.
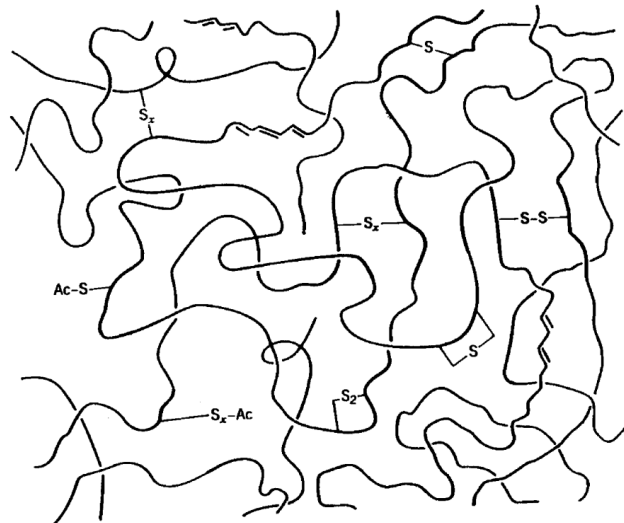
Figure 2.4 Schematic representation for different types of sulfidic linkage in rubber cured with sulfur vulcanization system (Coran., 2003) (Ac represents an accelerator).

2.2.2 Peroxide cured system

The oxygen-oxygen bonds in the molecular structure of an organic peroxide is susceptible to break under high temperature condition and to generate free radicals, as shown in Figure 2.5. These radicals are unstable and very reactive and they can readily react with the weak carbon-hydrogen bond in the polymer molecules and to transfer radicals to the polymer molecules, forming hydrocarbon radicals which are still very active (Henning, 2008). Then, the two active hydrocarbon radicals share free radical electrons to form a covalent bond as a cross-linking chain (Figure 2.5). In general, the α-methylene carbon atom is a sensitive location for the reaction with free radical to occur. Therefore, stronger covalent bond of carbon-carbon (bonding energy = 350 kJ) was formed instead of carbon-sulfur (bonding energy = 270 kJ) bond as seen in the sulfur vulcanization system (Henning, 2008). The stronger new formed C-C bond requires higher energy to break. Therefore, peroxide vulcanized rubbers provide superior heat resistance and compression set properties than the rubber products that are vulcanized by sulfur curing systems (Kruželák *et al.,* 2017).
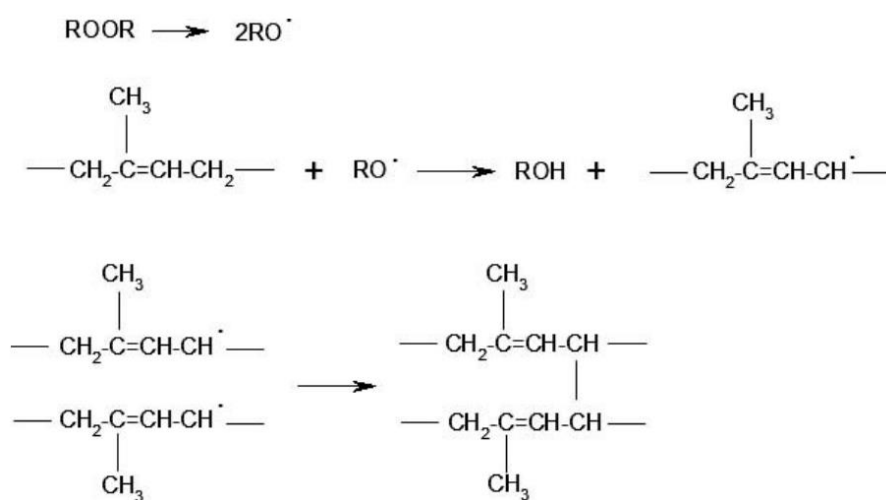
Figure 2.5 Peroxide cross-linking of NR (Kruželák *et al.,* 2017).

2.2.3 Phenolic cured system

Phenolic-resin is one of the most common polymeric binders in the composite due to its low cost, relatively high heat resistance and high degree of tackiness (Derakhshandeh *et al.,* 2008). Phenolic resins, (i.e., octyl phenol formaldehyde resin)

are widely utilized for crosslinking of butyl rubbers for high temperature environment applications. In crosslinking reaction, the reactive phenolic resin can form a cyclic ether via the reaction between the phenol-methylol groups and the C=C bond in the butyl rubber backbone (Lattimer *et al.*, 1984). Moreover, carbon black (CB) filled isobutylene isoprene rubber (IIR) composites cured with phenolic resin can improve thermal stability of IIR rubber vulcanizate (Li *et al.*, 2017). Figure 2.6 shows a reaction mechanism of phenolic resin cured diene rubber at high temperature (Imanifar, 2018).
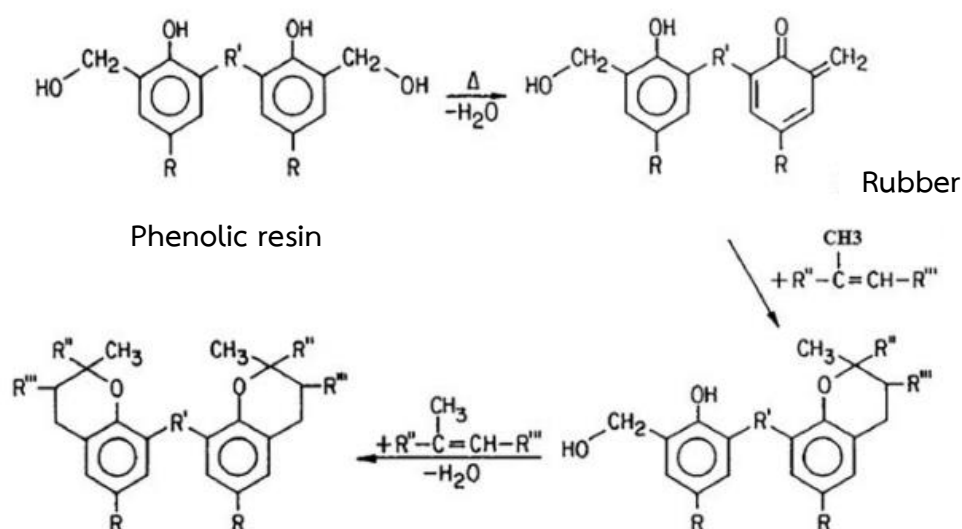
Figure 2.6 Reaction mechanism of phenolic resin cured diene rubber (Imanifar, 2018).

2.2.4 Metal oxide cured system

Metal oxide vulcanization is of importance for crosslinking of some types of rubber, especially chloroprene or neoprene rubber (CR) by ZnO and MgO (Mallon *et al.*, 1995). Furthermore, chloroprene rubber and butadiene rubber (BR) blends can be cross-linked by copper (I) oxide or copper(II) oxide with significant improvement of fire resistance (Olejnik *et al.*, 2018). A reaction mechanism for cross-linking of chloroprene and butadiene rubber blends with copper (I) oxide or copper(II) oxide is described in Figure 2.7. It is clear that the interelastomeric reactions between chloroprene and butadiene rubbers occur by the assist of copper oxides (Olejnik *et al.*, 2018).
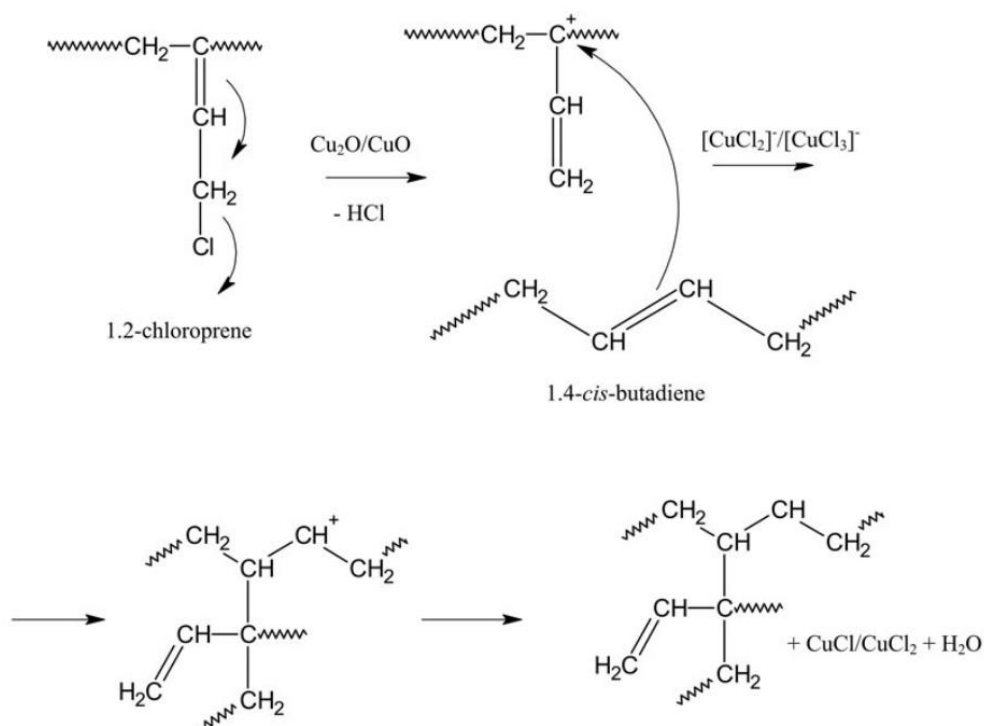
Figure 2.7 Reaction mechanism of cross-linking reaction of chloroprene and butadiene rubber blends (CR/BR, 75/25 wt%) in the presence of copper (I) oxide and copper(II) oxides (Olejnik *et al.*, 2018).

2.2.5 Coordination vulcanization system

Coordination compound or complex is defined as a class of substances with chemical structures in which a central metal atom is surrounded by bonding to nonmetal atoms or groups of atoms, called as "ligands. This coordination bonding provides the benefits of both the reversibility and stability (Kasyanenko *et al.,* 2009). The coordination linkage is generally considered as one of the most promising method for preparation of the reversible crosslinking of rubber and hence self-healable and re-processable rubbers (Kasyanenko *et al.,* 2009). Various types of metal ions can be formed coordination compound with polar rubbers. For instance, the acrylate rubber (AR) containing polar functional groups, were *in-situ* coordination crosslinking by mixing the rubber with $CuSO_4$ and cured at three different temperatures: 150, 180 and 210 °C. (Mou *et al.,* 2012). It was found that the tensile properties and crosslinking networks of the AR/$CuSO_4$ composites increased with increasing the $CuSO_4$ loading and

temperature. Furthermore, the coordination crosslinking of nitrile rubber (NBR) was carried out by mixing with copper sulfate in an open two-roll mill for 15 min at room temperature, as the reaction and crosslinked structure shown in Figure 2.8 (Shen *et al.,* 2007). It was found that this type of crosslinked NBR had high tensile strength of 45.2 MPa as compared with the traditional sulfur-vulcanized NBRs, filled with organoclay and a novel black liquor–montmorillonite complex, which had tensile strength lower than 30 MPa (Shen *et al.,* 2007). Furthermore, copper sulfate ($CuSO_4$) was mixed with nitrile rubber at 190 °C. for 20 min and found that the metal salts (i.e., $CuSO_4$) can cause coordination cross-linking reaction with NBR to create and form network structures similar to sulfur vulcanization (Shen *et al*., 2008). Therefore, the coordination reaction between the metal cations and the polar groups in rubber molecules occurred at high temperatures, at which the molecular chains were flexible enough.
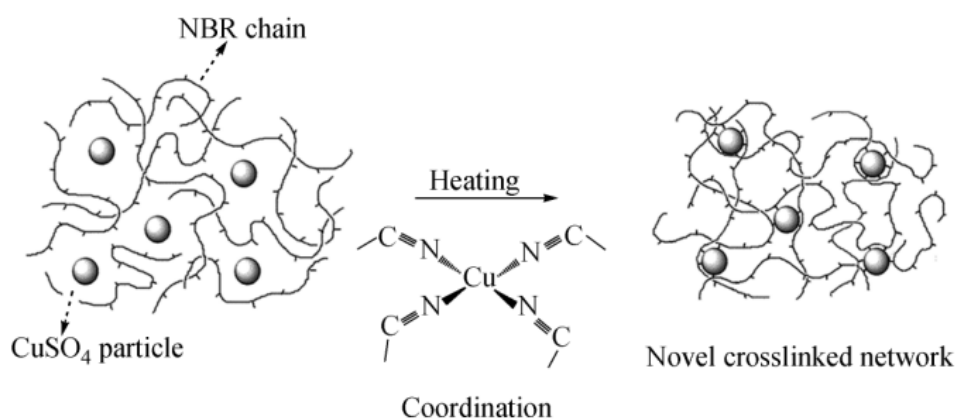
Figure 2.8 formation of coordination crosslinked rubber network: $CuSO_4$/NBR system (Shen *et al*., 2007).

Moreover, copper sulfate ($CuSO_4$) was mixed with nitrile rubber at 190 °C. for 20 min. It was found that the metal salts (i.e., $CuSO_4$) can cause coordination cross-linking reaction with NBR to create and form network structures similar to sulfur vulcanization (Shen *et al*., 2008). Therefore, the coordination reaction between the metal cations and the polar groups in rubber molecules occurred at high temperatures, at which the molecular chains were flexible enough. Recently, coordination crosslinking between carboxylate nitrile rubber (XNBR) and anhydrous $CuSO_4$ was investigated and found

that the crosslinking took place via both nitrile (–CN) and carboxylic (–COOH) groups of the XNBR. Therefore, the coordination bonds with copper were formed via the nitrile groups, while the ionic bonds were created *via the carboxylic* groups (Ibarra *et al*., 2009)

In general, type and size of the metal ions are an influential factor on coordination crosslinking (Petriuk *et al*., 2011). That is, larger metal diameters resulted in more defects and fewer cross-linking points. An ideal situation could be achieved when the diameters of metal particles reached their minimum limit. Therefore, it was important to decrease the particle size of metal salts to increase the cross-linking points as well as to improve their dispersion capability in the rubber matrix (Petriuk *et al*., 2011).

2.2.5.1 Coordination vulcanization of epoxy containing polymers

Reactions of metal ions and epoxy resins have been wildly investigated. These include reaction of epoxy resin with nickel Ni(II) with three different complexes based on three different ligands: diethylentriamine, pyrazole, and pyridine (Omrani *et al*., 2006). It was found that thermal stability of the coordination material increased with increasing amount of nickel(II) in the polymer chains (Omrani *et al*., 2006). Furthermore, copper (II) chloride complexes with four different ligands: ortho-phenylene diamine (OPD), para-phenylene diamine (PPD), diaminodiphenyl methane (DDM) and diaminodiphenyl sulphone (DDS) were used in curing of epoxy resin (Hamerton *et al*., 1995). It was found that the OPD structure with adjacent binding sites favor the formation of a chelate with copper good solubility in epoxy. However, the PPD ligand produces linear complex structures with poor solubility when formulating as the curing agent of epoxy resin. In addition, copper particles were mixed with epoxy resin to form the conductive adhesive with polyamide resin curing agent (Dang *et al*., 2012). It was found that the optimum condition of conductive adhesive resin composed of 16 wt% of epoxy resin, 8 wt% polyamide resin, 65 wt% of Cu microparticles and nanoparticles, 1.3 wt% of silane coupling agent, and 9 wt% of other additives with curing time of 4 h at 60°C. Moreover, the addition of silver particles in epoxy resin improved electrical

conductivity and crosslink density of the conductive adhesive composite (Khairul *et al.*, 2011).

Generally, the oxirane rings in an epoxy resin could react with different curing agents including aromatic amines, aliphatic amines, polyamides, phenols, anhydrides, acids and other suitable ring opening compounds (Lee *et al.*, 1967). It is noted that the epoxy resin cures primarily by a ring-opening mechanism in the anionic mechanism. That is, the oxirane rings may be opened in various fashions to produce an anion, as shown in Figure 2.9. This anion is an activated species which are capable of further reaction with metal ions.

Epoxy group   Epoxy anion
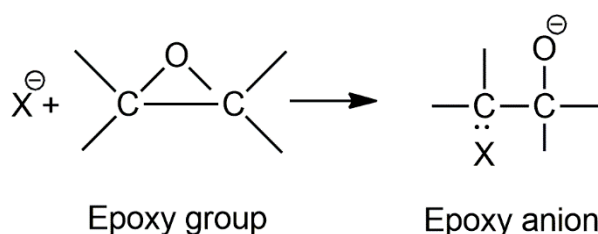
Figure 2.9 Anionic ring-opening mechanism of epoxy resin (Lee *et al.*, 1967).

Furthermore, the epoxy resin could be cured with ionic liquids: 1-ethyl-3-methylimidazolium chloride [EMIM]Cl and eutectic mixture of imidazole (IM) with choline chloride (ChCl) (Maka *et al.*, 2012). It was found that the [EMIM]Cl cured resin exhibited longer storage time and superior mechanical properties as compared with the cured resin based on the mixture of IM and ChCl (Maka *et al.*, 2012). In addition, epoxy resin could be cured with ammonium ionic liquids and palladium complex catalysts (Ostrowska *et al.*, 2013). It was found that the polymer-supported palladium catalysts have good catalytic stability. The model of coordination of Pd(II) complex formed by epoxy resin bisphenol A epichlorohydrin epidian 5 (EP5)/didecyldimethylammonium theophyllinate, (EP5/[d2m2am][thb]) is shown in Figure 2.10. It is seen that the particular disorientation of the purine ring of didecyldimethylammonium theophyllinate under the influence of Pd(II) indicates the possibility of the metal coordination to the =N- nitrogen atom (Figure 2.10(a)). While,

the bonding of the metal by the oxygen atom with a free pair of electrons is indicated in Figure 2.10(b).
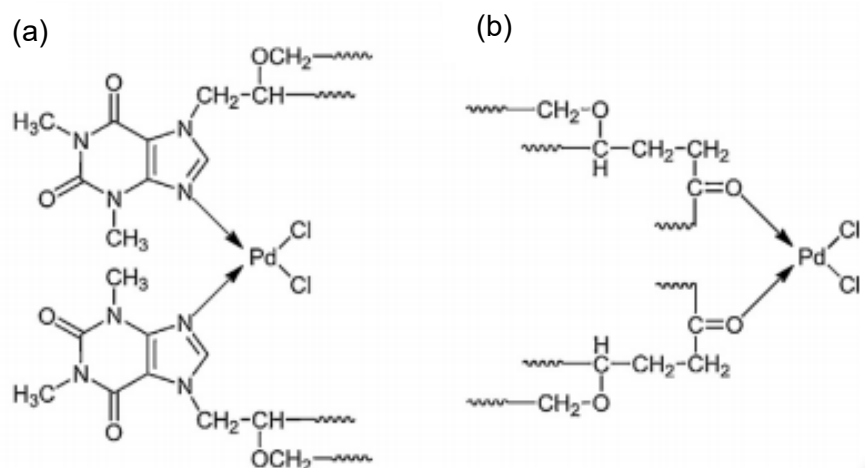
Figure 2.10 Model of coordination of Pd(II) complex by epoxy resin bisphenol A epichlorohydrin Epidian 5/didecyldimethylammonium theophyllinate support (Ostrowska *et al*., 2013).

2.2.5.2 Influence of metal ion on properties of natural rubber composites

Natural rubber (NR) composites have been prepared to tailor their properties and end use applications. NR was mixed with various metal ions including Ba^{2+}, Ca^{2+}, Mg^{2+} Cu^{2+} Fe^{2+} and Ca^{2+} (Utara *et al*., 2015). It has been found that the divalent metal ions (i.e., Cu^{2+}, Fe^{2+} and Ca^{2+}) caused decreasing curing rate by increasing the scorch time and cure time, as shown in Figure 2.11 (Utara *et al*., 2015). Furthermore, the modified natural rubber, epoxidized natural rubber (ENR) can be possibly crosslinked by reacting polar groups from opened epoxirane ring products with metal ions. There has been a limited number of studies relating to the reaction among metal ions and ENR or NR. In a such case, the active complex between metal ions and rubber molecules was formed due to the divalent metal ions act as a Lewis acid and the cure accelerator acts as a Lewis base (Utara *et al*., 2015). It was also established that the Lewis acid characteristic of the metal ion is inversely related to its radius (Utara *et al*., 2015). In addition, higher delta torque or torque difference and hence the cross-link

density of NR vulcanizate was found in the NR compounded with Cu^{2+}, rather than the NR compounded with Fe^{2+} and Ca^{2+}. However, it was found that the glass transition temperature (T_g) of NR filled these metal ions remains unaffected by either metal ion loading or type (Utara *et al.*, 2015).
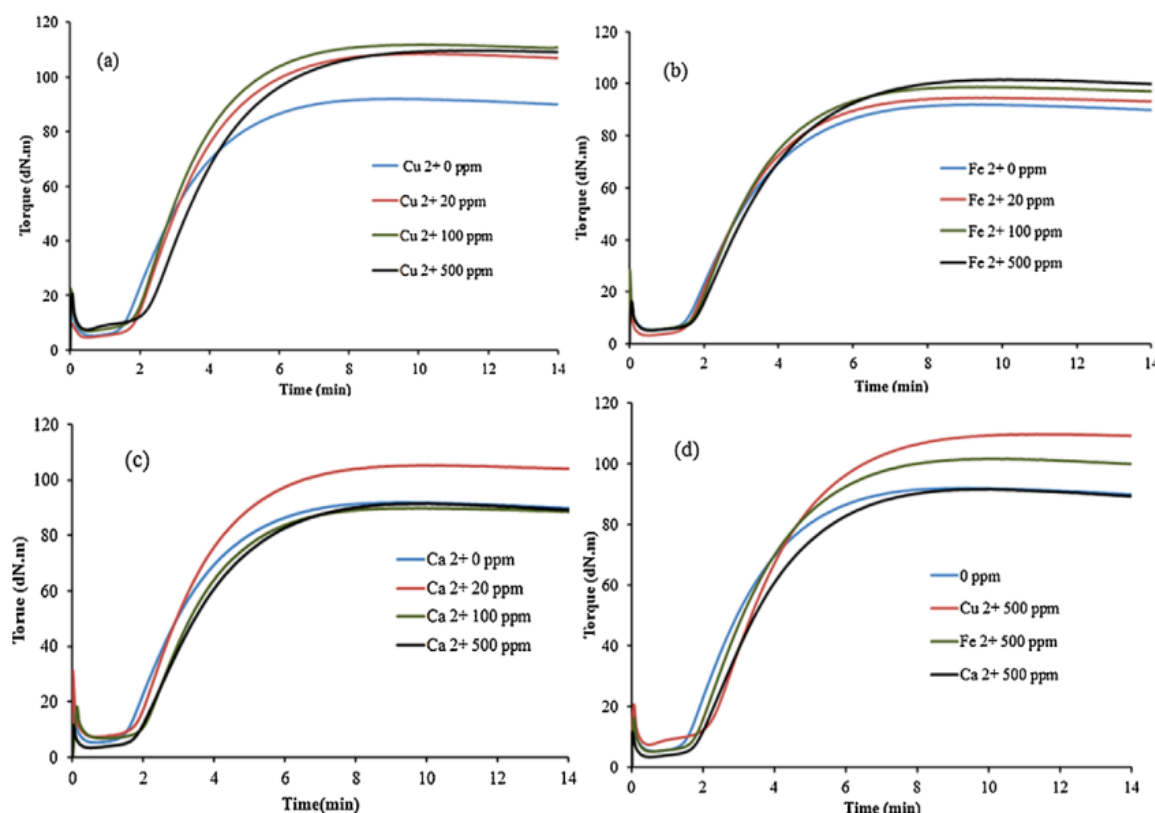
Figure 2.11 Effect of divalent metal ions on the torque-time curves of NR compounds; (a) Cu^{2+}; (b) Fe^{2+}; (c) Ca^{2+} and (d) comparison between Cu^{2+} Fe^{2+} and Ca^{2+} at the same concentration of metal ions (Utara *et al.*, 2015).

Furthermore, six types of divalent metal ions (i.e., calcium, magnesium, copper, manganese, iron, and zinc ions) were compounded with natural rubber and found that the calcium and zinc ions provided similar tensile and storage properties to raw natural rubber. However, the manganese and iron ions act as an accelerator in natural rubber vulcanization by decreasing scorch and cure times (Zhao *et al.*, 2018). Moreover, the magnesium ion caused suddenly increasing the storage stability at low concentration, while the copper ion showed the largest effect on the storage property (Zhao *et al.*,

2018). In addition, Gan *et al*., (1993) pointed out that different metal ions caused different effects on storage hardening of natural rubber latex. That is, the monovalent cations (i.e., Li^+, Na^+, K^+ and Cs^+) have small effect on storage hardening of natural rubber (Table 2.2). This might be attributed to lack of interaction between cations and nitrogenous groups in the rubber chains. However, the divalent cations (i.e., Ba^{2+}, Ca^{2+} and Mg^{2+}) could slowly displace and interact to the proteinous materials and amino acids of rubber molecules in latex particles, leading to less amino acid in NR molecules (Gan *et al*., 1993). This reflects by lower nitrogen contents, which consequently reduce the storage hardening phenomenon (Table 2.3). In addition, transition metal ions including Co^{2+}, Cu^{2+}, Mn^{2+}, Fe^{2+}, Ni^{2+} and Ag^+ promote oxidative degradation of NR molecules, causing the predominant chain scission reaction during storage of dry rubber (Gan *et al*., 1993).

Table 2.2 Effect of some monovalent cations on storage hardening of natural rubber (Gan *et al*., 1993).

Metal salt	Final pH	P_o	P_H	ΔP	%N
Control (none)	5.3	30	90	60	0.37
$LiNO_3.3H_2O$	5.6	31	85	54	0.38
$NaNO_3$	5.7	29	85	57	0.34
KNO_3	5.8	28	86	58	0.34

Table 2.3 Effect of Mg^{2+}, Ca^{2+} and Ba^{2+} on storage hardening of natural rubber (Gan *et al.*, 1993).

Metal salt	Final pH	P_o	P_H	ΔP	%N
Control (none)	5.5	30	90	60	0.32
$MgCl_2.6H_2O$	5.8	31	46	15	0.24
$CaCl_2$	5.7	32	46	13	0.18
$BaCl_2.2H_2O$	5.7	31	70	39	0.24

Different types of metal powder, such as aluminium powder (Vinod *et al.*, 2002), cobalt, nickel and iron powders were also used to prepare natural composites (Petriuk *et al.*, 2011). It was found that the higher dispersion of iron, cobalt and nickel caused electrical conductance increases slightly as long as the metal concentration did not exceed 20- 40% (Figure 2.12) (Petriuk *et al.*, 2011).
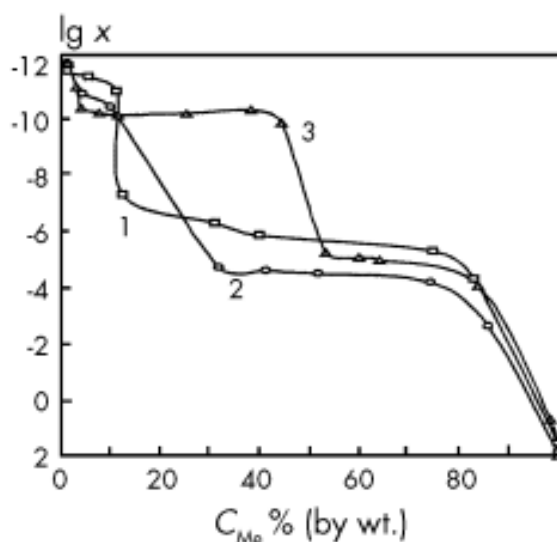
Figure 2.12 Electrical conductance of a composite system based on natural rubber containing highly-disperse particles of: 1–cobalt, 2 –nickel, and 3 – iron (Petriuk *et al.*, 2011).

In addition, particulate fillers, such as alumina nanoparticles have been exploited to modify properties of epoxidized natural rubber (ENR) and found that torque difference increased with increasing contents of alumina nanoparticles (Mohamad *et al.*, 2008). Furthermore, ENR and ethylene-methacrylic acid (EMA) ionomer blends were prepared with the aim to investigate the ability of intrinsic self-repairing systems (Rahman *et al.*, 2011). It was found that pure ethylene-methacrylic acid copolymers partially neutralized with sodium (i.e., EMNa) and ethylene-methacrylic acid copolymers partially neutralized with zinc ((i.e., EMZn) showed completely self-repairing in ballistic puncture tests. In addition, incorporation of di-cumyl peroxide (DCP) in EMNa/ENR blends caused significantly improvement of modulus and strength properties in comparison to the samples without DCP (Rahman *et al.*, 2011). However, the self-repairing effect was not found in the EMZn/ENR blends due to the rearrangement of coordinated complexes of Zn^{2+} ions (Rahman *et al.*, 2011).

The epoxirane rings in ENR molecules provide an effective conduction path of carrier ions. Therefore, the ENR electrolytes may yield flexible films with good adhesive property and high ionic conductivity (Idris *et al.*, 2001). Effect of salt concentration in the (ENR-50)-lithium bis(trifluoromethanesulfonyl)imide (LiTFSI) or ENR-50-LiTFSI electrolyte film on various properties was investigated and found that the conductivity of ENR-50-LiTFSI electrolyte film increased with the increase in LiTFSI concentrations (Zainal *et al.*, 2013). The increase in ionic conductivity is typically correlated to concentration of charge carriers and/or the migration rate of charge carriers. Influence of ENR with 50 mole % epoxide (i.e., ENR-50) mixed with carboxyl ionic liquids (i.e., 1-carboxymethyl-3-methylimidazoliumbis (trifluoromethylsulfonate) imine ((([(HOOC)C_1C_1Im][NTf$_2$])) on various properties was also studied (Lin *et al.*, 2015). It was found that increasing ([(HOOC)C_1C_1Im][NTf$_2$]) contents caused increasing amount of the side groups in the grafted ENR 50 but reducing the chain steadiness, causing hindering of ionic crosslinking reaction. Also, addition of lithium bis(trifluoromethanesulfonyl)imide (LiTFSI) electrolyte into the ENR 50/[(HOOC)C1C1Im][NTf2] hybrid system caused increasing electrical conductivity (Lin *et al.*, 2015).

2.2.5.3 Coordination crosslinking of natural rubber

Metal ions also cause coordination crosslinking of natural rubber contains polar groups like epoxirane rings in ENR. The ring opening reaction of epoxirane rings in ENR-50 molecules was conducted in the presence of $SnCl_2.2H_2O$ catalyst. The FTIR spectra revealed the presence of hydroxyl originating from diol and ketone and the estimated level of ring opening reaction based on ^{1}H NMR analysis was 7.5% (Hamzaha *et al.*, 2013). This caused formation of ENR/Sn hybrid complex via insertion of $SnCl_2$ in to the quaternary and methine carbon of ring opened epoxidized isoprene under CO_2 atmosphere (Hamzaha *et al.*, 2013). The ^{1}H NMR spectra demonstrated the extent of coordination reaction was up to 22.5% based on the new peaks assigned to methine, methylene and methyl carbon in the ENR/Sn complex. In addition, the formation of four-coordinated tin (Sn) complex was successfully characterized by NMR spectroscopy. Furthermore, TEM images display morphology of ring-coil shape with thick lining due to arrangements of ENR/Sn complex into layers via intermolecular hydrogen bonding (Figure 2.13). The proposed intermolecular hydrogen bonding between the oxygen atom of ENR/Sn complex and the methylene proton of isoprene is illustrated in Figure 2.14. It is seen that without the formation of ENR/Sn complex, the polymer chains are randomly distributed and form entangles amongst the chains due to the amorphous nature of ENR-50.
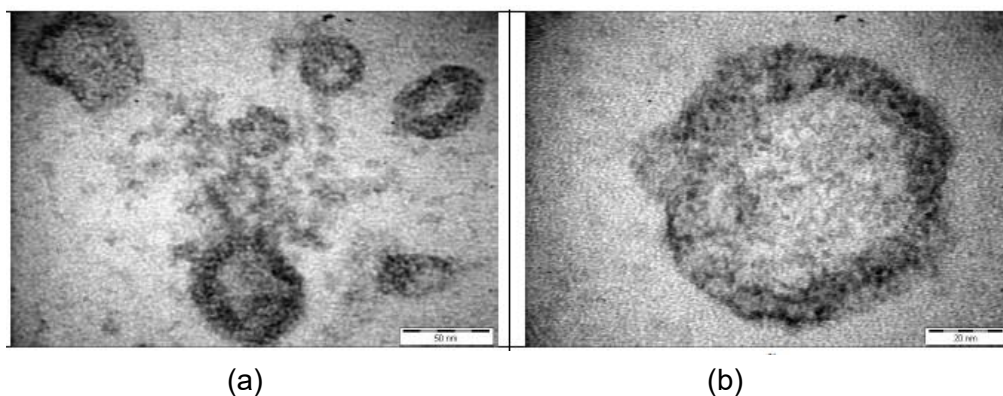
Figure 2.13 TEM micrographs of ENR/Sn complex hybrid at 5 hrs under CO_2 atmosphere (a) and enlargement of micrograph (b) (Hamzaha *et al.*, 2013).
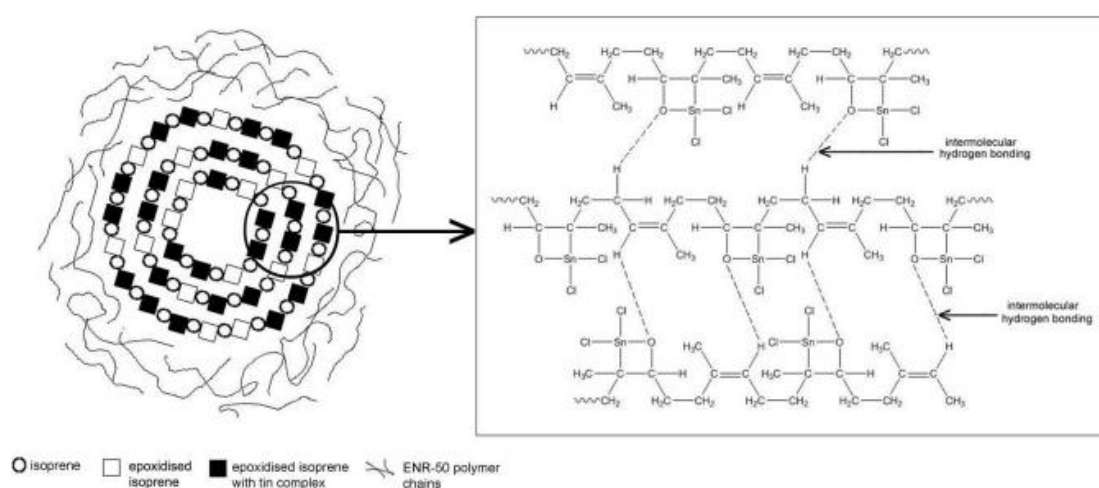
Figure 2.14 A proposed interaction of ENR-50/Sn complex (Hamzaha *et al.*, 2013).

Recently, the self-healable ENR has been prepared by reacting with $FeCl_3$ and diamine crosslinking agents via four reaction steps, as shown in Figure 2.15. It was found that some physical properties of the $FeCl_3$ crosslinked samples are comparable with the conventional sulfur crosslinked samples (Mandal *et al.,* 2021). Moreover, the availability of a nitrogen coordination site of the diamine along with the reactivity of the oxirane group of epoxidized natural rubber toward metal ions enables the re-establishment of cross-linking sites in a damaged polymer network. A slow release of

the metal ions from the metal amine complex to the ultra-active oxirane groups assists this reformation of the network, as shown in Figure 2.16 (Mandal *et al.,* 2021).
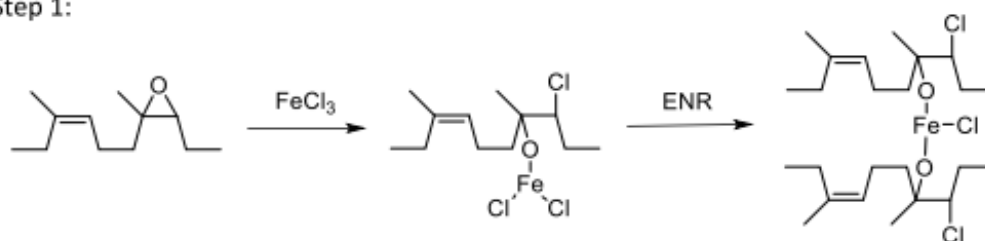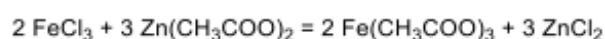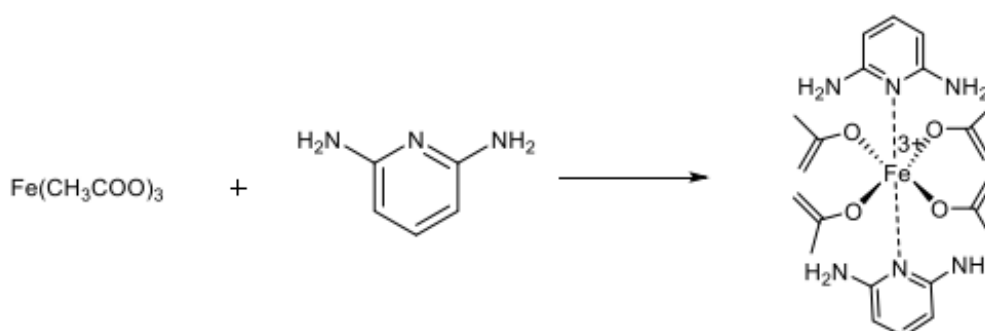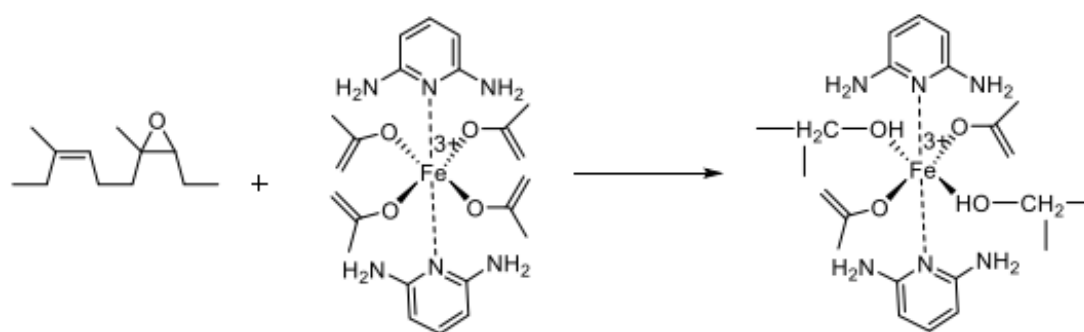
Figure 2.15 Reaction steps of ENR with $FeCl_3$ and diamine crosslinking agents; step 1. chemical interaction between ferric chloride and epoxidized natural rubber; step 2. ferric chloride and zinc acetate reacts to form ferric acetate and zinc chloride; step 3. complexation reaction between ferric acetate and DAP; and step 4. cross-linking of ENR by ferric ion from the ferric acetate–DAP complex (Mandal *et al.,* 2021).
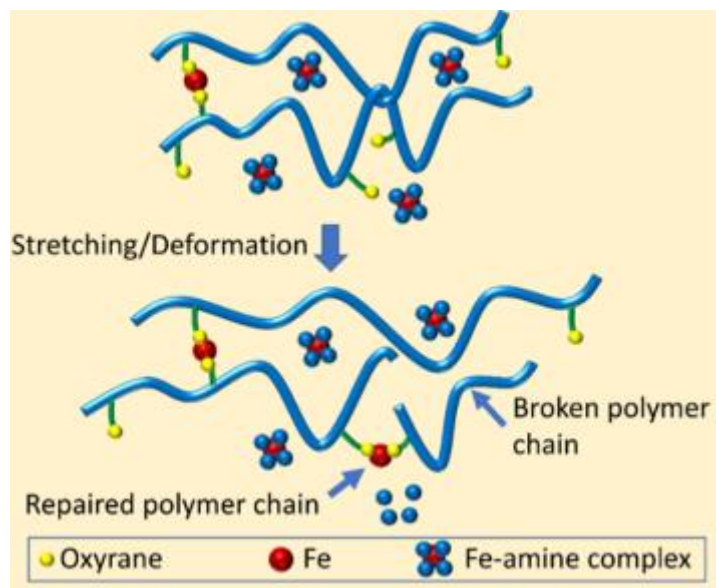
Figure 2.16 Controlled release mechanism of metal ion in self-healable epoxidized natural rubber (Mandal *et al.,* 2021).

2.3   Natural rubber composites

Natural rubber (NR) has been often used as a matrix of rubber composites with the main purpose to prepare smart materials with dramatic improvements in rubber performance. NR matrix composites (NMCs) have been prepared by incorporating different types of reinforcements. One of which is the ceramic fillers, i.e., barium titanate (BaTiO$_3$) and lead titanate (PbTiO$_3$) to form NR and ENR composites and found that ENR/BaTiO$_3$ exhibited higher mechanical strength than the NR/PbTiO$_3$ composites (Salaeh *et al.,* 2011). This is attributed to the polarity of ENR that caused formation of the linkage bridges between the polar functional groups of ENR molecules and polar groups at the filler surfaces. In addition, unmodified-clay, sodium montmorillonite (Na-MMT) and modified-clay or organoclay filled NR composites were studied by melt mixing technique (Sookyung *et al.,* 2014). It was found that higher mechanical strength was achieved in the composites with modified organoclay due to higher degree of clay dispersion, causing higher reinforcing efficiency of organoclay in NR matrix (Sookyung *et al.,* 2014). Furthermore, two different preparation methods: melt mixing and solution mixing methods were used to prepare NR composites with organoclay in the presence

of silane coupling agent (i.e., bis(trietoxysilyl propyl)tetrasulfide (TESPT) (Figure 2.17) (Manchado *et al.,* 2004). It was found that the solution mixing method offered better organoclay dispersion than the melt mixing process. Also, better compatibility between rubber molecules and clay surfaces was observed in the composites prepared by the solution mixing method. Furthermore, properties of NR/organoclay composites, in terms of tensile strength, modulus and hardness, were drastically improved after addition of TESPT in particular the adhesion performance between the interface of silicate layer of clay and rubber molecules (Manchado *et al.,* 2004).
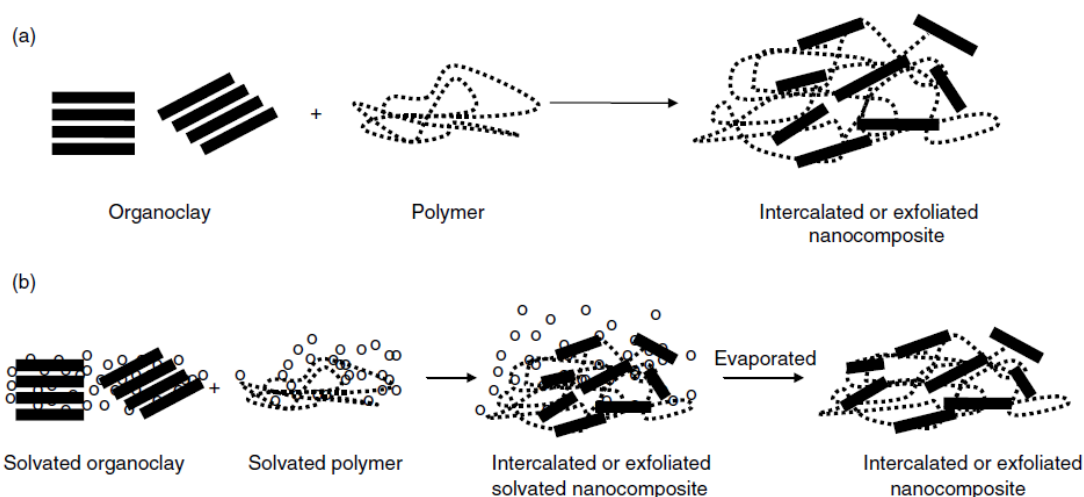
Figure 2.17 Schematic representation of dispersion in the elastomer matrix via the (a) mechanical (melt blending) and (b) solution mixing methods (Manchado *et al.,* 2004).

2.3.1 NR filled carbon black composites

Carbon-based fillers including carbon black, conductive carbon black, graphite, graphene and carbon nanotubes have been widely used as a conductive component to increase mechanical and electrical property of polymer composites. Generally, three types of carbon black have been exploited in industry including furnace black, channel black and thermal black. The chemical and physical properties of carbon black mainly depend on the manufacturing process. Conductive carbon black (CCB) contains high surface area, high structure and also high degree of porosity which are significantly improved mechanical property and electrical conductivity of rubber

composites at very low filler loading. That is, CCB filled NR and ENR composites had higher mechanical, dynamic, electrical properties and very low percolation threshold than NR and ENR without CCB (Matchawet *et al.*, 2015), as shown in Figure 2.18.
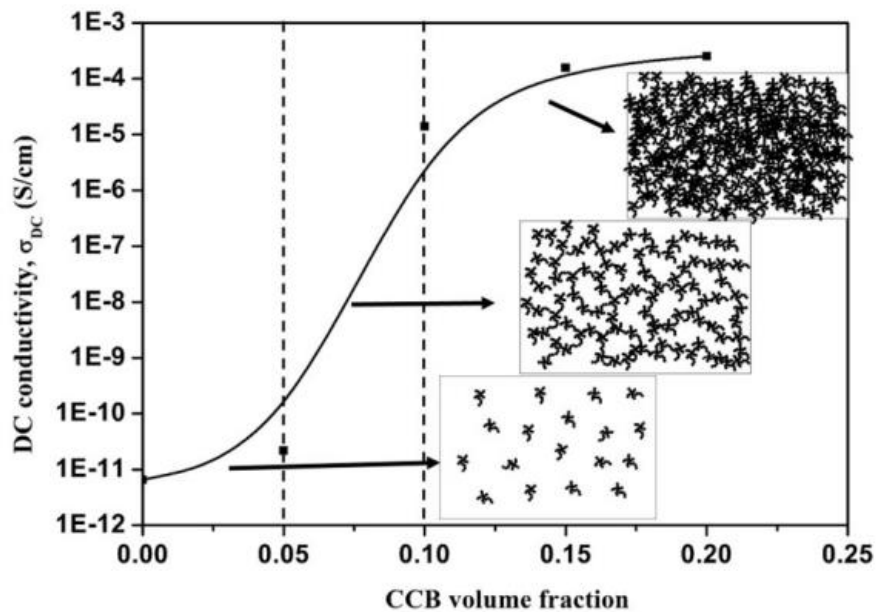
Figure 2.18 DC conductivity of ENR-50/CCB composite versus volume fraction of CCB. (Matchawet *et al.*, 2015).

The carbon black (CB) filled unmodified natural rubber (NR) and modified natural rubber (ENR-25, ENR-50 and MNR) using two types of CB: high abrasive furnace (HAF) and extra conductive furnace (ECF) were reported (Salaeh and Nakason, 2012). It was found that the ECF composites indicated higher Young's moduli but lower tensile strengths and elongations at break than the HAF composites (Figure 2.19). This is due to higher surface area and structure of ECF lead to more interfacial interaction, locking in place the ECF carbon black particles in the rubber matrix more rigidly than HAF particles.
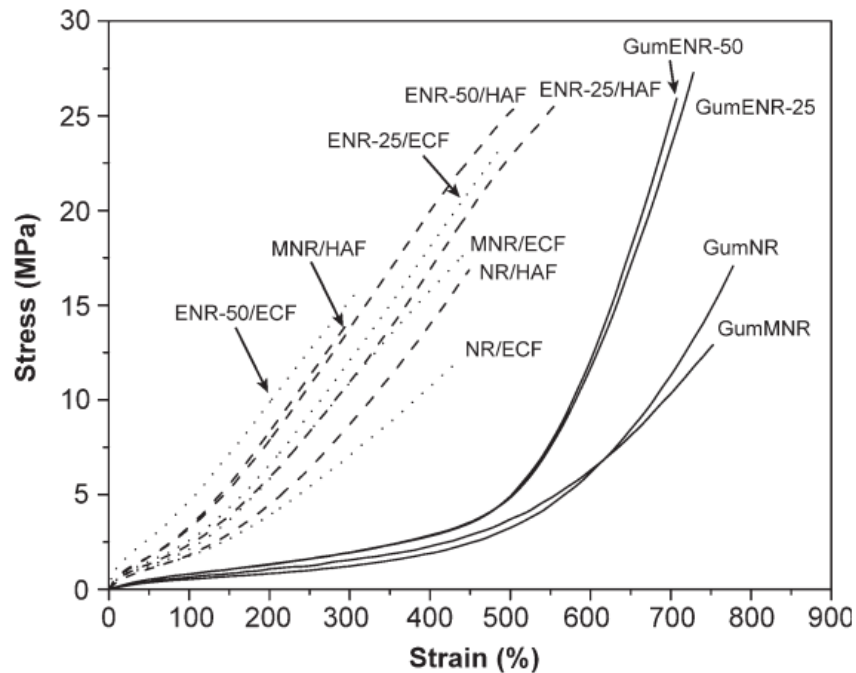
Figure 2.19 Stress–strain curves of gums and rubber/carbon black composites with different types of NR and carbon black (Salaeh and Nakason, 2012).

The hybrid filler combination of silica and carbon black was used to prepare natural rubber composites with various silica/CB ratios and at the same amount of hybrid filler of 50 phr. It was found that the vulcanizates containing 20 and 30 phr of silica in the hybrid filler provided better overall mechanical properties in terms of tensile strength and tear strength (Figure 2.20). This is due to good filler dispersion as a result of the lowest development of the CB and silica network in NR vulcanizates.
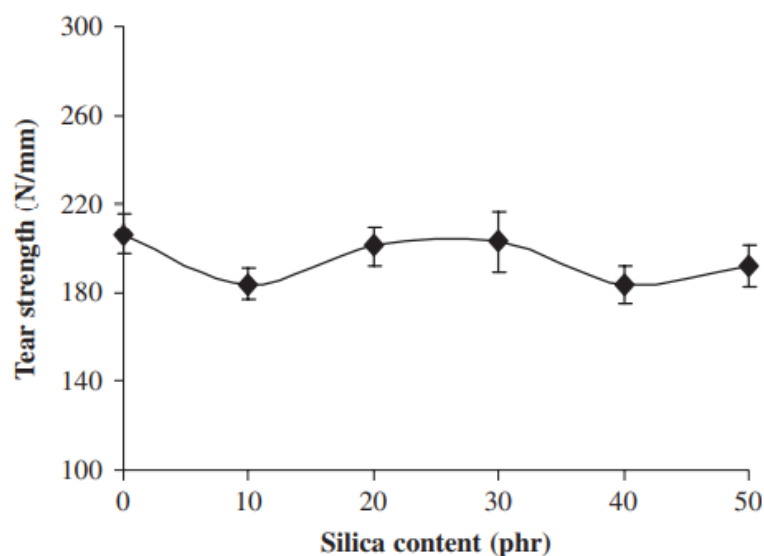
Figure 2.20 Tear strength of hybrid filler (silica/CB) filled NR vulcanizates with various silica/CB ratios (Rattanasom *et al*., 2007).

In addition, natural rubber without and with carbon black/nano-clay hybrid filler composites were prepared by mixing on two-roll mill (Qing-xiu *et al*., 2005). It was found that the NR filled with hybrid filler indicated the higher moduli at 100% and 300% elongation, tensile strength and tear strength than nano-clay nanocomposites without combination of CB. Moreover, CB/CNTs hybrid filler has also been reported as the details in the following section (2.3.3).

2.3.2 Carbon nanotubes (CNTs)

Carbon nanotubes (CNTs) is a member of the fullerene structural family that is considered as nano-fillers. It composes of a nanometer-sized (< 200 nm) in diameter and micrometer-sized in length. The carbon atoms in CNTs mostly arrange in sp^2-hybridization of hexagonal structures similar to graphite. The structure of CNTs consists of enrolled cylindrical graphitic or graphene sheet rolled up into a seamless cylinder with diameter in the order of nanometer (Figure 2.21).

(a)   (b)
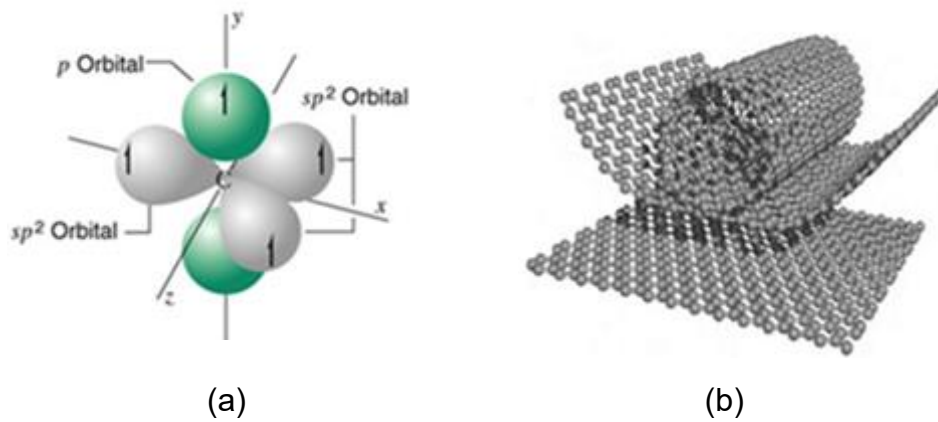
Figure 2.21 Sp^2 hybridization in carbon nanotubes (a). Single-wall carbon nanotube (SWCNTs) from a graphene sheet (b) (Tingaev *et al.,* 2017).

Carbon nanotube fundamentally fall into two classes: single-walled carbon nanotubes (SWCNTs) and multi-walled carbon nanotubes (MWCNTs) (Figure 2.22). Despite the obvious commonality, SWCNTs and MWCNTs have significantly different physical properties from each other because of their structural differences. The most important feature that distinguishes SWCNTs is that the wall of the nanotube consists of the only one graphene layer. In other words, single-walled carbon nanotubes can be described as graphene sheets seamlessly rolled up to form hollow cylinders. That is why they often referred to as graphene nanotubes (GNTs). Unlike a single-walled nanotube, a multi-walled carbon nanotube can be viewed as a concentric arrangement of SWCNTs. That is, they consist of multiple layers of graphene rolled up seamlessly into a tube shape, as shown in Figure 2.22
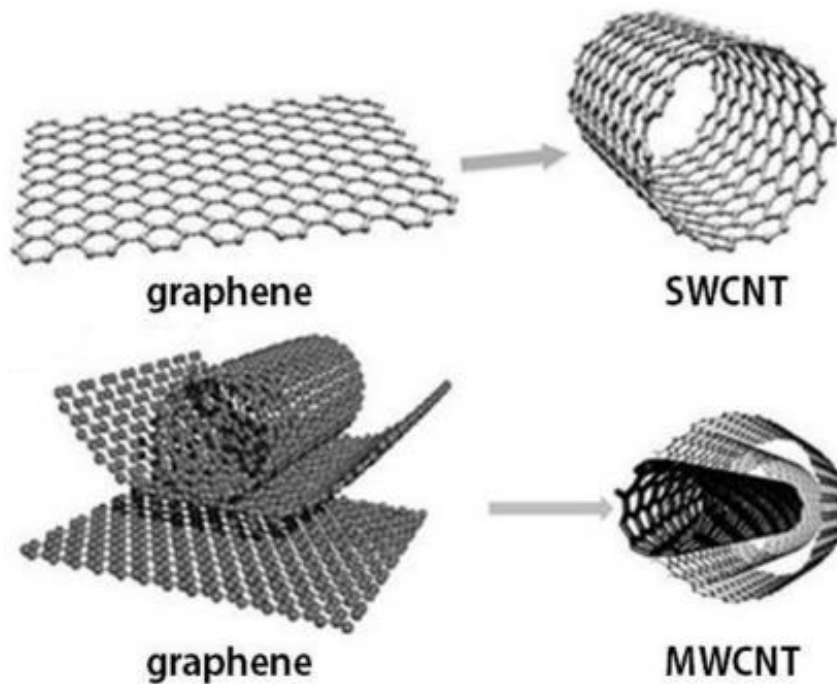
Figure 2.22 differences between single-walled and multi-walled carbon nanotubes (Vidu *et al.,* 2014).

Generally, several CNT properties depend on how the carbon atoms are arranged in the molecular structures (Ajayan, 1994). The CNTs are classified as the effectively one-dimensional (1D) carbon materials with high aspect ratio (L/D) that can exceed 1000. They could be envisioned as cylinders composed of rolled-up graphene planes with diameter in nanometer scale (Dresselhaus *et al*., 1995; and Ma *et al*., 2010). Also, the cylindrical nanotube usually has at least one end capped with a hemisphere of fullerene structure (Figure 2.23)
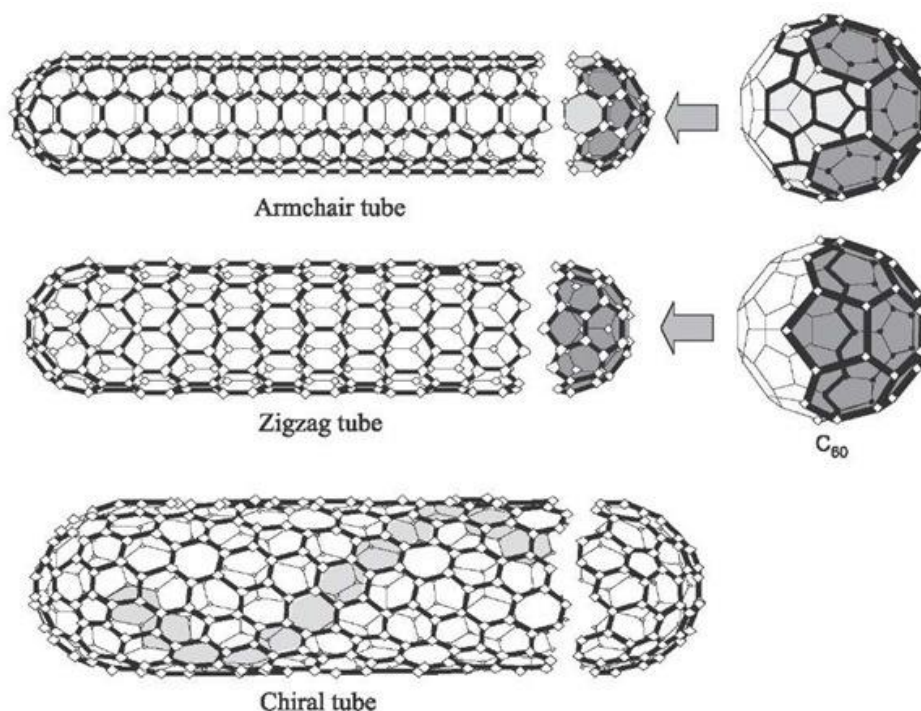
Figure 2.23 Three typical structural models for SWNTs, where the nanotubes are related to rolling a graphene sheet into a cylinder. Fullerene caps for the armchair and zigzag tubes are also indicated (Thostenson *et al*., 2001).

The graphene sheets of CNTs have typically different rolling angles of three chirality including armchair, zigzag and chiral. The tube chirality is defined by the chiral vector, Ch = na_1 + ma_2 (Figure 2.24), where the integers (n, and m) are the number of steps along the unit vectors (a_1 and a_2) of the hexagonal lattice (Dresselhaus *et al*., 1995). Using this naming scheme (n, and m), three types for orientation of the carbon atoms around the nanotube circumference are specified. If n = m, the nanotubes are called as ''armchair''. If m = 0, the nanotubes are called as ''zigzag''. Otherwise, they are called as ''chiral'' (Figure 2.24). The chirality of nanotubes has a significant impact on their transport properties, and particularly on the electronic properties. For a given (n, and m) nanotube, if (2n + m) is a multiple of 3, then the nanotube is metallic, otherwise the nanotube is a semi-conductor. Each MWCNT has several layers of graphene, and each layer could have different chirality, so the prediction of its physical properties is more complicated than the SWCNTs (Odom *et al*., 1998; and Ma *et al*., 2010).
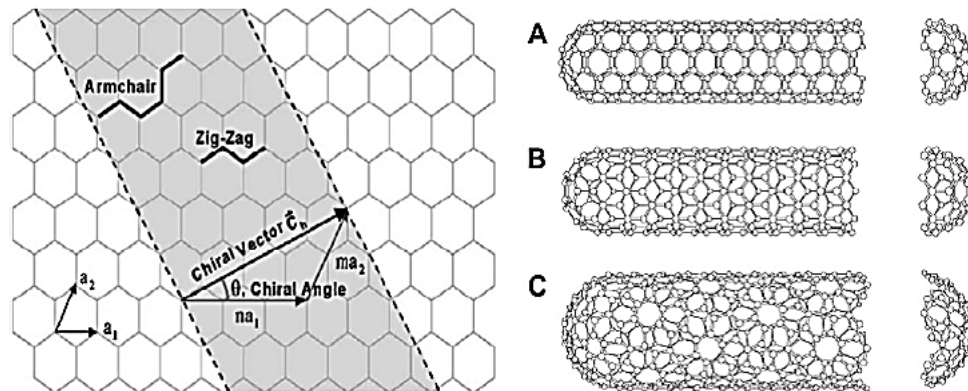
Figure 2.24 Schematic diagram showing how a hexagonal sheet of graphene is rolled to form a CNTs with different chiralities (A: armchair; B: zigzag; C: chiral) (Dresselhaus *et al*., 1995).

Figure 2.25 shows different forms of carbon allotropes, i.e., diamond, graphite, lonsdaleite, C60-fullerene, graphene, amorphous carbon, C540-fullerite, and single-walled carbon nanotube. Table 2.4 compares properties of four different forms of carbon materials including CNTs, graphite, diamond and fullerene (C_{60}). It is seen that the CNTs (i.e., SWCNT and MWCNT) exhibit unique electrical, and thermal properties. This is why the CNTs composites have been widely applied in some special applications, such as space explorations, aviation, automobile and sport application where high performance and lightweight structural materials are required (Dresselhaus *et al*., 1995).
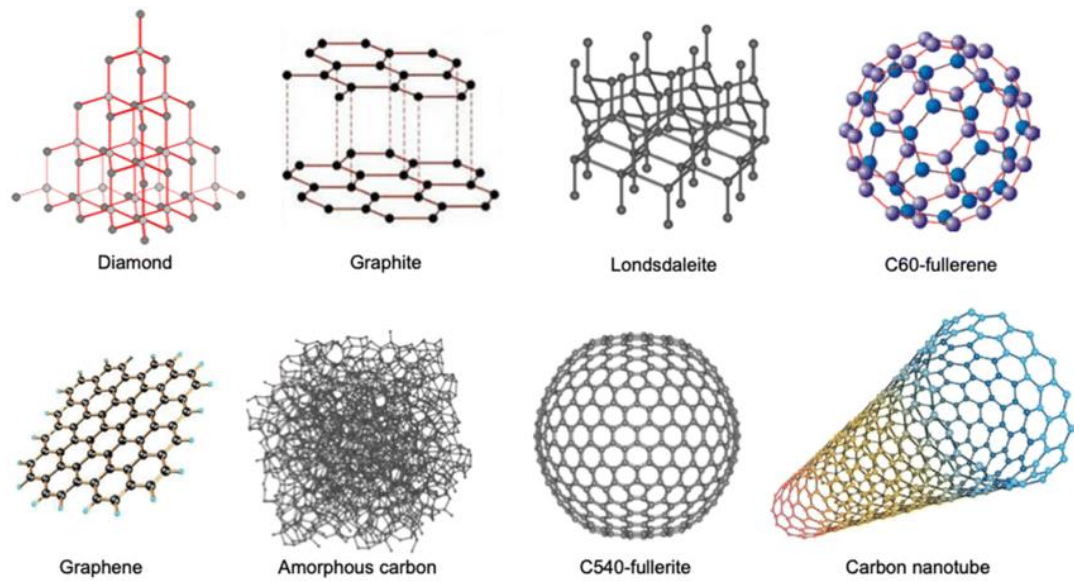
Figure 2.25 Carbon allotropes: diamond, graphite, lonsdaleite, C60-fullerene, graphene, amorphous carbon, C540-fullerite, and single-walled carbon nanotube (Negri *et al.,* 2020)

Table 2.4 Properties of carbon nanotubes along with other three types of carbon materials (Ma *et al*., 2010).

Properties	Materials				
	Graphite	Diamond	Fullerene	SWCNT	MWCNT
Specific gravity (g/cm^3)	1.9-2.3	3.5	1.7	0.8	1.8
Electrical conductivity (S/cm)	4000p, 3.3c	10^{-2}-10^{-15}	10^{-5}	10^2-10^6	10^3-10^5
Electron mobility(cm^2/(V.s))	2.0x10^4	1800	0.5-6	~10^5	10^4-10^5
Thermal conductivity (W/m.K)	298p, 2.2c	900-2320	0.4	6000	2000
Co-efficient of thermal expansion (K^{-1})	-1x10^{-6p}, 2.9x10^{-5c}	(1~3)x10^{-6}	6.2x10^{-5}	Negligible	Negligible
Thermal stability ($^\circ$C)	450-650	<600	<600	<600	<600

p = in-plane and c = c-axis

CNTs usually have extremely high tensile strength as compared to other carbon material counterparts. It exhibits 40% elongation without any forms of plastic deformation, brittle-like behavior, or rupture. This is attributed to the extra energy absorption required for the hollow structures of CNTs compared to other carbon materials. The tensile strength of CNTs has been reported to be on the order of a hundred giga-pascal (GPa), which is approximately a thousand time harder than steel (Demczyk *et al*., 2006). This excellent strength makes CNTs suitable for high reinforcing efficiency in the composite materials. It was also reported that addition of 5% of SWCNT caused increasing tensile strength and Young's modulus of the composites up to 90% and 150%, respectively, as compared to the composite without CNTs (Demczyk *et al*., 2006). In addition, excellent elastic property allows the CNTs store huge quantity of energy (Andrews *et al.,* 1999). It was found that incorporation of 0.5 phr MWCNT in NR composite caused increasing 61% of tensile strength, 75% of modulus and 59% of tear strength (Andrews *et al*., 1999). However, these properties increased with increasing CNT contents upto only 0.5 phr, but they were declined upon further addition of CNTs loading (George *et al.,* 2015).

CNTs have the chirality with $n = m$ tubes with no band gap energy (E_g) and it is metallic in nature. Also, CNTs are semi-conducting when $n \neq m$ with some band gaps (Figure 2.26). The subset with $n-m = 3q$, where q is an integer shows a small band gap induced by curvature of the graphene sheet, so-called semi-metallic, quasi-metallic, or small-gap semi conducting material. The band gaps of both semi-conducting and small-gap semi-conducting single-walled CNTs decrease with $1/r_t$ and $1/r^2_t$, respectively, as shown in Figure 2.27. The small band gap semi-conducting CNTs was formed due to the curvature effects are usually considered as metallic at room temperature, when ΔE_g is the minimum energy difference in the direction (Saito *et al.,* 1998).
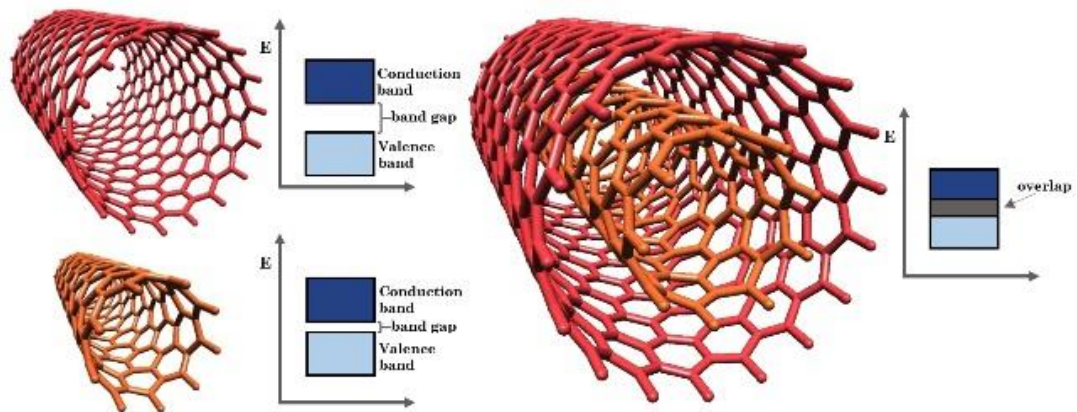
Figure 2.26 Tuning electronic properties: individual single carbon nanotubes (left) have band gaps (energy levels) and are semiconductors, but when combined (right), the band gaps overlap and make the double-walled structure a semimetal (Qian et al., 2020).
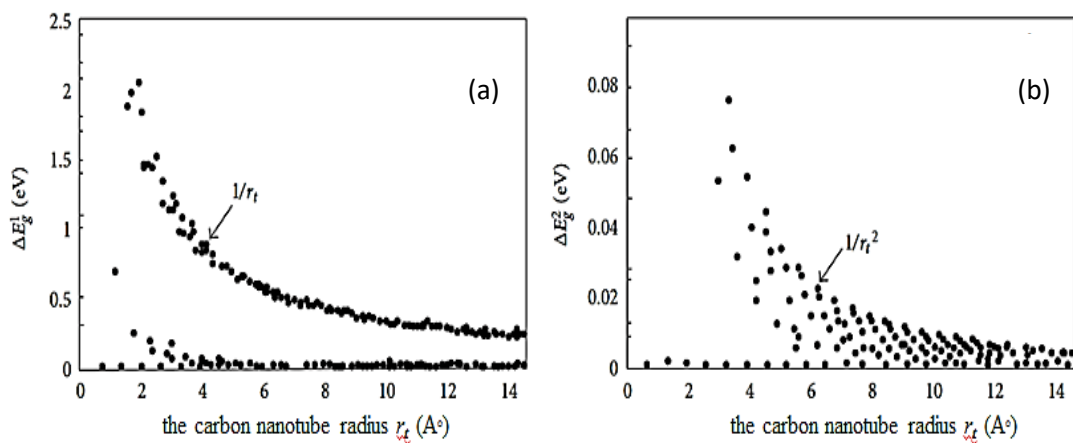
Figure 2.27 The energy band gap of the primary gap ΔE_g^1 (semi-conducting single-walled CNT) scales as $1/r$ (a), while for the curvature-induced band gap ΔE_g^2 (small-gap semi-conducting CNT) scales as $1/r^2$. At $\Delta E_g^1 = \Delta E_g^2 = 0$ relates to armchair nanotubes, which maintain their metallic character (b) (Saito *et al.,* 1998).

The electronic structure of multi-walled CNT is more complicated due to various coaxial arrangement of the single-walled CNTs. Electron transport in multi-walled CNTs is similar to that of the larger diameter single-walled CNTs. This is due to most of the electric current passing through a multi-walled CNTs from outside is mostly confined to the outermost cylindrical layer (Frank *et al.,* 1998; and Bachtold *et al.,* 1999).

Therefore, the excellent electronic properties of carbon nanotubes make them success in application in the electronic devices and sensor applications.

2.3.3   Hybrid composites of CNTs

To obtain rubber matrix composites with good mechanical and thermal properties, dispersion of filler in the rubber matrix must be carefully managed. As mentioned in section 3.2, CNTs have very high aspect ratio and strong Van-der Waals forces. They therefore cause strong agglomeration in rubber matrix and hence lead to inferior properties of rubber matrix composites. Incorporation of the second fillers into the rubber-CNTs composite system to form a hybrid filler may improve the CNTs dispersion and distribution in the rubber matrix, leading to enhancement of the mechanical properties, thermal stability, electrical conductivity and other related properties. Various studies were carried out to develop elastomer matrix composites using CNTs and ionic liquid (IL) with optimal electrical, mechanical, and thermal properties. This type of rubber matrix composites has been focused on applications like sensors and actuators (Subramaniam *et al.,* 2011). Moreover, the MWCNTs were modifiedby using the IL, namely 1-butyl-3-methyl-imidazolium-bis (trifluoromethylsulfonyl) imide (BMI), in different weight ratios of CNTs to BMI (i.e., 1:1, 1:5, 1:10, and 1:20). The CNTs and BMI was firstly mixed in a mortar and pestle at room temperature till a black mix was obtained (Subramaniam *et al.,* 2011). Then, the modified carbon tubes were incorporated into polychloroprene rubber along with other curatives on a two-roll mill at mixing temperature of 40 °C, as the preparation process shown in Figure 2.28 (Subramaniam *et al.,* 2013).

This technique is rather simpler than the conventional mixing techniques due to (a) reduced air pollution since CNT powders were incorporated into the matrix in a paste form, (b) short mixing cycles, and (c) no use of solvents (Subramaniam *et al.,* 2013).
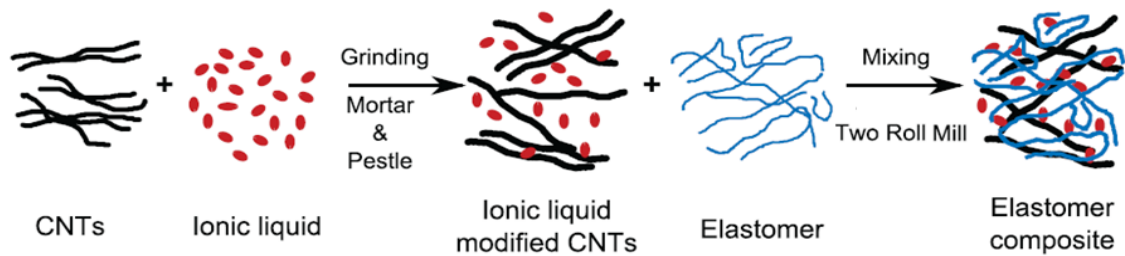
Figure 2.28 Preparation process of elastomer/CNT/IL composite (Subramaniam *et al.,* 2013).

Recently, natural rubber matrix composites with CNTs and IL hybrid filler, namely 1-butyl-3-methyl imidazolium bis (trifluoromethylsulphonyl)mide (BMI) was prepared and found that the NR/CNT-IL composite had higher electrical conductivity and lower percolation threshold concentration than the NR/CNT composite without IL (Krainoi *et al.,* 2019). Furthermore, AgNP particles were decorated on CNT surfaces by latex mixing method (Krainoi *et al.,* 2018). The enhancement of electrical conductivity of the hybrid composites was found due to reducing contact resistance of CNT junctions in a polymer matrix along with a simple approach to decorate carbon nanotube surfaces with silver nanoparticles (AgNPs), leading to enhancement of the electrical conductivity (Figure 2.29) (Krainoi *et al.,* 2018).
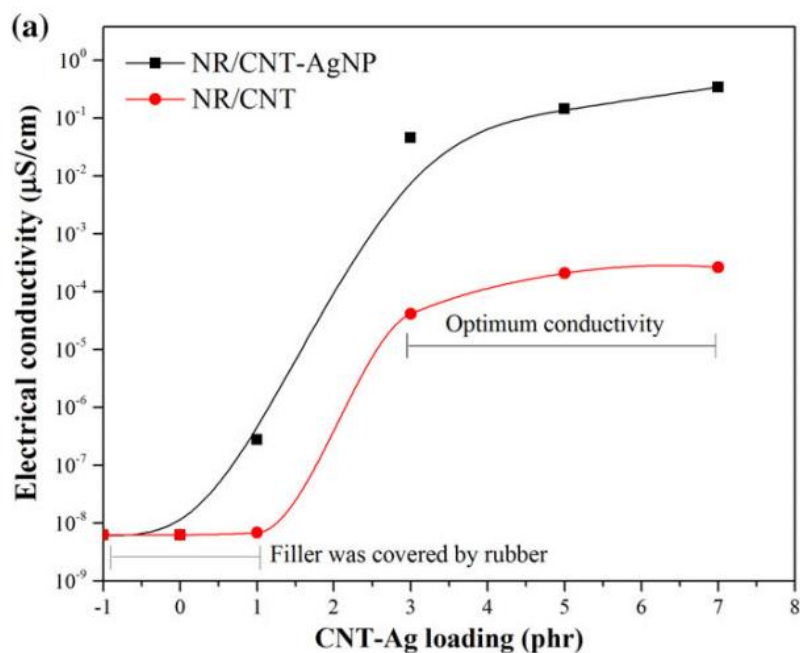
Figure 2.29 Electrical conductivity of CNT and CNT-AgNP filled NR vulcanizates with various CNT and CNT-AgNP loadings (Krainoi *et al.,* 2018).

Decoration of CNT bundle surfaces with ZnO nanoparticles was also performed and mixed with in natural rubber (Thongkong *et al*., 2020). It was found that hybrid filler with 3 phr CNT and 3 phr ZnO filled NR caused improvement of initial stress, bound rubber content, storage modulus and electrical properties (Thongkong *et al*., 2020). This is attributed to good dispersion and distribution of CNT and ZnO fillers in the NR matrix with strong CNT/ZnO network formation and stronger filler-rubber interactions (Figure 2.30).
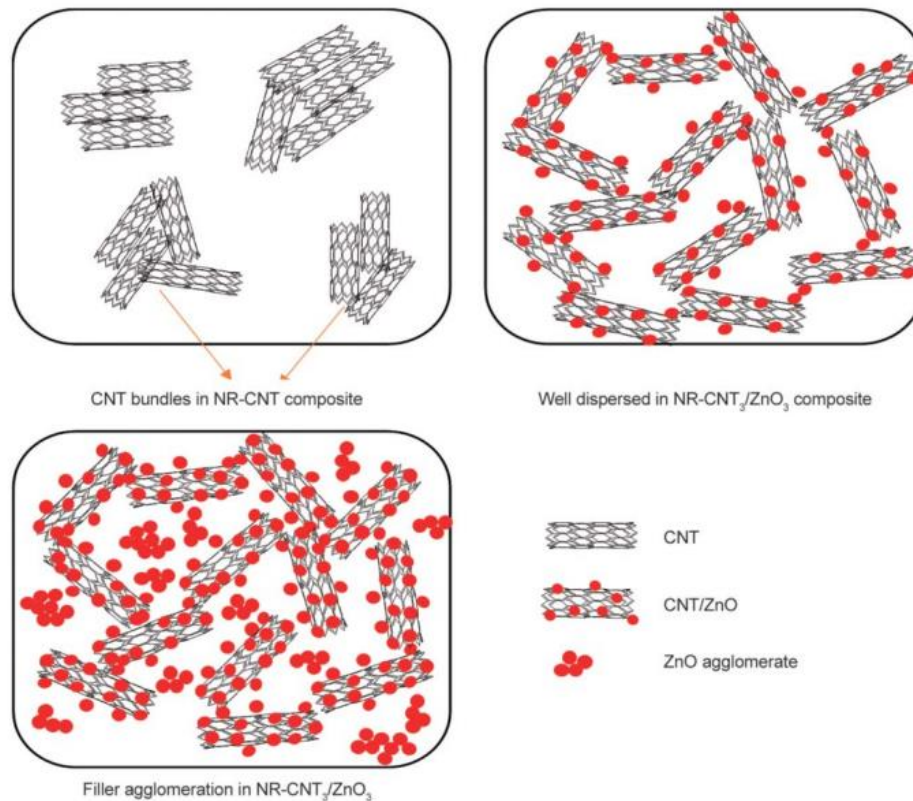
Figure 2.30 A proposed model for dispersion of CNT and CNT/ZnO hybrid filler in NR matrix (Thongkong *et al.*, 2020).

CNTs and conductive carbon black (CCB) are conducting fillers with distinct geometric shapes, aspect ratios and dispersion characteristics. This offers a unique synergy that gives rise to enhancement of mechanical properties, electrical conductivity and other related properties of the rubber matrix nanocomposites with CNTs and carbon black hybrid filler. Incorporation of small amount of CNTs into CB/polymer composite can significantly enhance the composites properties. This may be possible to design and to prepare low-cost polymer composites with novel, desirable morphology and useful properties by using combination of CB and CNTs. These mixed conductive fillers are possible to partly replace expensive fillers (Szeluga *et al.*, 2015). The potential application of the CB-CNT hybrid filler was reported in epoxy nanocomposite with the CB/CNTs ratio at 1:1 (Sumfleth *et al.* 2009). It was found that the enhancement of electrical behavior of the hybrid nanocomposite

system (i.e., ternary system of epoxy/CB-CNTs) was observed as compared with the conventional single filler CNT filled epoxy (binary) system. This might be due to the synergistic effect of the network formation and the charge transport in the epoxy composite with CB-CNTs hybrid filler (Figure 2.31)
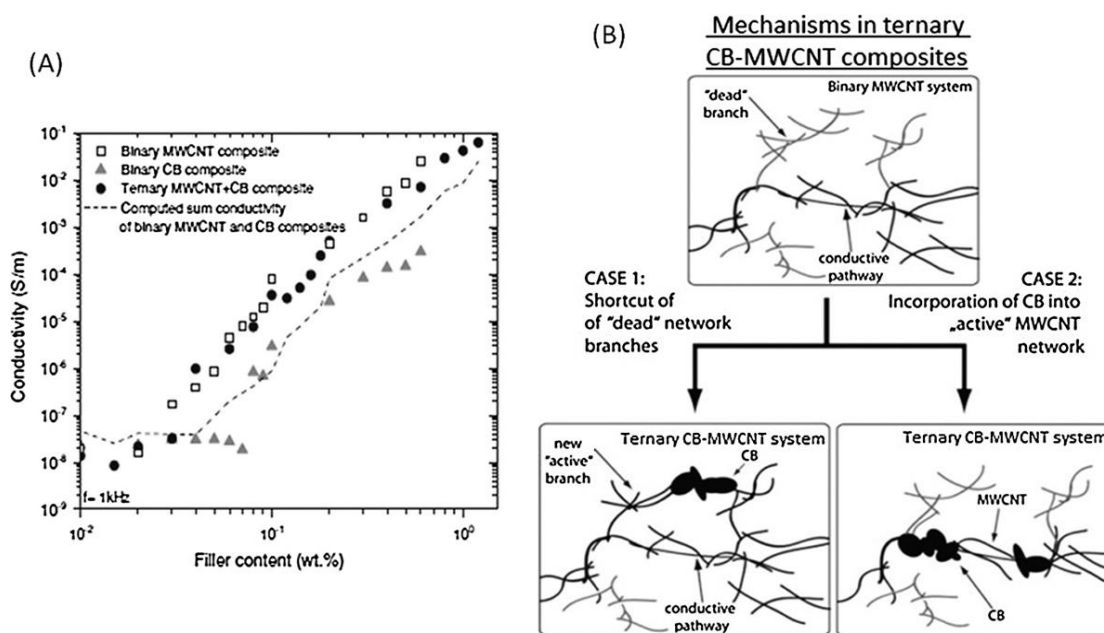
Figure 2.31 Electrical conductivity for the binary (CB and CNT/epoxy) and ternary CB–CNT/epoxy) nanocomposites exhibiting percolation behavior (A): and principles of conductive pathway formation in ternary CB–CNT/epoxy systems (B) (Sumfleth *et al.*, 2009).

Figure 2.31 (A) shows electrical conductivity as a function of filler contents of the binary and ternary epoxy nanocomposites. It was found that the electrical percolation thresholds of approximately 0.025 wt% was observed in the ternary CB–CNT/epoxy but about 0.03 wt% was observed in the binary CNT/epoxy composite (Sumfleth *et al.*, 2009). Conversely, the binary CB/epoxy nanocomposite exhibited three times higher percolation threshold concentration of approximately 0.085 wt%. To understand the synergistic effects in ternary composites or the utilization of CB-CNT hybrid filler in the epoxy matrix, two theoretical situations were described in Figure 2.31 (B) shortcut of dead network branches (case I) and incorporation of CB into active CNT networks (case II). Incorporation of CB caused connecting of the dead ends of the

CNTs network (case I) and hence facilitate the electron or charge transfer in the nanocomposites. Therefore, addition of CB aggregates leads to the formation of new conductive pathways between ''dead'' CNT branches. This caused increase in conductivity of hybrid CB–CNT composites which resulted in reduction of the tunneling distances when CB particles are located between "dead'' CNT networks (Sumfleth *et al*. 2009). Therefore, the tunneling distance between CNTs determines the overall conductivity in CNT/polymer composites (Li *et al*. 2007). Thus, the electrical conductivity of the ternary CB-CNT system is higher than that of the binary CNT system. On the other hand, incorporation of CB into active CNT networks in case II (Figure 2.31 (B) the CB was incorporated into the conductive ''active'' CNT pathways that are the mainly contributed to the electron movement throughout the composites. Thus, incorporation of CB in this case was not significantly enhanced the connection among the CNT encapsulates. Therefore, the conductivity of the composites has no significant increase, since the most active electrons are moved only in the active CNT pathways within the composites (Ma *et al*., 2009; Sumfleth *et al*., 2009; and Szeluga *et al*., 2015).

Conductive carbon black (CCB) has been investigated by incorporating electrically conductive fillers into the insulating rubber composites. It was found that the MWCNTs and CCB filled ENR were compared and found that the ENR/S-MWCNTs composite had the lower percolation threshold concentration at 3 phr (Matchawet *et al*., 2015). In addition, the filler network formations in NR matrix (Figure 2.32) (Nakaramontri *et al.,* 2017). This could reduce the Van-der Waals attraction among CNT particles and hence lead to finer and better dispersion of CNTs in the NR matrix. This is confirmed that the secondary filler contributes to improve the CNTs dispersion in ENR matrix.
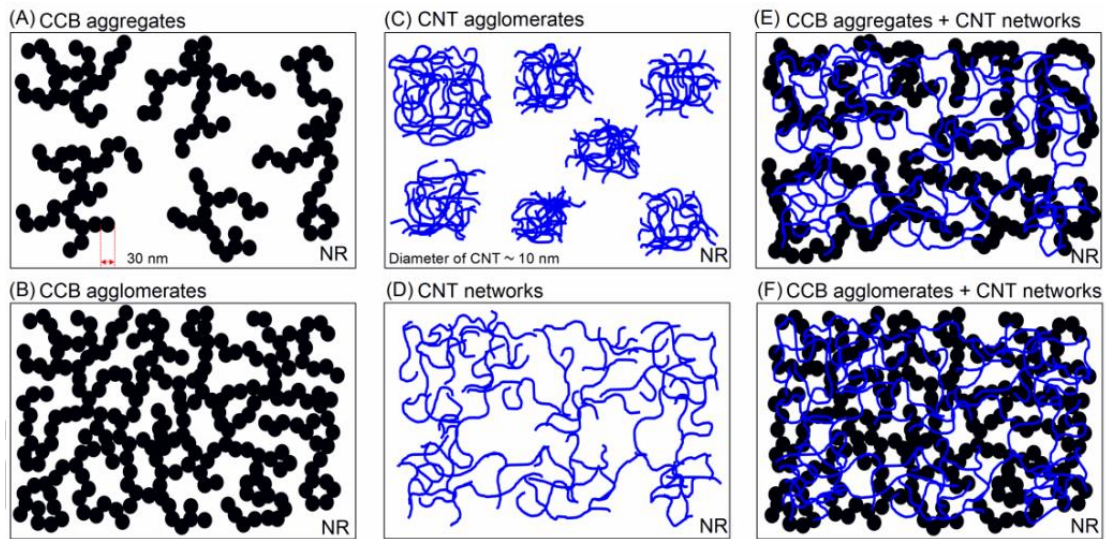
Figure 2.32 Proposed models of filler network formations in an NR matrix with various filler types: CCB (A and B), CNT (C and D), and CNT/CCB (E and F) (Nakaramontri *et al.,* 2017).

2.4   Percolation threshold

Fundamental theoretical basis describes the conductive behavior of conductive particles-polymer is percolation theory. At very low filler loading, the conductive particles scatter in the matrix as isolated particles or clusters, and the conductive particles-filled polymer is either insulated or barely conductive. After more particles are added into the matrix, the isolated clusters grow and would eventually "percolate" to form a connected network or conductive bridge in the matrix. This could transform the polymer from being insulated to conductive material. At the critical concentration of the filler that is the polymer experiences a drastic jump in conductivity. At this position, it is termed as *the percolation threshold concentration* or *critical volumetric (v_c),* as seen in Figure 2.33. This also corresponds to abruptly decreasing trend of the surface resistivity, as shown in Figure 2.34. At the filler concentration higher than percolation region, the connected network of conductive particles become denser, thus continuing to raise the polymer conductivity albeit at increasingly slower rate (Pham, 2008).
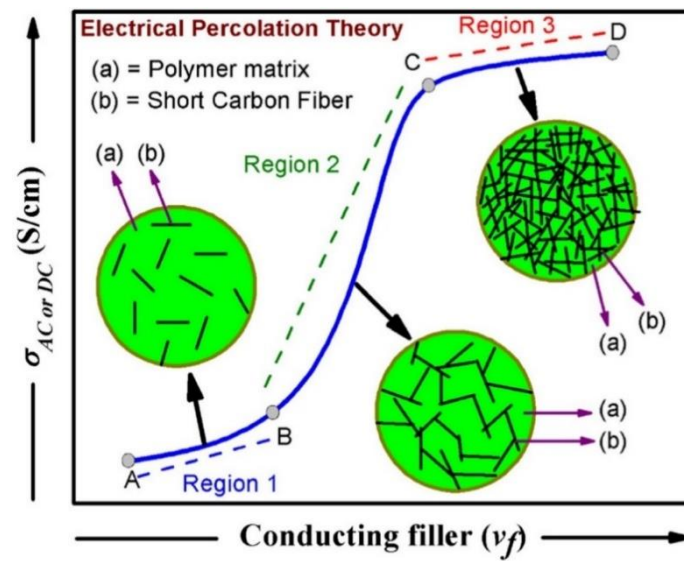
Figure 2.33 Schematic diagram representation of the percolation behavior in polymer/conducting filler (Ram, 2016).
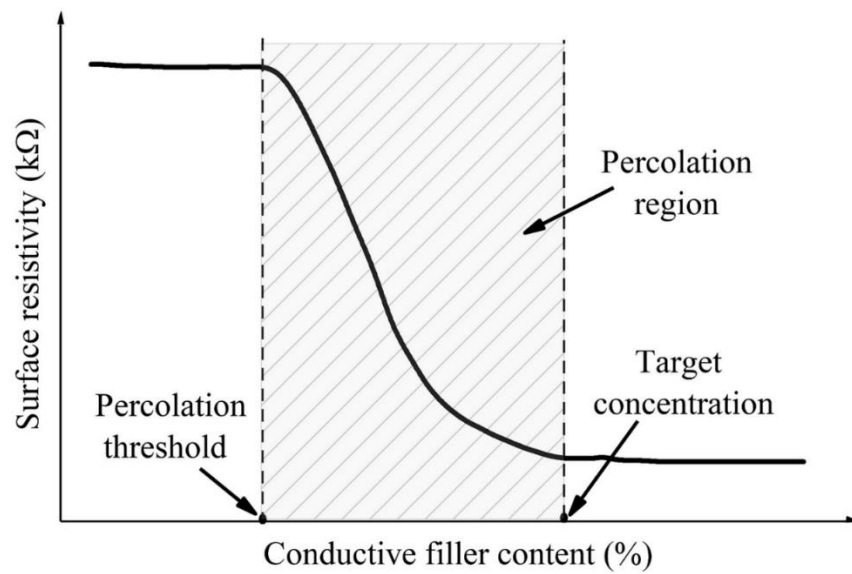
Figure 2.34 Schematic diagram of percolation theory of the conductive polymer (Cui *et al.,* 2019)

CHAPTER 3

MATERIALS AND EXRERIMENTAL METHODOLOGY

3.1 Materials

3.1.1 Ferric chloride (FeCl$_3$)

Ferric chloride (FeCl$_3$) with a molecular weight of 162.20 g/mol, melting temperature of 304 °C was used as a curing agent of epoxidized natural rubber (ENR) by coordination linkages. It was manufactured by Sigma-Aldrich Pte., Ltd., Darmstadt, Germany.

3.1.2 Natural rubber (NR)

Two types of natural rubber were used as a matrix in the rubber compounds:

3.1.2.1 Unmodified natural rubber (NR)

Unmodified natural rubber (NR), air dried sheet (ADS) with density of 0.93 g/cm^3 and Mooney viscosity [ML (1+4) 100 °C] of approximately 82, was used to prepare rubber vulcanizates with FeCl$_3$. It was manufactured by Von Bundit Co., Ltd., Surat Thani, Thailand.

3.1.2.2 Epoxidized natural rubber (ENR)

Epoxidized natural rubber (ENR) of epoxide content of 25 mol% (ENR-25) and 50 mol% (ENR-50) with a density of 0.93 g/cm^3 was used to prepare rubber vulnerates with metal ions (FeCl$_3$) and sulfur vulcanization systems. It was manufactured by Muangmai Guthrie Co., Ltd., Surat Thani, Thailand.

3.1.3 Zinc oxide (ZnO)

Zinc oxide (ZnO) with a density of 5.61 g/cm^3, molecular weight of 81.38 g/mol and melting temperature of 419 °C was used as a cure activator in sulfur vulcanization system of rubber. It was manufactured by Global Chemical Co., Ltd., Samut Prakarn, Thailand.

3.1.4   Steric acid

Steric acid ($C_{18}H_{36}O_2$) with a density of 0.85 g/cm^3 molecular weight of 332.47 g/mol, boiling and melting temperatures of 383.0°C and 69.6 °C, respectively. It was used as a co-activator of ZnO in the sulfur vulcanization system. It was manufactured by Imperial Industry Chemical, Pathum Thani, Thailand.

3.1.5   Mercaptobenzothiazole disulfide

2-Mercaptobenzothiazole disulfide or 2,2'-Dithiobis-(benzothaiazole) (MBTs) with a specific gravity of 1.50 g/cm^3, molecular weight of 332.47 g/mol and melting temperature of 177°C was used as a cure accelerator in sulfur vulcanization system. It was manufactured by Flexsys, Termoli, Italy.

3.1.6   Sulfur

Sulfur with a density of 2.07 g/cm^3 and a melting temperature of 115 °C was used as a curing agent. It was manufactured by Ajax Chemical Co., Ltd., Samut Prakan, Thailand.

3.1.7   Toluene

Toluene with a density of 0.87 g/cm^3 and a boiling temperature of 110.6 °C was used as a solvent for determination of crosslink density and bound rubber contents of rubber vulcanizate. It was manufactured by CSC jäklechemie GmbH & Co. KG. Nuremberg, Germany.

3.1.8 Carbon nanotubes

The multiwall carbon nanotubes (CNTs), NANOCYL^{TM} NC7000, with a density 1.35 g/cm^3, 9.5 nm diameter, 1.5 μm length, and 90% purity, were manufactured by Nanocyl S.A., Sambreville, Belgium.

3.1.9 Conductive carbon black

Conductive carbon black (CCB), Vulcan XC72R, with a density of 1.70 g/cm^3, and 30 nm diameter was used as a conductive filler in the rubber composites. It was manufactured by Cabot Corporation, Texas, USA.

3.2   Equipment

3.2.1   Internal mixer

Brabender Plasticorder (Figure 3.1), model 835205 with a mixing chamber capacity of 70 cm^3 was used to prepare the rubber compounds. The mixer is equipped with tangential rotors, and with a thermocouple for measuring and recording the mixing temperature. This machine is also equipped with a built-in torque sensor, which is used to determine mixing torque. It was manufactured by Brabender® GmbH & Co. KG, Duisburg, Germany.

Figure 3.1 Internal mixer, model 835205 (Brabender Plasticorder).

3.2.2   Open mill mixer

Two-rolls mill, model YFCR 6" with the diameter and length of the rolls of 14 and 16 inch with the fixed speed of the front and back rolls at 21.4 and 25.7 rpm, respectively. (Figure 3.2). It was manufactured by Yong Fong machinery Co., Ltd., Samut Sakorn, Thailand. It was used to improve dispersion of chemical ingredients in ENR compounds after dumping from the internal mixer. In addition, two-rolls mill was also used to sheet out the rubber composites prior to the compression molding process.

Figure 3.2 Two-rolls mill, model YFCR 6" (Yong Fong machinery Co., Ltd).

3.2.3 Moving die rheometer (MDR)

Moving die rheometer (MDR), MDR 2000, Alpha technologies (Ohio, USA) (Figure 3.3) was used to characterize cure characteristics of rubber compounds, according to ASTM D5289 with a fixed frequency of 1.67 Hz at 160°C and strain amplitude of 1° arc.

Figure 3.3 Moving die rheometer (MDR), MDR 2000 (Alpha technologies).

3.2.4 Compression molding machine

Compression molding machine, model PR1D-W400L450PM with electrically heated elements and a heating platen size of 296 x 296 mm, capacity of the press of 40 ton, together with the operated mold temperature and pressure 160 °C and 1500 psi, respectively (Figure 3.4), manufactured by Charon Tut Co, Ltd., Bangkok, Thailand. It was used to fabricate the rubber compounds to vulcanizate's sheets for further testing and characterization.

Figure 3.4 Compression molding machine, model PR1D-W400L450PM (Charon Tut Co, Ltd.)

3.2.5 Fourier transform infrared spectrophotometer (FTIR)

The FTIR spectra of ENR and its compounds were determined in transmission mode by using the Fourier Transform Infrared Spectrophotometer model spectrum two, Perkin Elmer Co. Ltd (Massachusetts, USA) (Figure 3.5). It was used to characterize the molecular structure of polymers in particular the functional group in ENR molecules together with the new formed linkage from reaction of ENR and metal ions. The analysis was carried out over the wide wavenumber ranges of 4000-400 cm^{-1} with a resolution 2 cm^{-1}.

Figure 3.5 Fourier transform infrared spectrophotometer (FTIR).

3.2.6 Tensile testing machine

Tensile properties of rubber vulcanizates were determined according to ISO 527 (type 5A) by a Universal tensile testing machine, model 10 ST (Figure 3.6). The machine was manufactured by Tinius Olsen, Co., Ltd (Honey Crock Lane, UK). The tensile machine was fitted to the load cell with a load capacity of 10 kN and operated at a crosshead speed of 200 mm/min at 23 ± 2 °C.
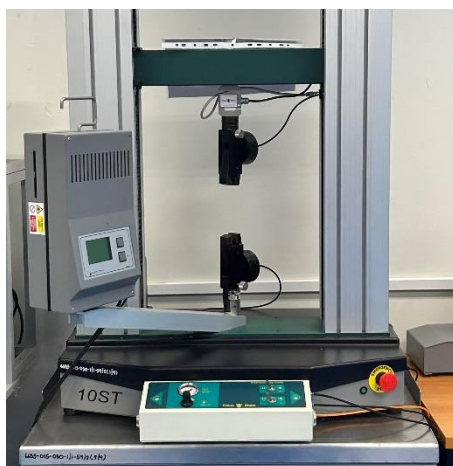
Figure 3.6 Universal tensile testing machine, model 10 ST (Tinius Olsen, Co., Ltd).

3.2.7 Hardness tester

Shore hardness tester, model HT3000 was manufactured by Mon Tech, Werkstoffpeüfmaschinen GmbH., Buchen, Germany (Figure 3.7). It was used to test the hardness of rubber vulcanizates according to ISO 868.

Figure 3.7 Hardness tester, HT3000 (Mon Tech, Werkstoffpeüfmaschinen GmbH).

3.2.8   Scanning electron microscope (SEM)

Scanning electron microscopy (SEM), Quanta 250, FEI Company (Černovice, Czech Republic). (Figure 3.8). It was used to investigate the morphological properties of the ENR compounds and its nanocomposites by achieving a magnification of over 10,000x with high resolution imaging in a digital format. It offers acceleration voltage of 20 kV. The elemental composition of various ENR-25 compounds were investigated by a scanning electron microscope, SEM/EDX. The rubber vulcanizates were first cryogenic cracked in liquid nitrogen and then gold coated before SEM characterization.

Figure 3.8 Scanning electron microscopy (SEM), Quanta 250 (FEI Company)

3.2.9 Dynamic mechanical analyzer (DMA)

Dynamic mechanical analysis was carried out using DMA, model DMA 8000 (Figure 3.9), manufactured by Perkin Elmer Inc., (Waltham, Massachusetts, USA). The DMA was used to analyze thermal properties under dynamic forces at various temperatures of the rubber compounds and its composites. The machine was operated in a tension mode at a fixed frequency of 1 Hz in the temperature ranges of -100 to 100 $^\circ$C. The dynamic properties in terms of storage modolus (E$'$), loss modulus (E$''$) and loss tangent (tan δ) in wide temperature ranges were investigated.

Figure 3.9 Dynamic mechanical analyze, model DMA 8000 (Perkin Elmer Inc).

3.2.10 Thermogravimetric analyzer (TGA)

TGA, model TGA-SDTA 851, manufactured by Mettler Toledo, (Greifensee, Switzerland) (Figure 3.10). It was used to investigate thermal stability of ENR-50, ENR compounds and vulcanizates in the temperature ranges 30 to 1000 °C, under nitrogen atmosphere and oxygen atmosphere.

Figure 3.10 Thermogravimetric analyzer, model TGA-SDTA 851 (Mettler Toledo).

3.2.11 Rubber process analyzer (RPA)

Rubber process analyzer, RPA 200 was manufactured by Alpha Technologies., (Ohio, USA) (Figure 3.11). It was used to determine dynamic properties at a fixed temperature of 100°C. The machine was operated in a strain variation mode in the strain amplitude ranges from 0.56 to 100% at a fixed frequency of 1.0 Hz. In this work, the storage modulus as a function of strain amplitude was determined to verify the Payne effect of the rubber composites.

Figure 3.11 Rubber process analyzer, RPA 2000 (Alpha Technologies).

3.2.12 Temperature scanning stress relaxation tester (TSSR meter)

TSSR meter was manufactured by Brabender GumbH & Co.KG., (Duisburg, Germany) (Figure 3.12). It was used to characterize stress relaxation behaviors of rubber vulcanizates under non-isothermal condition. The machine has a heating and a cooling chamber with electrical heating and air cooling in the temperature ranges of 20 to 220°C with the heating rate of 0-4°C/min. The specimen is fixed in a running traverse driven by a linear lifting motor which is stretched at the tensile strain of 50%.
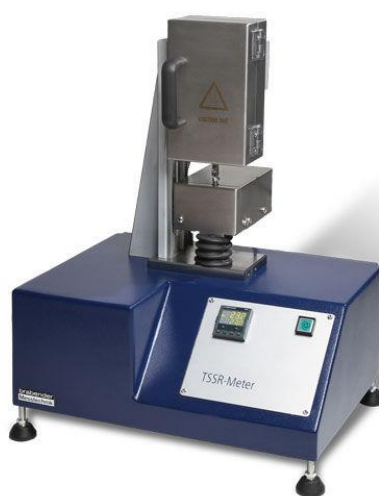
Figure 3.12 TSSR meter (Brabender GumbH & Co.KG).

3.2.13 LCR meter

LCR meter, model IM 3533, was manufactured by Hioki E.E., Corporation., (Nagano, Japan) (Figure 3.13). The LCR meter was connected to the electrode plates of a dielectric test fixture model 16451B dielectric test fixture, Test Equipment Solutions Ltd., (Berkshire, United Kingdom) with 5 mm electrode diameter. It was used to determine electrical properties in terms of electrical conductivity (σ) and dielectric constant (ε') of the ENR-50 and its composites. It can be operated in wide frequency ranges of 20 Hz to 200 kHz with 5 digits measurement resolution. The testing mode can be possibly chosen from the primary and secondary measurements. The primary measurement includes; capacitance (C), inductance (L), impedance (Z), resistance (R). On the other hand, the secondary measurement covers dissipation factor (D), quality factor (Q)(=1/D) and phase angle (θ).

Figure 3.13 LCR meter model IM 3533 (Hioki E.E., Corporation)

3.3   Experimental

3.3.1   Preparation of ENR-25 compounded with $FeCl_3$

ENR-25 was first dried in a hot air oven at 60°C for about 24 h and then mixed with different concentrations of ferric chloride at i.e., 1, 3, 5, 7 and 10 mmol in an internal mixer (Brabender Plasticorder) with a measuring mixer type 50 EHT (Duisburg, Germany) at 60°C and a rotor speed of 60 rpm. In the mixing process, ENR was masticated for about 3 min before incorporating of ferric chloride with continued mixing until reaching a total mixing time of 8 min, as compounding formulation and mixing schedule shown in Table 3.1 The rubber compound was dumped from the mixing chamber and sheeted out by passing through the 1 mm nip of an open two-rolls mill model YFCR 600, Yong Fong machinery Co., Ltd (Samut Sakorn, Thailand) at ambient temperature. The rubber compound was then conditioned in a desiccator at room temperature for about 24 h. Cure characteristic was eventually investigated by moving die rheometer, MDR 2000, Alpha-technologies, (Ohio, USA) at 160°C. Finally, the vulcanized rubber sheets were prepared by compression molding using PR1D-W400L450PM molding machine, Charon Tut Co, Ltd (Bangkok, Thailand) at 160°C and the respective cure time based on the rheometer test.

Table 3.1 Compounding formulations and mixing schedule of ENR-25 with $FeCl_3$

Ingredients	Quantities (phr)
Epoxidized natural rubber 25 mol % (ENR-25)	100 phr
Ferric chloride ($FeCl_3$)	0, 1, 3, 5, 7 and 10 mmol

3.3.2 Preparation of ENR-50 and NR compounds with $FeCl_3$ and ENR cured with the conventional sulfur vulcanization (CV)

ENR-50 was first dried in a hot air oven at 60°C for about 24 h and then mixed with different concentrations of ferric chloride at 1, 3, 5, 7 and 10 mmol using an internal mixer (Brabender Plasticorder, 50 EHT, Duisburg, Germany). The initial mixing temperature was set at 60°C and at a rotor speed of 60 rpm. ENR was masticated for about 3 min before addition of ferric chloride in the mixing chamber with continued mixing for another 8 min. NR was also compounded for a comparison purpose by masticating of NR for 3 min, then 7 mmol $FeCl_3$ was added and the mixing was continued to reach the total mixing time of 8 min. Furthermore, ENR cured with the conventional sulfur vulcanization (CV) system was also prepared for a comparison purpose. That is, ENR was compounded with various chemical ingredients, as shown in Table 3.2. This was done by masticating of ENR-50 about 3 min and then activators, (i.e., zinc oxide and stearic acid), cure accelerator (MBTs) and curing agent (sulfur) were sequentially added. The rubber compound was then dumped from the mixing chamber and sheeted out by passing through the 1 mm nip of an open two-rolls mill model YFCR 600, Yong Fong machinery Co., Ltd. (Samut Sakorn, Thailand) at ambient temperature. The rubber compound was then conditioned in a desiccator at room temperature for about 24 h. Cure characteristics were eventually investigated by using moving die rheometer, MDR 2000, Alpha-technologies, (Hudson, OH, USA) at 160°C. Finally, the vulcanized rubber sheets were prepared by compression molding model PR1D-W400L450PM molding machine, Charon Tut Co, Ltd., (Bangkok, Thailand) at 160 °C.

Table 3.2 Compounding formulation of ENR and NR with FeCl$_3$ and ENR compounded with conventional sulfur (CV) vulcanization system

Ingredients	ENR with FeCl$_3$	NR with FeCl$_3$	ENR with CV cured system
Epoxidized natural rubber 50 mol % (ENR-50)	100 phr	-	100 phr
Natural rubber (NR)	-	100 phr	-
Ferric chloride (FeCl$_3$)	1, 3, 5, 7 and 10 mmol	7 mmol	-
Zinc Oxide (ZnO)	-	-	5 phr
Stearic acid	-	-	1 phr
2,2-Dithiobis-(benzothiazole) (MBTs)	-	-	0.5 phr
Sulfur (S)	-	-	2.5

3.3.3 Preparation of ENR-CNTs nanocomposites

The ENR-50 was first compounded with an optimum dose of FeCl$_3$ at 7 mmol, according to the results from section 3.3.2. The mixing was performed by a tangential internal mixer, Brabender Plasticorder with Mixer 50 EHT model: 835205 (Duisburg, Germany) at 60°C, a rotor speed of 60 rpm and a total mixing time of 8 min (Table 3.3). The ENR-50 was first masticated for about 2 min and then 7 mmol FeCl$_3$ was added and continued mixing to reach the total mixing time of 8 min. This rubber product is later called as "ENR-FeCl$_3$" In the preparation of ENR-50/CNTs nanocomposites, various loadings of CNTs (1, 3, 5, 7 and 10 phr) were each mixed in the ENR-FeCl$_3$ and continued mixing to reach the total mixing time of 8 min. It is noted that the CNTs are in powder forms that can be gradually incorporated into the mixing chamber until they almost became a homogeneous mix with the ENR before closing the mixing chamber with the incorporated time of CNTs was controlled at about 4 min. The ENR-FeCl$_3$/CNTs compound was then dumped from the mixing chamber and passed through the 1 mm nip of an open two-roll mill, model YFCR 600, Yong Fong Machinery Co., Ltd. (Samut

Sakorn, Thailand) at an ambient temperature for many cycles, involving cutting and banding of the rubber compounds. This was aimed to have better dispersion and distribution of the CNTs in the ENR matrix. The rubber compound was then conditioned in a desiccator at room temperature for about 24 hrs. Cure characteristic was investigated by a moving die rheometer (MDR), model MDR 2000, Alpha Technologies, (Ohio, USA) at 160°C. Finally, the compression molding, model PR1DW400L450PM, Charon Tut Co., Ltd, (Bangkok, Thailand) was used to prepare the rubber sheet at 160°C using the respective cure time based on the rheometer test.

Table 3.3 Formulations and mixing schedule for preparation of ENR-FeCl$_3$/CNT compounds

Ingredients	Quantity (phr)	Mixing time (min)
ENR-50	100	2
FeCl$_3$	7 mmol	2
CNTs	0, 1, 3, 5, 7 and 10	4

3.3.4 Preparation of ENR/CNT-CCB hybrid nanocomposites

The ENR-50 was first compounded with an optimum loading dose of FeCl$_3$ and CNTs at 7 mmol and 7 phr according to the results in sections 3.3.2 and 3.3.3, respectively. The mixing was performed by an internal mixer, Brabender Plasticorder with Mixer 50 EHT model: 835205, (Duisburg, Germany) at 60°C and a rotor speed of 60 rpm, according to the formulation shown in Table 3.4. The ENR-50 was first masticated for about 2 min and then 7 mmol FeCl$_3$ were mixed for about 2 min and 7 phr of CNTs was then added and continued mixing for 6 min to reach the total mixing time of 10 min. This sample is designated as "F7-CNT7". In a preparation of ENR/CNTs-CCB hybrid compounds, ENR-50 was also first masticated and mixed with 7 mmol FeCl$_3$ and 7 phr of CNTs in the same manner as the F7-CNT7 but mixing was conducted for about 3 min after incorporating of CNTs before adding various loadings of CCB at 2.5, 5.0, 7.0, 10.0 and 15.0 phr. Then, the compounds were continued mixing for 3 min to

reach the total mixing time of 10 min. These samples are designated as "CNT7/CCBX", where x is the CCB loading in phr. The mix (i.e., ENR-FeCl$_3$/CNT-CCB hybrid nanocomposite) was then dumped from the mixing chamber and passed through the 1 mm nip of an open two-rolls mill, model YFCR 600, Yong Fong machinery Co., Ltd (Samut Sakorn, Thailand) at an ambient temperature. This was aimed to have better dispersion and distribution of the hybrid fillers in ENR matrix. The rubber compound was then conditioned in a desiccator at room temperature for about 24 h. Cure characteristic was investigated by a moving die rheometer (MDR), MDR 2000, Alpha Technologies, (Ohio, USA) at 160°C. Finally, the compression molding, PR1D-W400L450PM, Charoen Tut Co., Ltd, (Bangkok, Thailand) was used to prepare the vulcanizate sheets at 160°C using the respective cure time based on the rheometer test.

Table 3.4 Chemical ingredients and compounding formulation of ENR-FeCl$_3$ filled with CNTs-CCB hybrid filler.

Ingredients	Quantity (phr)
Epoxidized natural rubber (ENR-50)	100
Ferric chloride (FeCl$_3$)	7(mmol)
Carbon nanotubes (CNTs)	7
Conductive carbon black (CCB)	0, 2.5, 5.0, 7.0, 10.0 and 15.0

3.4   Testing and characterization

3.4.1   Cure characteristic

Cure characteristics of rubber compounds were determined at 160°C by a moving die rheometer (MDR 2000), Alpha Technologies, (Ohio, USA) with a fixed frequency of 1.67 Hz and strain amplitude of 1° arc. The optimum scorch time (t_{s1}), cure time (t_{c90}), minimum torque (M_L), maximum torque (M_H), and torque difference (M_H-M_L), were determined from the curing curves.

3.4.2 Tensile properties

The tensile test specimens were mechanically prepared by die cutting from the vulcanized rubber sheet to form a dumb bell shape specimen according to ISO 527 (type 5A). The samples were then clamped with the sample holder of the Universal tensile testing machine, model a 10 ST, Tinius Olsen, Co., Ltd (Honey Crock Lane, UK). The test was then performed at room temperature by extending the samples with a crosshead speed of 200 mm/min according to ISO 527. The stress-strain curves were captured and tensile strength, modulus at 100% elongation and elongation at break were recorded from these curves.

3.4.2.1 Tensile strength

Tensile strength or stress at break is the maximum tensile stress applied in stretching a specimen to rupture. It can be calculated in units of force magnitude at a material failure (F) per cross-section area (A) of unstrained specimen, as follows:

$$\text{Tensile strength (MPa)} = \frac{F}{A} \tag{3.1}$$

3.4.2.2 Tensile modulus

Tensile modulus is a tensile stress at any specified elongation. It can be calculated, as follows:

$$\text{Modulus at x \% (MPa)} = \frac{Fx}{A} \tag{3.2}$$

Where, Fx is the force at x% of elongation and A is cross-sectional area of unstained specimen.

3.4.2.3 Elongation at break

Elongation at break is the ratio between change in length (ΔL) and initial length (L_0) after breakage of the test specimen. It can be calculated, as follows:

$$\text{Elongation at break} = \frac{\Delta L}{L_0} \times 100 \tag{3.3}$$

3.4.3 Hardness

The hardness Shore A of rubber compounds was determined by hardness tester, model HT3000, Mon Tech Werkstoffpeüfmaschinen GmbH., (Buchen, Germany), according to ISO 868. The indentation hardness is inversely related to the penetration and is dependent on the elastic modulus and viscoelastic behavior of material. In this work, hardness of rubber composites with a thickness of least 6 mm was determines at room temperature.

3.4.4 Fourier transform infrared spectrophotometry (FTIR)

Attenuated total reflection Fourier transform infrared (FTIR) spectroscopy was performed using a Fourier Transform Infrared Spectrophotometer (FTIR, Spectrum two, Perkin Elmer, (Massachusetts, USA). Different samples, including a neat ENR, ENR compounds with $FeCl_3$ and sulfur cured system, and ENR composites with CNTs composites were characterized by ATR-FTIR. The analysis was performed over the wide wavenumber ranges from 4000 to 400 cm^{-1}.

3.4.5 Crosslink density

Crosslink density of ENR vulcanizates and nanocomposites was determined by two different approaches: the equilibrium swelling measurement and the temperature scanning stress relaxation (TSSR) test.

3.4.5.1 Determination of crosslink density by equilibrium swelling measurement

In equilibrium swelling measurements, the tests were carried out to determine the crosslink density of the rectangular 10 x 10 x 2 mm^3 rubber specimens. The samples were first weighed before immersing into toluene at room temperature for seven days. The swollen rubber samples were then removed and excess solvent on the specimen surfaces was removed by blotting with filter paper. After that, the specimens were dried in a vacuum oven at 40°C for 24 h. Finally, the samples were weighted, dried, and weighted again. The crosslink density of the rubber vulcanizates

was eventually determined according to the Flory–Rehner relation (Flory and Rehner, 1943):

$$\text{Crosslink density } (V) = \frac{-\ln(1-\emptyset p)+\emptyset p + \chi \cdot \emptyset_p^2}{V_L \cdot (\emptyset_p^{1/3} - \frac{\emptyset p}{2})} \tag{3.4}$$

where $\emptyset_p$ is the volume fraction of rubber in the swollen network, V_L is the molar volume of toluene and χ is the interaction parameter of polymer and solvent (for ENR and toluene, the value is 0.34) (Flory and Rehner, 1943).

3.4.5.2 Determination of crosslink density by TSSR measurement

Crosslink density of the ENR vulcanizates was also estimated by the temperature scanning stress relaxation (TSSR) test. Typically, the apparent crosslink density can be estimated from the maximum slope in the initial part of the stress-temperature curve of the TSSR result, using equations (3.5) and (3.6).

$$V_e = \frac{k}{R^*(\lambda - \lambda^2)} \tag{3.5}$$

$$V_e = \frac{\rho}{M_C} \tag{3.6}$$

where V_e is the apparent crosslink density (mol/m^3), R^* is the universal gas constant, λ is the nominal strain ratio, k is the temperature coefficient of stress (the derivative of mechanical stress with respect to temperature), ρ is the mass density, and M_C is defined as the average molar mass of the elastically active network chains (Matchawet *et al.*, 2017).

It is note that derivative of equation (3.6) is based on the rubber elasticity theory, which applies to rubber network. Consequently, equation (3.6) provides apparent crosslink density of the ENR vulcanizes. (Nakaramontri *et al.*, 2014).

3.4.6 Morphological properties

The morphological properties of the ENR-FeCl$_3$ compound and ENR-FeCl$_3$ filled with CNTs and its hybrid filler with CCB were characterized by scanning electron microscopy (SEM), Quanta 250, FEI Company (Černovice, Czech Republic). The

elemental composition of various ENR compounds were investigated by a scanning electron microscope, SEM/EDX. Each specimen was first cryogenically cracked in liquid nitrogen to create a fresh cross-sectional surface. Then, the dried surface was gold coated and examined by SEM at high resolution and magnification.

3.4.7 Dynamic properties

Two routes of dynamic properties were exploited: dynamic mechanical analyzer (DMA) and rubber process analyzer (RPA).

3.4.7.1 Dynamic mechanical analysis (DMA)

Dynamic mechanical analysis (DMA) was carried out using Perkin Elmer DMA 8000, Perkin Elmer Inc., (Waltham, USA) using rectangular sample with dimensions $30 \times 10 \times 2$ mm^3. The storage modulus (E'), storage modulus (E'') and loss tangent (tan δ) were measured in a tension mode, in the temperature ranges from -100 to 80 °C with a heating rate of 3 °C/min and a fixed deformation frequency of 1 Hz.

3.4.7.2 Rubber process analyzer (RPA)

The storage shear modulus (G') as a function of strain amplitudes was determined at 100°C by using a rubber process analyzer, RPA 2000, Alpha Technologies (Ohio, USA). The test was performed by measuring the storage shear modulus (G') of each filled un-vulcanized rubber compound under shear deformation in the strain amplitude ranges from 0.56 to 100% at a fixed frequency of 1.0 Hz and 100°C. The main aim was to determine the Payne effect of ENR nanocomposites. It is noted that the Payne effect was quantified from the difference between storage moduli at very low strain ($G'_{0.56}$) and at very high strain (G'_{100}) regimes. That is, the Payne effect is typically estimated from the difference between moduli at very low and very high strain regimes (i.e., $G'_0 \longrightarrow G'_{100}$) (Payne and Whittaker, 1971), as follows,

$$G'_0 - G'_{100} = \Delta G' \qquad (3.7)$$

where G'_0 and G'_{100} are the minimum (i.e., $G'_{0.56}$) and the maximum storage moduli (i.e., at the strain amplitude 100%).

Therefore, the Payne effect of various ENR compounds were estimated by the following equation (Pötschke *et al*., 2002):

$$\% \text{ Payne effect} = \frac{G'max - G'min}{G'min} \, x \, 100 \qquad (3.8)$$

where G'_{max} and G'_{min} are maximum and minimum of storage moduli *(G')*.

3.4.8   Thermal resistant properties

Thermal stability of the ENR compounds with $FeCl_3$ without and with CNTs was examined by thermogravimetric analysis (TGA) using TGA-SDTA 851, Mettler Toledo (Greifensee, Switzerland). The measurement was performed under a nitrogen atmosphere at 30–600 °C before switching to an oxygen atmosphere until 900 °C with the same heating rate of 10°C /min.

3.4.9   Bound rubber contents

Bound rubber contents of the ENR compounds with $FeCl_3$, ENR-$FeCl_3$ filled with CNTs and CTNs-CCB hybrid filler were estimated by the swelling method (Flory and Rehner, 1943). The sample was initially immersed in toluene and conditioned to the equilibrium state at room temperature for at least 72 h, renewing the toluene in every 24 h. The sample was later separated from the solvent and then dried at 105°C for at least 24 h. In the same manner, the ENR compound sample was immersed in toluene for at least 72 h at room temperature either in the normal state or in an ammonia atmosphere with the renewal of toluene every 24 h. Then, the solvent was separated, and dried at 105°C for 24 h and eventually weighted. It is noted that the ammonia was used to cleave the physical linkages between rubber molecules and filler surfaces. The bound rubber content was then determined as follows: (Wolff *et al*.,1993)

$$\text{Bound rubber content [\%]} = \frac{W_{fg} - W_f}{W_p} \qquad (3.9)$$

where W_f and W_p are the weights of filler and rubber in the specimens, respectively. W_{fg} is the weight of filler with bound rubber absorbed on it after toluene extraction (Wolff *et al*.,1993).

3.4.10 Temperature scanning stress relaxation (TSSR)

The temperature scanning stress relaxation (TSSR) measurements of rubber vulcanizates were performed using a TSSR meter, Brabender® GmbH & Co. KG, (Duisburg, Germany). The TSSR instrument consists of an electrical heating chamber, where the tensile dumbbell-shaped specimens (type 5A) according to ISO 527 was placed between the two clamps. A linear drive unit attached with the clamps was used to apply certain uniaxial tension to the sample. A thermocouple was placed near the center of the rubber specimens to detect the tested temperature. Also, a signal amplifier and a high-resolution AD-converter were exploited to capture and digitize the analogue signals from the force transducer and thermocouples. All signals were eventually transferred to a personal computer which a special software program was installed for display and evaluation the tested results to gather with for a control purpose. In the test procedure, the sample was first annealed in a hot air oven at 100°C for at least 30 min to eliminate thermal history and storage hardening effect of natural rubber molecules (Wu *et al.*, 2013). The samples were then cooled down to room temperature for about 30 min before placing in the sample holder of the TSSR machine. Then, the rubber sample was stretched to 50% elongation as compared with its original length at 23°C and then conditioned at this temperature (i.e., isothermal condition) for about 2 h. After that, the non-isothermal test was performed by raising temperature from 23°C to 220°C (Figure 3.14) with a constant heating rate of 2 K/min (*v*). The stress at each temperature was then recorded and reported in terms of relationship between stress and tested temperature and hence relaxation modulus and temperature. It is noted that the relaxation spectrum (*H(T)*) was also calculated based on the relationship between relaxation modulus (*E(T)*) and temperature (*T*), as follows (Wu *et al.*, 2013):

$$H(T) = -T \left[\frac{dE(T)}{dT} \right]_{v=const} \qquad (3.10)$$
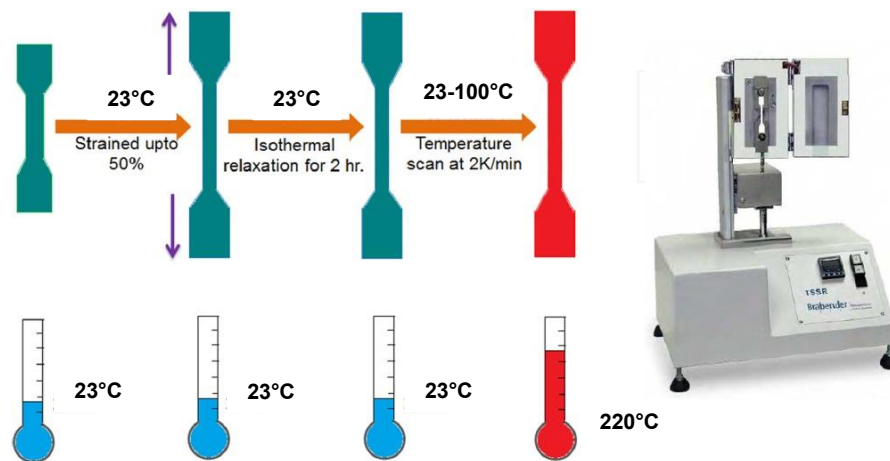
Figure 3.14 Schematic representation of TSSR test procedure and the TSSR instrument (Modified from Chatterjee *et al.,* 2017).

3.4.11 Electrical properties

Electrical properties of the ENR-FeCl$_3$ compound and ENR-FeCl$_3$/CNT-CCB hybrid nanocomposites in terms of electrical conductivity (**σ**) and dielectric constant (**ε′**) were measured at room temperature by an LCR meter, Hioki IM 3533, Hioki E.E. Corporation (Nagano, Japan) in the frequency ranges of 1 to 10^5 Hz. The LCR meter was connected to the electrode plates of a dielectric test fixture model 16451B dielectric test fixture, Test Equipment Solutions Ltd. (Berkshire, United Kingdom) with 5 mm electrode diameter. The electrical conductivity (**σ**), and dielectric constant (**ε'**) were determined, as follows (Du *et al.,* 2003):

$$\sigma = \frac{1}{\rho} = \frac{d}{(R_p)A} \qquad (3.11)$$

$$\varepsilon' = \frac{C_p(d)}{A(\varepsilon_0)} \qquad (3.12)$$

where *d* and *A* refer to the sample thickness and the area of an electrode, respectively. The parameter **ε**$_0$ is the dielectric constant of the free space, which is 8.854x10^{-12} F/m. The factor **ρ** is the volume resistivity which is reciprocal of conductivity.

CHAPTER 4

FERRIC CHLORIDE CROSS-LINKED EPOXIDIZED NATURAL RUBBER WITH 25 MOL% EPOXIDE (ENR-25)

4.1 Introduction

In recent years, a number of works have demonstrated that the introduction of covalent and non-covalent bonds within polymers which can build networks that break and reorganize in response to external stimuli, thus conferring self-healing and remodeling ability to the material (Wang *et al.,* 2022). This can be formed by many dynamic covalent (i.e., transesterification reactions (Chen *et al*., 2018a; Salaeh *et al*., 2021), disulfide bonds (Cheng *et al.,* 2019; Xiang *et al*., 2019), Diels–Alder reactions (Bai *et al.,* 2015; Feng *et al*., 2019), boronic ester bonds (Chen *et al*., 2018b; Huang *et al*., 2021), Schiff base bonds (Chao *et al.,* 2016), etc. Non-covalent bonds have been also used to prepare self-healable and recyclable polymers by forming hydrogen bonding (Cao *et al., 2019*; Shen *et al*., 2021; Xu *et al.,* 2019), and metal coordination (Cao *et al.,* 2021a; Fan *et al*., 2021), together with ionic clusters (Wu *et al*., 2021; Xu *et al.,* 2016), etc.).

The metal coordination of rubber molecules have been one of special bonds that have been used to tailor rubber properties. Also, some divalent transition metal ions (i.e., Mn^{2+}, Cu^{2+} and Fe^{2+}) were found to accelerate oxidative degradation of dried rubber by degradation of poly-isoprene chains (Ripple *et al*., 2002). Coordination crosslink reaction of carboxylated nitrile rubber (XNBR) was found by reacting with anhydrous copper sulfate (Ibarra *at al*., 2009). It was found that crosslink density increased with increasing concentration of anhydrous copper sulfate due to the coordination crosslinking reaction between copper ions and XNBR molecules. Recently, self-healable epoxidized natural rubber (ENR) has been prepared by coordination crosslinking with ferric ions based on ferric chloride and 2,6-diaminopyridine (DAP) (Mandal *et al*., 2021). It was found that some physical properties of the metal ion crosslinked samples are comparable with the conventional sulfur crosslinked samples. Additionally, strong and tough elastomers have been developed

by introduction of deformable microphase-separated granules with rich epoxy–ferric ions coordination into a ductile rubber network of epoxidized natural rubber (Zhang *et al.*, 2018).

In this chapter, epoxidized natural rubber with 25 mole % epoxide (ENR-25) was vulcanized by metal ions namely ferric ions from ferric chloride ($FeCl_3$) at various loadings of 0, 1, 3, 5, 7 and 10 mmol by mixing ENR-25 and $FeCl_3$ at high temperature. Various properties including cure characteristics, mechanical and morphological properties and crosslink densities were investigated.

4.2   Preparation of ENR-25 compounded with $FeCl_3$

The ENR compounds were prepared by mixing method according to the experimental procedure described in section 3.3.1.

4.3   Testing and characterization

ENR with 25 mol% epoxide (ENR-25) compounds were prepared with various concentrations of $FeCl_3$ at 1, 3, 5, 7 and 10 mmol, as designated by E25F1, E25F3, E25F5, E25F7 and E25F10, respectively were also prepared by the mixing method and the experimental procedure, as described in section 3.4.

4.3.1   Curing characteristics

Curing characteristic of various ENR compounds was determined by using MDR test, as the experimental procedure described in section 3.4.1. Figure 4.1 shows the mixing torque-time curves or curing curves of the ENR-25 compounded with various concentrations of $FeCl_3$ at 1, 3, 5, 7 and 10 mmol compared with the neat ENR-25. It is clearly seen that the neat ENR-25 showed no response of mixing torque-time relation. This indicates absent of the crosslinking reaction between ENR molecules. The flat curves were also seen in the ENR-25 compounded with 1 and 3 mmol $FeCl_3$ due to very low concentration of $FeCl_3$. However, dramatically increasing torque-time curve is obvious when incorporation of $FeCl_3$ was higher than 5 mmol, indicating as the marching curing curves. This is attributed to chemical reaction between oxirane rings

in ENR molecules and $FeCl_3$. The crosslinking reaction is described in detailed in chapter 5.
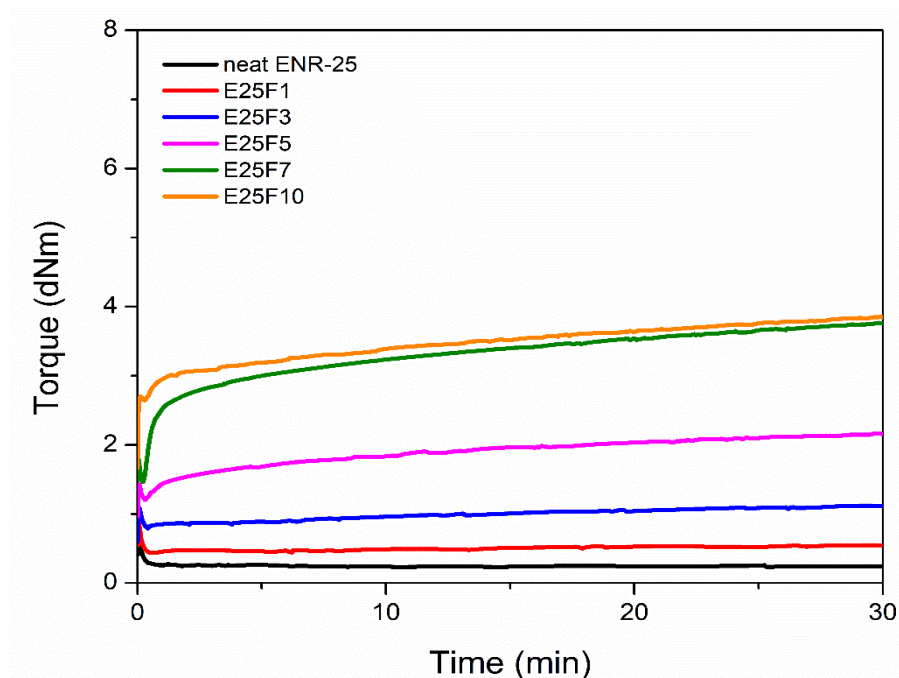
Figure 4.1 Cure curves of neat ENR-25 and ENR-25 compounded with various concentrations of $FeCl_3$ at 1, 3, 5, 7 and 10 mmol (i.e., E25F1, E25F3, E25F5, E25F7 and E25F10.

4.3.2 SEM/EDX analysis

Morphological properties and metal content of ENR compounds were determined by using SEM/EDX Analysis, as the experimental procedure described in section 3.4.6. Figure 4.2 shows SEM images together with EDX spectra of the neat ENR-25 and 7 mmol of $FeCl_3$ (E25F7). As might be expected, the main elements of the neat ENR-25 consist of carbon (C) ($\sim$ 82 wt%) which arises from hydrocarbon chains and oxygen (O) ($\sim$ 18 wt%) which are mainly from the epoxirane rings in ENR molecules. In Figure 2 (a), it is also seen that the smooth homogeneous surface is clearly seen in the SEM micrograph of the neat ENR-25. In Figure 2(b), the main elements in the E25F7 are carbon (C) ($\sim$ 70 wt%), oxygen (O) ($\sim$ 17 wt%), iron (Fe) ($\sim$5%) and chlorine (Cl) ($\sim$ 7%). These two new elements (i.e., Fe and Cl) are arose from the incorporation of

ferric chloride molecules. This confirms the presence of Fe and Cl elements in the epoxidized natural rubber molecules. Furthermore, SEM micrograph of E25F7 in Figure 2(b) indicates inhomogeneous distribution of $FeCl_3$ in ENR matrix. This might reflect high cross-linking structure as the rigid networks of ENR molecules.
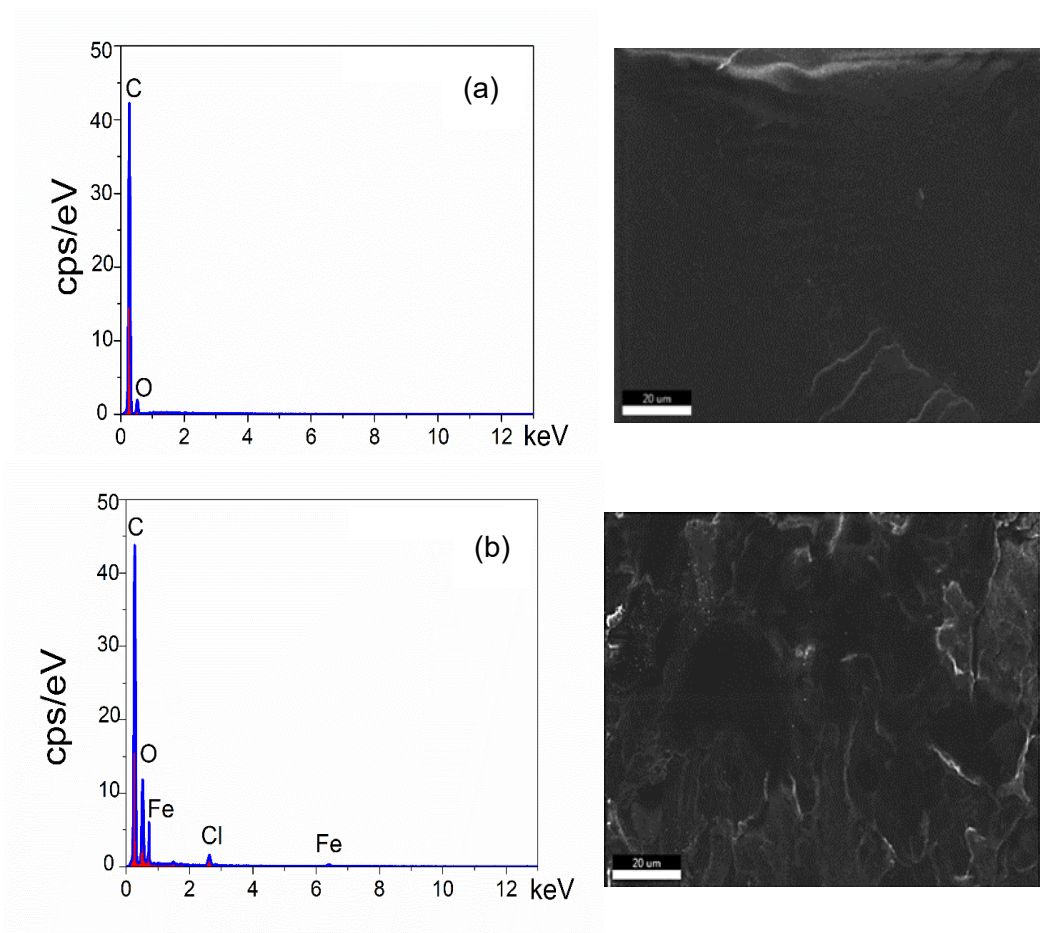
Figure 4.2 SEM images with the EDX spectra of neat ENR-25 (a) and ENR-25 compounded with 7 mmol of $FeCl_3$ (E25F7) (b).

4.3.3 Mechanical properties

Tensile properties of ENR-25 compounded with $FeCl_3$ were characterized as the experimental procedure described in section 3.4.2. Figure 4.3 shows stress-strain curves of the ENR-25 compounded with various concentrations of $FeCl_3$ compared to the neat ENR-25. It is seen that ENR-25 compounded with $FeCl_3$ exhibited significantly increased in the Young's moduli (i.e., slope of the initial curves) with increasing

concentrations of $FeCl_3$. Also, the toughness as indicated by the area underneath of the stress-strain curve also increased with increasing concentrations of $FeCl_3$. This is attributed to increasing level of crosslinking reaction and hence the linkages between oxirane rings in ENR-25 molecules and $FeCl_3$ to form more rubbery networks. On the other hand, the elongation at break decreased with increasing the $FeCl_3$ contents. This is due to the restriction of the rubber chain mobility of ENR molecules caused by increasing concentrations of $FeCl_3$.
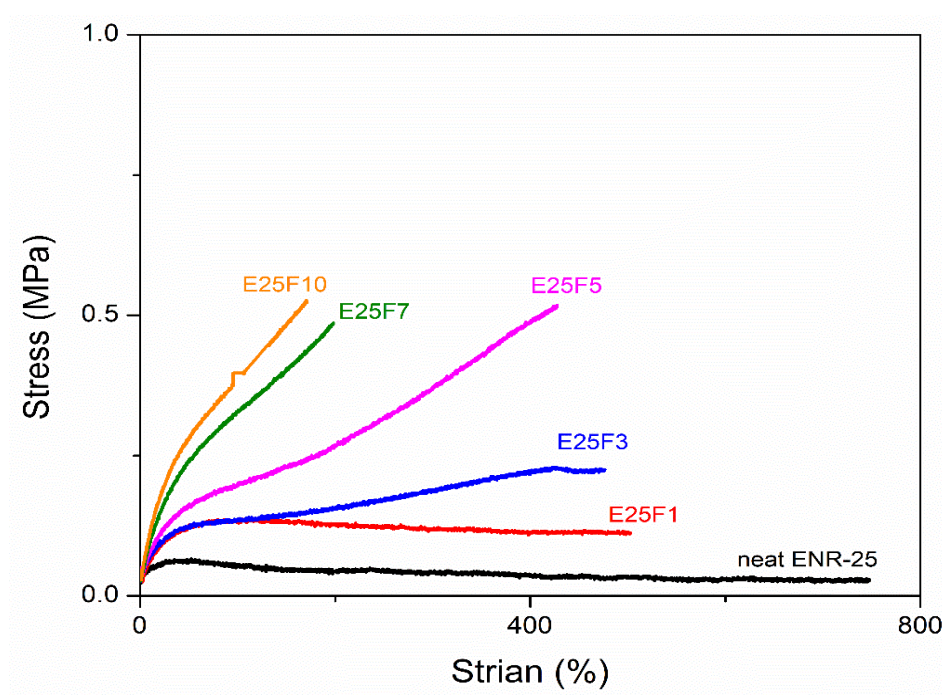
Figure 4.3. Stress-strain curves of neat ENR-25 and ENR compounded with various concentrations of $FeCl_3$ at 1, 3, 5, 7 and 10 mmol (i.e., E25F1, E25F3, E25F5, E25F7 and E25F10, respectively).

4.3.4. Crosslink density

Crosslink density of ENR compounded with $FeCl_3$ was determined as the experimental procedure described in section 3.4.5. Figure 4.4 shows the crosslink densities of ENR-25 compounded with various concentrations of $FeCl_3$ at 1, 3, 5, 7 and 10 mmol. It is clearly seen that the crosslink densities increased with increasing $FeCl_3$ contents due to the higher new by formed coordination cross-links between Fe^{3+} and

the oxygen atom in the oxirane rings of ENR molecules. This indicates a higher level of chemical crosslinks between ENR molecules and hence higher contents of -O-Fe-O linkage in ENR networks. This result correlates with the magnitude of torque in Figure 4.1.
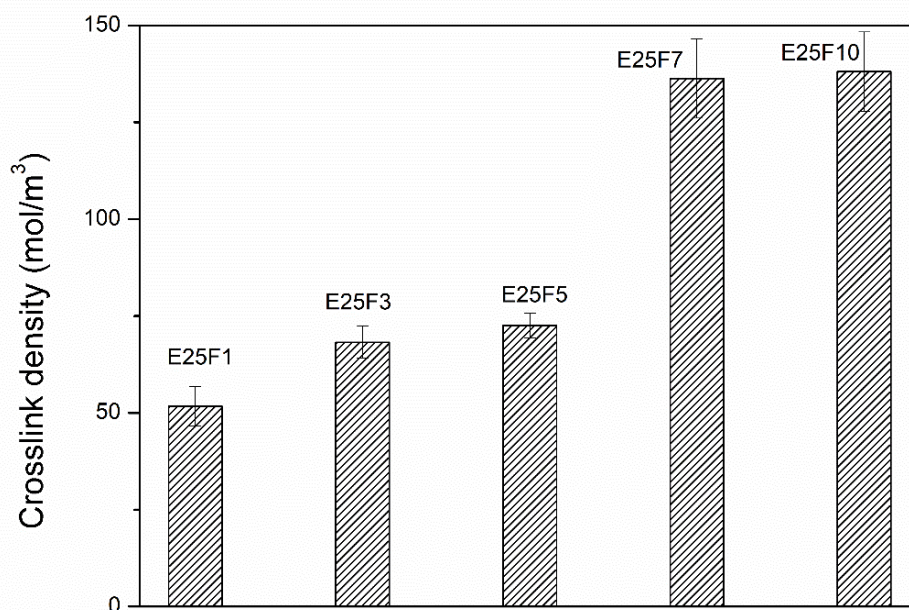
Figure 4.4. Crosslink density of ENR-25 compounded with various concentrations of $FeCl_3$ at 1, 3, 5, 7 and 10 mmol (i.e., E25F1, E25F3, E25F5, E25F7 and E25F10, respectively).

4.4 Conclusions

ENR-25 was successfully vulcanized with $FeCl_3$ by a crosslinking reaction between opened ring products of an oxirane ring in ENR and Fe^{3+} to create metal–oxygen coordination (–O-Fe-O–) cross-links. It was found that the ENR-25 compounds with $FeCl_3$ showed good tensile properties with increased curing torque, as the $FeCl_3$ concentration increased. This is attributed to chemical reaction between oxirane rings in ENR molecules and Fe^{3+} ion to form rubbery network.

CHAPTER   5

CROSS-LINKED OF EPOXIDIZED NATURAL RUBBER WITH 50 MOL% EPOXIDE (ENR-50) BY FERRIC CHLORIDE

5.1   Introduction

Vulcanization of rubber is a process to form permanent rubber network structures with useful properties. Typically, vulcanization is performed by sulfur vulcanization process to form sulfidic linkages between rubber chains. The presence of unsaturation in the chemical structure of rubber macromolecules enables this crosslinking process. The examples of sulfur vulcanization systems in various rubber types are in styrene butadiene rubber (SBR) (Marzocca and Mansilla., 2006), natural rubber (Vennemann *et al*., 2014; Krainoi *et al*., 2019; Nun-anan *et al*., 2020), and epoxidized natural rubber (ENR) (Matchawet *et al*., 2015; Nakaramontri *et al*., 2015; Yangthong *et al*., 2019). Typically, the sulfur vulcanization system provides three different types sulfidic linkages with mono-, di-, and poly-sulfidic bonds in the rubber vulcanizates (Hernandez *et al*., 2016). Generally, the sulfur cured vulcanizates exhibit good mechanical, thermal and other related technical properties, but the chemistry behind of such crosslinking reactions is rather complex. The sulfur vulcanization system consists of at least three different chemical ingredients including activator, accelerator and curing agent. Other commonly used vulcanization systems of rubber are peroxide, phenolic and metal oxide cured systems (Smejda-Krzewicka *et al*., 2019). The peroxide system typically improved heat resistance and compression set properties more superior than rubber products based on the sulfur curing systems (Kruželák *et al.,* 2017). In addition, the phenolic resin increases the crosslinking density of styrene-butadiene rubber (SBR) and nitril-butadiene rubber (NBR) phase due to the curative effects (Derakhshandeh *et. al*., 2008).

Incorporation of metal ions in epoxidized natural rubber (ENR) can lead to crosslinking reaction, and it is supposed that the network formation may be associated with coordination crosslinks or the complex which consists of metal central atom and rubber molecules or other chemical ligands (Zhang *et al*., 2016). It has been obvious

that the research dealing with reaction of metal ions and rubber is still limited. Therefore, more research work on the related topics may lead to great benefits to the research and innovation of rubber. Reaction of metal ions and polar polymers for instance, epoxy resin has been more or less investigated rather than in rubber materials. The epoxy cured with ammonium ionic liquids and palladium complex catalyst was studied and found that the palladium catalysts have good catalytic stability (Ostrowska et al., 2013). Furthermore, three different divalent metal ions (i.e., Ca^{2+}, Cu^{2+} and Fe^{2+}) were mixed with ENR and found that the metal ions caused alteration of curing characteristics (i.e., scorch and cure times, and cure rate index) together with dynamic properties (storage modulus and damping peaks) of ENR compounds (Utara et al., 2015). In addition, the transition metal ions (i.e., Co^{2+}, Cu^{2+}, Mn^{2+}, Fe^{2+}, Ni^{2+} and Ag^{+1}) promoted oxidative degradation of natural rubber molecules, causing the predominant chain scission reaction during storage of dry rubber (Rodrıgues et al., 1998). Furthermore, the type and concentration of divalent metal ions (i.e., Ca^{2+}, Sr^{2+}, Mg^{2+}, Cu^{2+}, Zn^{2+}) influenced on intrinsic viscosity of natural rubber latex (Rodrıgues et al., 1998). Additionally, the thermal behavior and non-isothermal degradation of magnetite (Fe_3O_4)/epoxidized natural rubber (ENR-50) composites, lithium triflate ($LiCF_3SO_3$)-ENR-50 polymer electrolytes and $LiCF_3SO_3$-Fe_3O_4/ENR-50 composite polymer electrolytes were investigated using differential scanning calorimetry (DSC) and thermogravimetric analysis (TGA). It was found that the glass transition temperature (T_g) and other related thermal properties of these materials generally follow the increasing trend (Tan and Bakar, 2014). Furthermore, Zn^{2+} was incorporated in butadiene–styrene–vinylpyridine rubber (VPR) to construct additional Zn^{2+}-pyridine coordination complex in rubber network and to tailor the mechanical performance (Tang et al., 2016). Other metal ions including Ni^{2+}, Co^{2+}, Fe^{3+}, and La^{2+} were incorporated in VPR at the stoichiometric equivalence of pyridine and metal ions (Tang et al., 2016). It was found that the metal–ligand bonds are formed through the coordination reaction between the pyridine groups in butadiene–styrene–vinylpyridine rubber (VPR) and metal ions. This contributes to increase the stiffness of the material at small increasing strain, and also a complete recovery was achieved after stretching (Tang et al., 2016).

In this chapter, epoxidized natural rubber with 50 mol% epoxide (ENR-50) was mixed with small amount of $FeCl_3$ ranging from 1 to 10 mmol and the compounds were systematically characterized with the main aim to understand the mode of crosslinking reaction and related mechanisms. The metal ion crosslinked materials were then compared with the ENR vulcanizates cured by the conventional sulfur cured system in terms of attenuated total reflection (ATR) fourier transform Infrared spectrophotometer (FTIR), cure characteristics, mechanical properties, crosslink density, dynamic properties, morphological, thermal properties, temperature scanning stress relaxation and electrical conductivities.

5.2   Preparation of ENR-50 compounded with $FeCl_3$

The ENR compounds were prepared by mixing method according to the experimental procedure described in section 3.3.2.

5.3   Testing and characterization

ENR with 50 mol% epoxide (ENR-50) compounds were prepared with various concentrations of $FeCl_3$ at 1, 3, 5, 7 and 10 mmol, as designated by E50-F1, E50-F3, E50-F5, E50-F7 and E50-F10, respectively. For a comparison purpose the conventional sulfur compounds and NR compounded with 7 mmol of $FeCl_3$ were also prepared by the mixing method and the experimental procedure, as described in section 3.4.

5.3.1 Attenuated total reflection (ATR) fourier transform infrared spectrophotometer (FTIR)

The ATR-FTIR was used to identify chemical structure and chemical linkages in various types of cured system of NR and ENR-50, as experimental procedure described in section 3.4.4. Figure 5.1 shows ATR-FTIR spectra of the neat ENR-50, ENR-50 compounded with 7 mmol of $FeCl_3$ (E50-F7), and conventional sulfur vulcanization (E50-CV), together with unmodified NR (ADS) compounded with 7 mmol $FeCl_3$ (NR-F7). It is clear that the FTIR absorption peak at the wavenumber 878 cm^{-1} is clearly seen in the FTIR spectrum of the neat ENR-50, which indicates the presence of the asymmetric C-O stretching vibration in epoxide rings of ENR molecules (Harun and Chan, 2016). Additionally, the main absorption peaks at the wavenumbers 878 cm^{-1} and 838 cm^{-1} are also observed in the FTIR spectra of ENR-$FeCl_3$. They assigned to the asymmetric C-O stretching vibration in oxirane rings and =C-H out of plane bending in ENR molecules (Zhang *et al*., 2005). However, a broad new absorption peak at wavenumber of 565 cm^{-1} is clearly observed in the FTIR spectra of ENR-$FeCl_3$. This broad peak may be consisting with many other peaks more particularly, at 544 and 444 cm^{-1}, which are well identified as Fe-O bond in the structure of **α**-Fe_2O_3 (Biju., 2018). Hence, this indicates the existence of the Fe-O stretching vibration in ENR-$FeCl_3$ compounds (Zhang *et al*., 2005). Therefore, the newly formed linkages between ENR and $FeCl_3$ molecules is responsible for the absorption peak at wavenumber 470 cm^{-1} (Biju., 2018). In Figure 5.1, it is also clear that incorporation of 7 mmol $FeCl_3$ in ENR-50 caused a reduction of the peak intensity at wavenumber 838 cm^{-1}, which might represent the disappearance of some oxirane rings in ENR molecules.
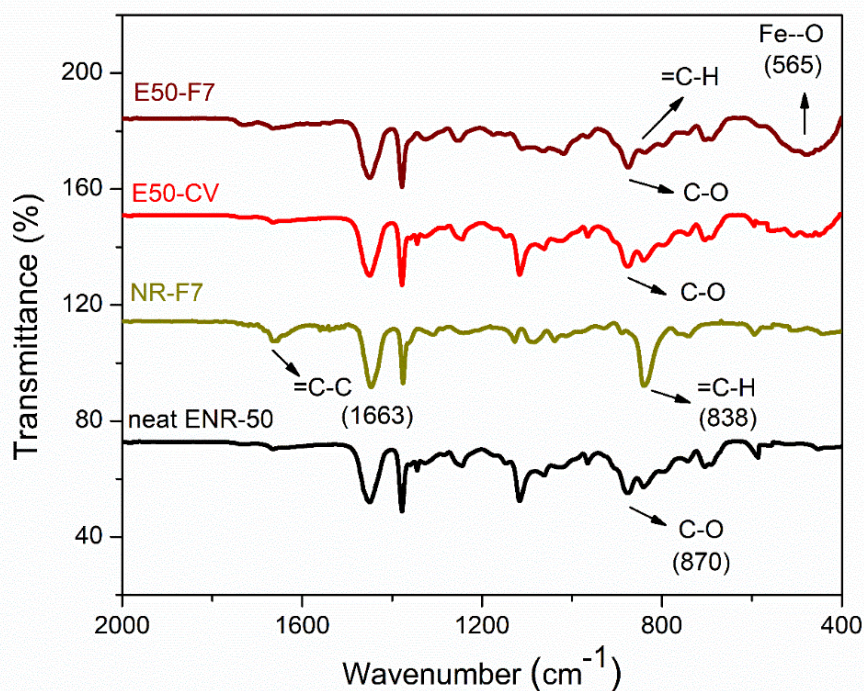
Figure 5.1 ATR-FTIR spectrum of the neat ENR-50, ENR-50 compounded with 7 mmol of FeCl$_3$ (E50-F7) and the conventional sulfur vulcanization (E50-CV) as well as the unmodified NR (ADS) compounded with 7 mmol of FeCl$_3$ (NR-F7)

5.3.2 Curing characteristics

Curing characteristic of various ENR compounds was determined by using MDR test, as the experimental procedure described in section 3.4.1. Figure 5.2 shows the mixing torque-time curves of the ENR-50 compounded with various concentrations of FeCl$_3$ at 1, 3, 5, 7 and 10 mmol. The conventional sulfur compound (i.e., E50-CV) is also considered for comparison. It is clearly seen that the neat ENR-50 and unmodified NR (ADS) with 7 mmol FeCl$_3$ had no response of mixing torque-time relation, indicating no establishment of network structure. However, slightly increasing torque is obvious when ENR-50 was mixed with 1 mmol of FeCl$_3$ (E50-F1). Furthermore, increasing concentrations of FeCl$_3$ from 1 to 10 mmol caused abruptly increasing of torque at a given testing time in particularly, at high loadings of FeCl$_3$. Additionally, the steepness of the mixing torque-time curves is increased with increasing concentrations of FeCl$_3$, resulting a marching nature of the crosslinking reaction. Therefore, the curing curves of ENR-FeCl$_3$ compounds have not reached to the equilibrium curing state within the

experimental time of 1 h. Table 5.1 shows cure characteristics in terms of minimum torque (M_L), maximum torque (M_H), torque difference (M_H-M_L), scorch time (t_{s2}) and cure time (t_{c90}) of various ENR-50 compounds. It is seen that the maximum rheometric torque is increased with increasing $FeCl_3$ concentration. This might be attributed to more chemical reaction between oxirane rings of the ENR molecules and Fe^{3+} ion to form more crosslinking network structures via -O-Fe-O- linkages, as evidenced in the FTIR peak of E50-F7 compound at a 565 cm^{-1} in Figure 5.1. Therefore, the proposed reaction mechanism of crosslinking reaction of ENR is shown in Figures 5.3 to 5.5. It is noted that under the given conditions at high temperature, the oxirane rings in ENR molecules are prone to ring opening reaction with a product (i.e., diols) that are able to form new linkages with another ring opened ENR fragment via Fe^{3+} bridges. In Figures 5.2-5.4, different types of crosslinking structures are described (Bořkovec, 1958; Childers *et al.*, 2014). As far as the chemical scheme of Figures 5.2 and 5.3 are concerned, the microstructure in Figure 5.3 where the nucleophilic chloride is attached with **α** position with respect to the methyl group is more favorable. This is due to presence of methyl group that enables the adjacent carbon atom less nucleophilic nature. It could enhance the possibility of nucleophilic attack by chloride ion to the carbon atom without the methyl group. Furthermore, the strong reactivity of ethylene oxide or propylene oxide with ferric chloride is very well-known and described very well (Bořkovec, 1958). That is, the epoxy group containing molecules can even undergo an "internal polymerization" type of reaction and yield many exchanged and complicated polymeric microstructures. In the present case, the epoxy groups are most probably following similar types of reaction pathways and can result in very strong crosslinking structures as described in Figure 5.5. Due to the remarkable reactive character of ferric chloride, the epoxy group can follow a ring opening type "internal polymerization" resulting highly dense network structure.

In Figure 5.2, it is also seen that the ENR-50 compounded with conventional sulfur vulcanization system (ENR-CV) exhibits a typical curing curve with dramatically reversion phenomenon at the curing time beyond 10 min. This is due to the destruction of newly formed sulfidic linkages due to high temperature treatment. In Table 5.1, it is also clear that the ENR-50 compounded with $FeCl_3$ over 7 mmol showed

higher maximum rheometric torque and curing time than the E50-CV. This may reflect a higher content of crosslink density. It is also clear that increasing concentration of ferric chloride caused a decrement of the cure rate index (CRI). This may be attributed to the cure retarding effect of chloride ion of $FeCl_3$ (Figure 5.2).
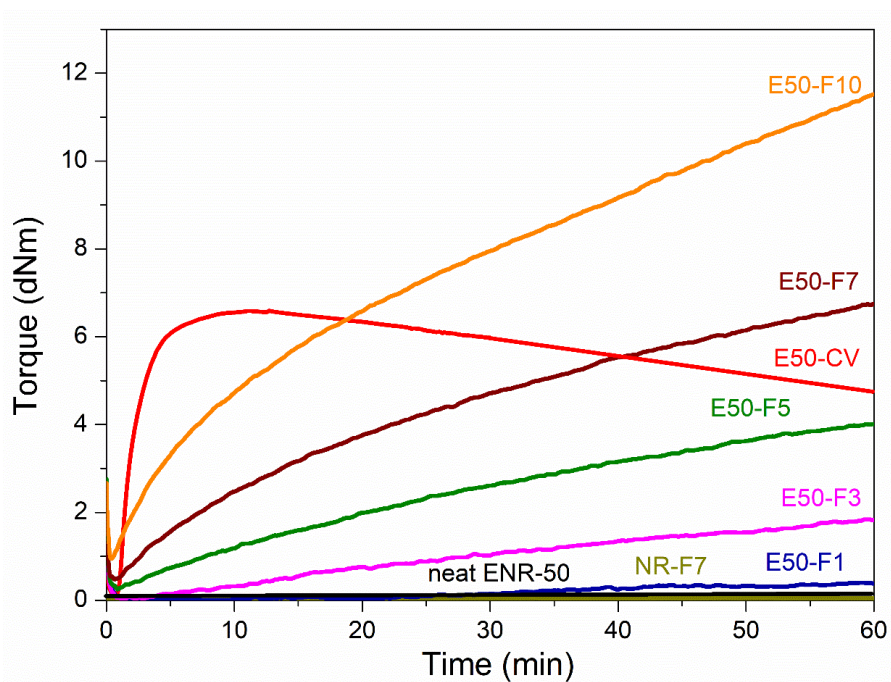

Figure 5.2 Cure curves of ENR-50 compounds with various concentrations of $FeCl_3$ at 1, 3, 5, 7 and 10 mmol (i.e., E50-F1, E50-F3, E50-F5, E50-F7 and E50-F10, respectively), and the conventional sulfur vulcanization (i.e., E50-CV), neat ENR-50 and unmodified NR (ADS) with 7 mmol of $FeCl_3$ (NR-F7).

Table 5.1 Cure characteristics in terms of minimum torque (M_L), maximum torque (M_H), torque difference (M_H-M_L), scorch time (T_{s2}) and cure time (T_{c90}) of various ENR-50 compounds.

Compounds	M_L	M_H	M_H-M_L	T_{s2}	T_{c90}	CRI
	(dNm)	(dNm)	(dNm)	(min)	(min)	
E50-CV	0.22	6.18	5.96	2.11	7.36	19.04
E50-F1	0.12	0.47	0.35	3.75	6.40	37.73
E50-F3	0.20	1.84	1.64	3.23	6.38	31.74
E50-F5	0.25	4.01	3.76	2.49	7.01	22.12
E50-F7	0.48	6.75	6.27	2.20	7.40	19.23
E50-F10	0.95	11.52	10.57	1.39	8.21	14.66
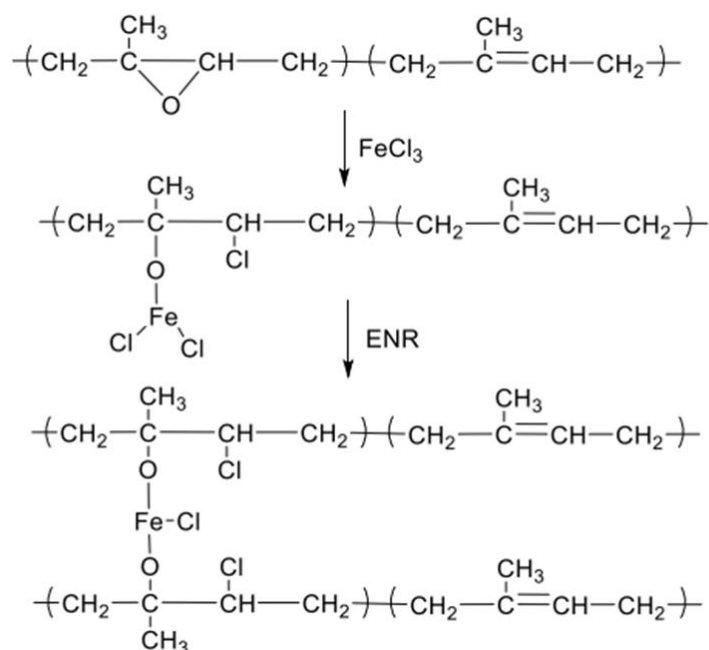
Figure 5.3 A proposed reaction mechanism between epoxidized natural rubber and ferric chloride. The nucleophilic chloride is attached with **α** position with respect to the methyl group.
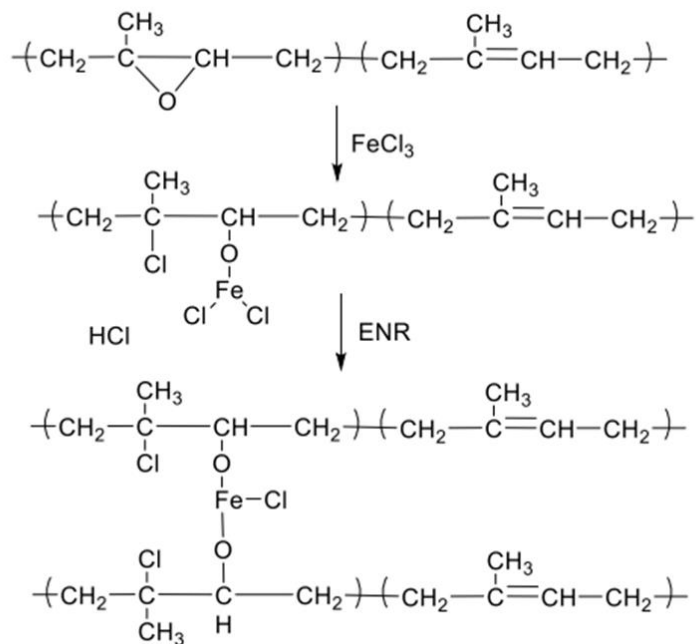
Figure 5.4 A proposed reaction mechanism between epoxidized natural rubber and ferric chloride. The nucleophilic chloride is attached with **β** position with respect to the methyl group.
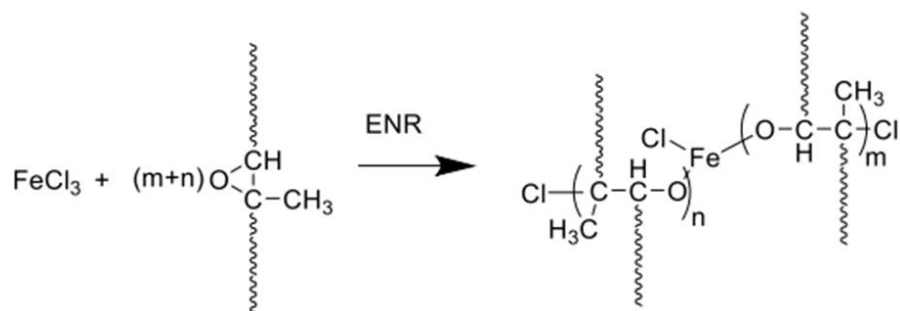
Figure 5.5 A proposed reaction mechanism between epoxidized natural rubber and ferric chloride. In the mechanism, the ring opening type polymerization of the epoxy group is described, which can be correlated with "internal polymerization" of the epoxy group of epoxide natural rubber.

5.3.3 Mechanical properties

Tensile properties of ENR-50 compounded with $FeCl_3$ and conventional sulfur vulcanization system were characterized as the experimental procedure described in section 3.4.2. Figure 5.6 shows stress–strain curves of ENR-50 compounded with various concentrations of $FeCl_3$ compared with the ENR-50 cured by the conventional sulfur vulcanizate (i.e., E50-CV). Additionally, mechanical properties in terms of 100% modulus, tensile strength, elongation at break and hardness (Shore A) of various ENR-50 compounds are summarized in Table 5.2. It is seen that ENR-50 compounded with $FeCl_3$ offered significantly stronger initial modulus (Young's moduli) (i.e., slope of the initial curves) with increasing concentrations of $FeCl_3$. Additionally, the toughness as indicated by the area underneath of the stress–strain curve also increased with increasing concentrations of $FeCl_3$. This is attributed to the increasing level of crosslinking reaction and hence the linkages between oxirane rings in ENR molecules and $FeCl_3$ to form more rubber network structures due to coordination linkages of -O-Fe-O- (Figures 5.3 and 5.4) and internal polymerization (Figure 5.5). In Table 5.2, it can be observed that a lower 100% modulus and tensile strength of ENR-50 compounded with low concentration of $FeCl_3$ (i.e., 1, 3 and 5 mmol) as compared with the ENR-50 compounded with the conventional sulfur vulcanization. However, with higher $FeCl_3$ concentration in ENR-50 at 7 and 10 mmol, 100% modulus and tensile strength are increased as compared with the data obtained from E50-CV. This might be due to higher contents of the crosslinking structures from the coordination reaction of Fe^{3+} with epoxide groups together with the internal polymerization of the epoxide rings. On the other hand, the elongation at break decreased with increasing the $FeCl_3$ contents (Table 5.2). This might be attributed to the restriction of the rubber chain mobility caused by increasing concentrations of $FeCl_3$, which provided higher contents of strong rubbery network with higher crosslinking density. In Table 5.2, it is also clear that hardness of the ENR-50 compounds with $FeCl_3$ increased with increasing concentrations of $FeCl_3$. This can be explained by increasing internal polymerization products and also contents of -O-Fe-O linkages between ENR-50 molecules to cause higher level of crosslinking density. In addition, the ENR-50 compounds with higher amounts of $FeCl_3$ show hardness values that are the higher than those of the E50-CV.

This confirms a denser rigid crosslinking network. This observation is also reflected in the maximum rheometric torque values (Table 5.1). In Figure 5.6, it is also seen that the stress–strain curve of E50-F10 exhibits a rigid solid-like behavior with the highest hardness (Table 5.2) and brittle properties, as indicated by high moduli, but less elongation at break.
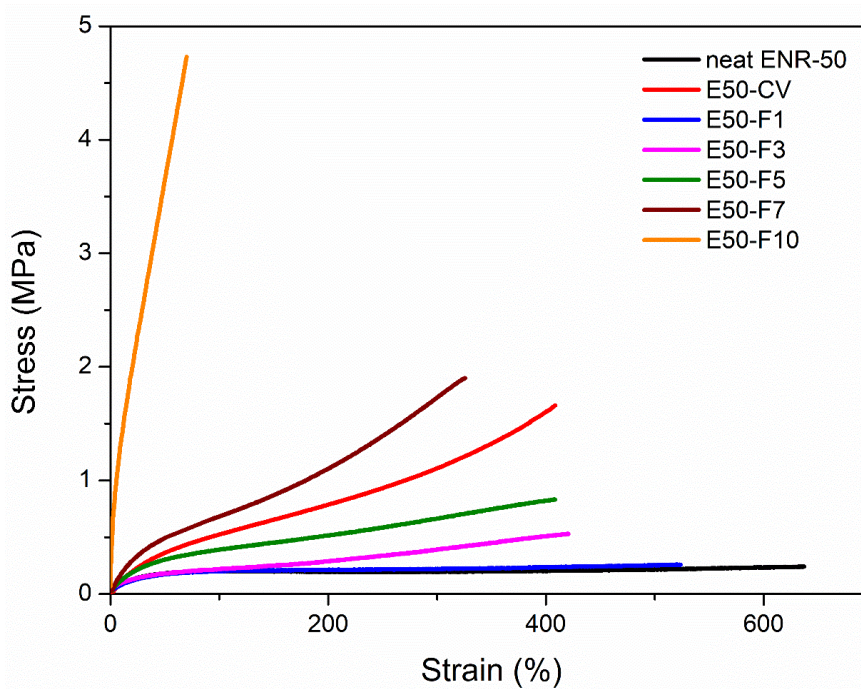
Figure 5.6 Stress–strain curves of ENR-50 compounded with various concentrations of FeCl$_3$ at 1, 3, 5, 7 and 10 mmol, and the conventional sulfur vulcanization (i.e., E50-CV).

Table 5.2 Mechanical properties in terms of 100% modulus, tensile strength, elongation at break and hardness (Shore A) of ENR-50 compounded with various concentrations of $FeCl_3$ at 1, 3, 5, 7 and 10 mmol and the conventional sulfur vulcanization (i.e., E50-CV).

Samples	100% Modulus (MPa)	Tensile Strength (MPa)	Elongation at Break (%)	Hardness (Shore A)
E50-CV	0.42±0.03	1.63±0.21	408.60±56.13	30.40±2.00
E50-F1	0.15±0.03	0.22±0.02	527.90±15.12	20.11±1.15
E50-F3	0.19±0.02	0.49±0.09	420.70±19.81	22.80±1.10
E50-F5	0.26±0.06	0.76±0.10	406.50±10.93	28.70±1.90
E50-F7	0.89±0.18	1.89±0.11	325.70±20.21	44.50±1.00
E50-F10	1.47±0.32	4.71±0.16	70.00±3.00	62.50±2.10

5.3.4 Crosslink density

Crosslink density of ENR-50 compounded with $FeCl_3$ and conventional sulfur vulcanization system was determined as the experimental procedure described in section 3.4.5. Table 5.3 shows the crosslink densities of ENR-50 compounded with various concentrations of $FeCl_3$ at 1, 3, 5, 7 and 10 mmol and the conventional sulfur vulcanizates (i.e., E50-CV). It is clearly seen that the crosslink densities of ENR-50 compounded with $FeCl_3$ over 7 mmol are higher than the E50-CV. In addition, the crosslink densities increased with increasing $FeCl_3$ contents due to the higher crosslinks between Fe^{3+} and oxygen (i.e., -O-Fe-O-) of the oxirane rings as well as the impact of the internal polymerization. Moreover, E50-F7 and E50-F10 show higher crosslinking density than E50-CV. This indicates higher level of chemical crosslinks between ENR molecules and hence higher contents of -O-Fe-O- linkage in the elastomer networks. This result correlates with the value of maximum rheometric torque in Table 5.1.

Table 5.3 Crosslink densities of ENR-50 compounded with various concentrations of FeCl$_3$ and the conventional sulfur vulcanization (i.e., E50-CV).

Sample	Crosslink densities (mol/m^3)
E50-CV	99.16±4.52
E50-F1	43.52±8.18
E50-F3	64.45±1.12
E50-F5	84.49±1.98
E50-F7	112.76±1.76
E50-F10	142.38±0.27

5.3.5   Thermogravimetric analysis

Thermogravimetric analysis (TGA) of ENR-50 compounded with FeCl$_3$ and conventional sulfur vulcanization system was performed as the experimental procedure described in section 3.4.8. Figure 5.7 shows the TGA and DTG thermograms of the neat ENR-50 and ENR-50 compounded with various concentrations of FeCl$_3$ and the conventional sulfur vulcanization system (i.e., E50-CV). It is noted that TGA was performed under nitrogen atmosphere in the temperature ranges between 23-600 °C, before switching to oxygen atmosphere and heated until 900 °C with the same heating rate at 10 °C/min.

The TGA thermograms of ENR-50 in Figure 5.7(a), the rubber compounded with FeCl$_3$ show double degradation steps in the temperature ranges around 240–290°C and 418–433 °C. The first DTG peaks (Figure 5.7(b)) at around 240–290°C (T_{d1} in Table 5.4) can be associated with dissociation of water molecules in the crystal structure of FeCl$_3$. The second DTG peaks are seen around 418–433°C (T_{d2} in Table 5.4), indicating the degradation of hydrocarbon in ENR molecules. In addition, an increase in concentrations of FeCl$_3$ causes shifting of the degradation temperature of ENR molecules (i.e., T_{d2}) to higher temperature (Table 5.4). This might be due to higher thermal resistance of the material with the coordination linkage, –O-Fe-O- linkages. On the other hand, the degradation of the neat ENR-50 and E50-CV showed a single degradation stage with no significant difference in the TGA thermograms with the DTG peaks (i.e., decomposition temperature (T_d)) around 402 and 411°C, respectively. This is attributed to the degradation of ENR molecules. Nevertheless, in the last region under the oxygen atmosphere of TGA thermogram (Figure 5.7(a) and Table 5.4), the ENR50-CV exhibited the highest remained residue, as compared to the ENR-50 compounded with FeCl$_3$ and the neat ENR-50, respectively. This might be more particulate chemicals involved in the conventional sulfur vulcanization system, such as ZnO.
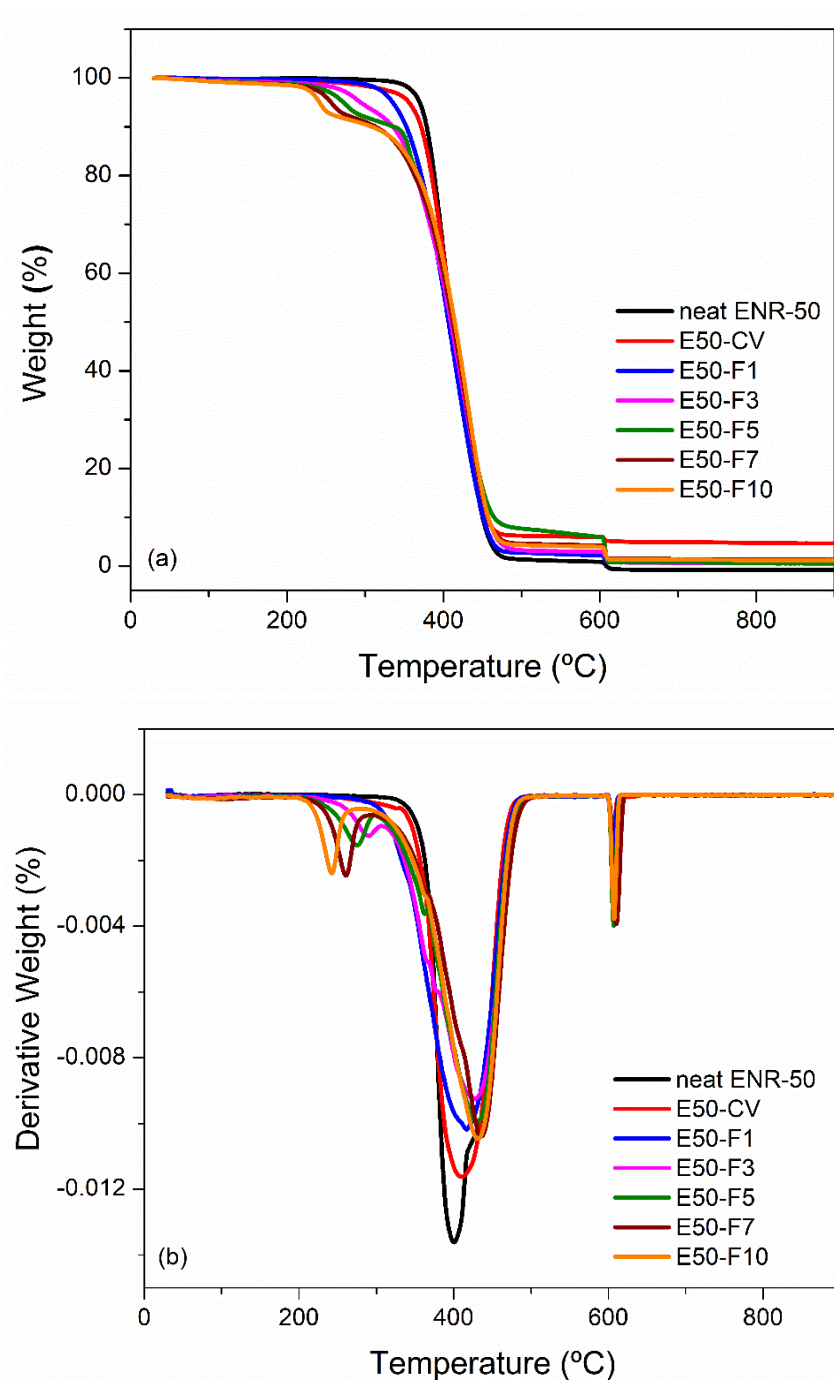
Figure 5.7 TGA (a) and DTG thermograms (b) of neat ENR-50 and ENR-50 compounded with various concentrations of FeCl$_3$ at 1, 3, 5, 7 and 10 mmol the conventional sulfur vulcanization system (i.e., E50-CV).

Table 5.4 Degradation temperature (T_d) of the neat ENR-50 and ENR-50 compounded with various concentrations of FeCl$_3$ and the conventional sulfur vulcanization (i.e., E50-CV).

Sample	T_{d1} (°C)	T_{d2} (°C)	Weight loss (%) under the nitrogen atmosphere	weight loss (%) under the oxygen atmosphere
Neat ENR-50	402.11	-	94.10	0.83
E50-CV	411.58	-	94.06	5.13
E50-F1	290.02	418.23	93.51	1.38
E50-F3	285.45	423.14	93.07	1.75
E50-F5	273.56	426.89	92.00	1.80
E50-F7	258.67	430.34	88.14	2.20
E50-F10	240.79	433.31	76.65	2.36

5.3.6 Temperature scanning stress relaxation (TSSR)

Temperature scanning stress relaxation of ENR-50 compounded with FeCl$_3$ and conventional sulfur vulcanization system was performed as the experimental procedure described in section 4.4.10. Figure 5.8 shows the relaxation modulus as a function of temperature of ENR compounded with 7 mmol of FeCl$_3$ (E50-F7) and the conventional sulfur vulcanizate (E50-CV). It can be seen that the E50-F7 shows higher initial modulus than the E50-CV. This might be due to the higher level of crosslink structures. This can be corelated with the data of delta torque (Table 5.1), the 100% modulus (Table 5.2) and crosslinking density (Table 5.3). In Figure 5.8, it is also seen that that the initial relaxation modulus of E50-F7 is marginally increased, but E50-CV is remarkably increased with increasing temperature in the initial region. This might be contributed to the entropy effect, which typically happens in the rubber vulcanizates (Vennemann *et al.*, 2006). Another part of the modulus curves in the temperature ranges from 30 to 90°C indicated the deterioration of the physically bound rubber molecules. Furthermore, the thermal degradation of sulfidic crosslinks and rubber chains are observed in the temperature ranges between 90-160°C and 160-220°C,

respectively (Vennemann *et al.*, 2006). In Figure 5.8, it is clear that the E50-F7 has a higher entropy effect than the sulfur crosslinked sample, E50-EV. Additionally, the relaxation modulus of E50-CV showed rapidly decreasing to nearly zero in the temperature ranges 80-220°C. This is attributed to lower thermal resistance of the E50-CV than E50-F7. This result correlates to lower degradation temperature (T_d) of E50-CV than E50-F7 in Table 5.4.
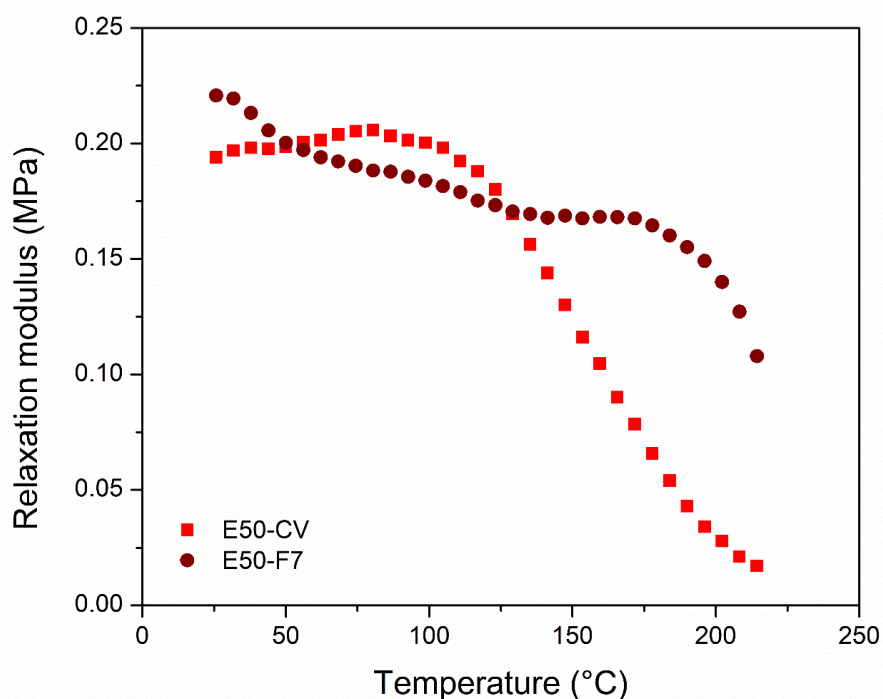
Figure 5.8 Representative relaxation modulus of ENR-50 compounded with 7 mmol of FeCl$_3$ (E50-F7) and the conventional sulfur vulcanizate (i.e., E50-CV).

5.3.7 Dynamic mechanical analysis (DMA)

Dynamic mechanical analysis (DMA) of ENR-50 compounded with FeCl$_3$ and conventional sulfur vulcanization system was performed as the experimental procedure described in section 3.4.7.1. Figure 5.9 shows the storage modulus (E') and the loss tangent (tan δ) as a function of temperature of the neat ENR-50 and ENR-50 compounded with various concentrations of FeCl$_3$ and with the conventional sulfur vulcanization (i.e., E50-CV). In Figure 5.9 (a), it is clearly seen that the storage moduli in

the glassy regions of E50-F7 and E50-F10 are higher than the E50-CV and other types of materials investigated. This might be due to formation of the stronger rubber networks that contain high amount of -O-Fe-O- linkages in the E50-F7 and E50-F10 vulcanizates. In the ENR-50 with lower $FeCl_3$ concentration than 7 mmol, it is clear that lower and weaker molecular networks of ENR are formed. This might be due to the lower extent of crosslinking reactions and hence lower newly formed amount of -O-Fe-O- coordination linkages. In Figure 5.9 (a), it is seen that increasing temperature approaches the glass transition zone where the glass transition temperature (T_g) of various materials are seen, as the tan δ peaks in Figure 5.9 (b). It is clear that increasing concentration of $FeCl_3$ in ENR-50 compounds caused higher glass transition temperature (T_g). This may be associated with the increase in the crosslinking densities (Table 5.3) with more restriction in the rubber chain mobility. It is also clear that the ENR compounds with $FeCl_3$ indicate only a single glass transition temperature (T_g), which is seen from the single tan δ peak in Figure 5.9 (b). Furthermore, in Figure 5.9 (b), it is clearly seen that the ENR-$FeCl_3$ compounds with $FeCl_3$ greater than 3 mmol had lower tan δ peak height. This is attributed to lower level of chain mobility of the materials with higher crosslinking density and hence higher glass transition temperature (T_g). In the rubbery region, E50-F7 and E50-F10 showed higher storage moduli than the E50-CV and other types of materials (Figure 5.9 (a)). This is due to the higher crosslinking density based on strong reactions between $FeCl_3$ and the epoxide groups of the ENR molecules.
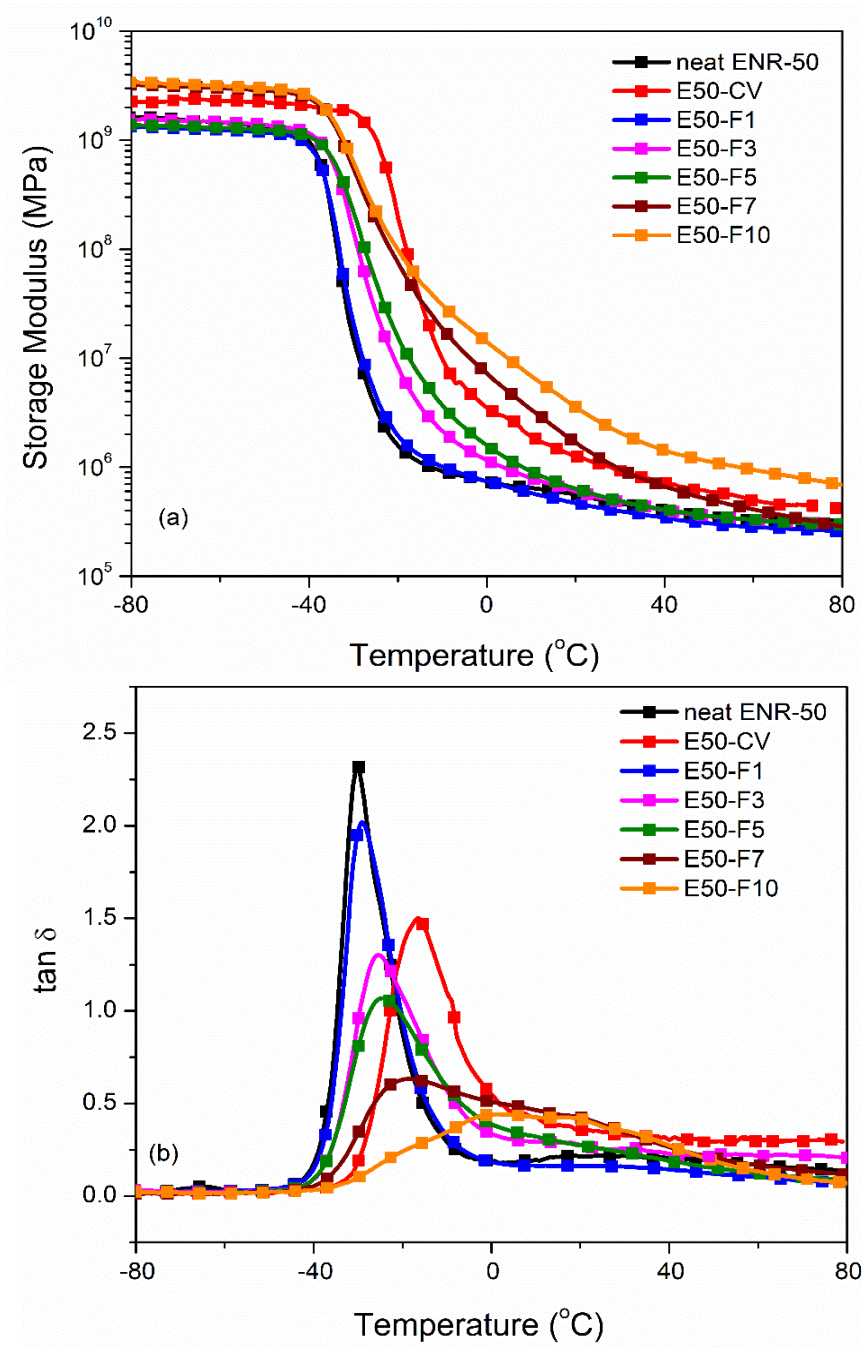
Figure 5.9 Storage modulus (a) and tan δ (b) as a function of temperature of the neat ENR-50, ENR-50 compounded with various concentrations of $FeCl_3$ compared and the conventional sulfur vulcanization system (i.e., E50-CV).

5.3.8   Electrical properties

Electrical properties of ENR-50 compounded with $FeCl_3$ and conventional sulfur vulcanization system were determined as the experimental procedure described in section 3.4.11. Figure 5.10 shows electrical conductivities of ENR compounds as a function of frequencies. It seen that the neat ENR and E50-CV show lower electrical conductivity. However, upon addition of various concentrations of $FeCl_3$ in ENR-50, suddenly improvement of the electrical conductivity of the ENR-$FeCl_3$ compounds is clearly seen. Additionally, the electrical conductivities increased with increasing concentrations of $FeCl_3$ in ENR-50 with a strong increment with the concentration of $FeCl_3$ beyond 5 mmol. This might be due to higher electrical conductivity of $FeCl_3$, causing powerful transferring of electrical currents and enhances the conductivity of rubber compound significantly.
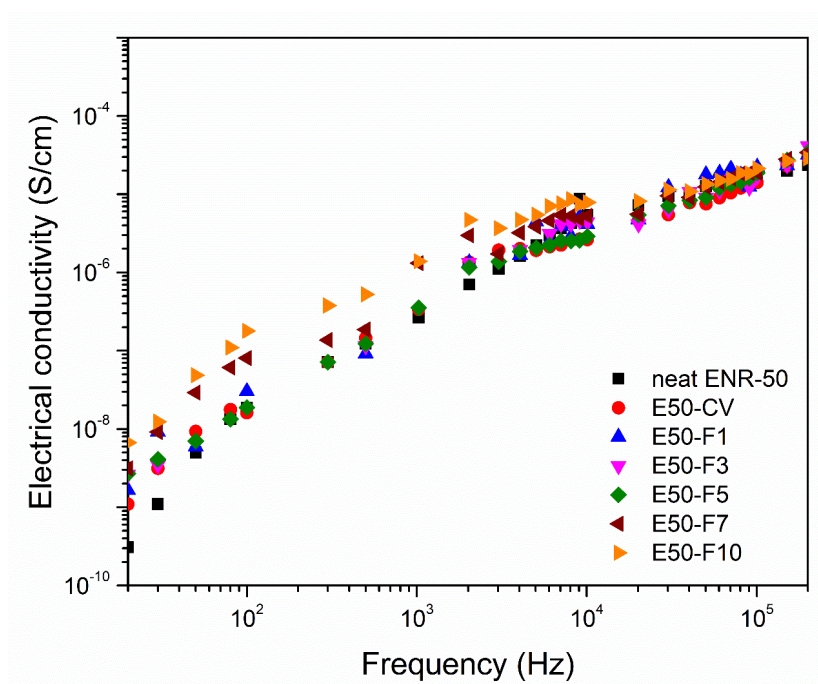
Figure 5.10 Electrical conductivity as a function of frequency of the neat ENR-50, ENR-50 compounded with various concentrations of $FeCl_3$ and the conventional sulfur vulcanization system (i.e., E50-CV).

5.4   Conclusions

ENR-50 can be very efficiently crosslinked by using Fe^{3+} from $FeCl_3$. In the present case, a small amount of $FeCl_3$ was used to cure ENR. The linkages between $FeCl_3$ and oxirane ring in the ENR molecule (i.e., -O-Fe-O) was confirmed from the FTIR studies. The epoxy group can follow a ring opening type "internal polymerization" that is, increasing the network formation of ENR and $FeCl_3$ via the coordination -O-Fe-O-linkages. Moreover, it was found that an increased concentration of $FeCl_3$ improved the properties of ENR-50 compounds, including maximum rheometric torque, crosslinking densities, tensile strength, dynamic properties, electrical conductivity and thermal properties. The conventional sulfur vulcanization of ENR-50 compounds and unmodified NR compounded with 7 mmol $FeCl_3$ were used for comparison and it is found that $FeCl_3$ cannot cure NR. Furthermore, the ENR-50 compounded with $FeCl_3$ at 7 and 10 mmol showed higher crosslinking densities and mechanical properties than the ENR-50 cured with conventional sulfur cured system. This might be due to higher crosslinking structures of the cured samples. Additionally, the internal polymerization of epoxy moieties with $FeCl_3$ offers very dense network structures, which are reflected in mechanical and dynamic mechanical properties. Additionally, T_g values increased with increasing concentrations of $FeCl_3$. This is due to the increase in the crosslinking densities that restricted the mobility of ENR molecules. Furthermore, the ENR-50 compounded with $FeCl_3$ showed the highest electrical conductivity than the other samples without $FeCl_3$. Additionally, thermal resistance was increased with increasing concentration of $FeCl_3$. The reaction between ENR and $FeCl_3$ could be very rapid at a higher temperature and the principle can be applied for other epoxy-based materials.

CHAPTER 6

CROSSLINKED EPOXIDIZED NATURAL RUBBER BY FERRIC CHLORIDE FILLED
WITH CARBON NANOTUBES

6.1　Introduction

Natural rubber (NR) is an agricultural product which can be obtained from
renewable resources and also biodegradable. Typically, NR exhibits many excellent
properties, including mechanical, dynamic properties and elasticity, but its weathering
and oil-resistant property are rather poor. To improve mechanical properties, electrical
conductivity and other related properties of NR, various conductive fillers are normally
incorporated in the compounding formulation of NR (Salaeh and Nakason, 2012;
Matchawet *et al*., 2016). Also, the modified NR like epoxidized natural rubber (ENR)
(Teh *et al*., 2004), maleated natural rubber (Sahakaro and Beraheng, 2008) and NR
grafted with polar monomers (Saramolee *et al*., 2014) have also been exploited to
improve some important properties of NR. Currently, natural rubber nanocomposites
have also been prepared by incorporating different types of nanofillers, including
carbon nanotubes (Krainoi *et al*., 2018), graphene (Matos *et al*., 2014) and conductive
carbon black (Nakaramontri *et al*., 2018). Furthermore, ceramic fillers, such as barium
titanate ($BaTiO_3$) and lead titanate ($PbTiO_3$) were also investigated (Salaeh *et al*., 2011).
It was found that the gum ENR and ENR/$BaTiO_3$ composites exhibit higher mechanical
properties and electrical conductivities than those of the gum NR and NR/$PbTiO_3$
composites. This is attributed to the higher polarity of ENR than the unmodified NR,
which makes them enable to promote the interactions between functional groups of
ENR and at the ceramic filler surfaces (Salaeh *et al*., 2011).

Nanocomposites based on elastomer and carbon nanotubes (CNTs) have been
found in various applications with high thermal stability and electrical conductivity
(Ebbesen and Ajayan., 1992; Das *et al*., 2012; Mensah *et al*., 2015). However, the decent
properties of ENR/CNT nanocomposites depend mainly on dispersion and distribution
of CNTs and their three-dimensional network formation in ENR matrix. Typically, CNTs
have high aspect ratio and strong van der Waals forces among the particles that cause

strong agglomeration of CNTs in ENR matrix (Nakaramontri *et al*., 2014). Thus, addition of carbon nanotubes-based filler in ENR has been widely studied with the main aims to enhance various ENR properties including cure characteristics, mechanical properties, thermal stability and electrical conductivity (Matchawet *et al*., 2015; Shanmugharaj and Ryu., 2013; Nakaramontri *et al*., 2015; Ismail *et al*., 2012; Nakaramontri *et al*., 2015). Also, CNTs have been used as a hybrid filler in combination with other types of fillers in different rubber composites, for instance in chloroprene rubber (CR) (Subramaniam *et al*., 2011) and in solution styrene butadiene rubber (S-SBR) filled with the hybrid filler consisting of the multi-walled carbon nanotubes and ionic liquid (IL) (Das *et al*., 2009). It was found that the NR/CNT with IL hybrid nanocomposite indicates comparatively high electrical conductivity with lower percolation threshold concentration than in the NR/CNT without IL (Krainoi *et al*., 2019)

In this chapter, epoxidized natural rubber (ENR) was compounded with ferric chloride to assist the crosslinking reaction and then filled with carbon nanotubes via the melt mixing method. Various properties, including cure characteristics, infrared spectroscopy (FTIR), mechanical properties, Payne effect, morphological properties, bound rubber contents, thermogravimetric analysis, dynamic mechanical analysis and electrical conductivities were investigated in the ferric ion crosslinked and CNTs filled ENR composites.

6.2   Preparation of carbon nanotubes filled epoxidized natural rubber crosslinked by ferric chloride

The ENR compounds were prepared by mixing method according to the experimental procedure described in section 3.3.3.

6.3   Testing and characterization

ENR with 50 mol% epoxide (ENR-50) with a fixed 7 mmol $FeCl_3$ and with various CNTs loadings at 1, 3, 5, 7 and 10 phr (i.e., F7C1, F7C3, F7C5, F7C7 and F7C10) was prepared and compared with ENR-50 compounds with a fixed 7 mmol $FeCl_3$ without CNTs, according to the experimental procedure described in section 3.4

6.3.1 Cure characteristics

Curing characteristic of various ENR compounds were determined by using MDR test, as the experimental procedure described in section 3.4.1. Figure 6.1 shows torque-time curves or cure curves of the ENR-$FeCl_3$ compounds in combination with different CNTs loadings at 1, 3, 5, 7 and 10 phr (i.e., F7C1, F7C3, F7C5, F7C7 and F7C10, respectively). Cure characteristics in terms of minimum torque (M_L), Maximum torque (M_H), torque difference (M_H-M_L), scorch time (T_{s2}) and cure time (T_{c90}) of ENR-$FeCl_3$ without and with CNTs are summarized in Table 6.1. It is seen that the cure curves of all ENR-$FeCl_3$ compounds exhibited the marching cure behavior, i.e., an increase in mixing torques as increasing of mixing time. This is due to internal polymerization and coordination reaction of the epoxy group resulting crosslinking networks. Most probably the reaction is not complete as the there are many epoxy groups which are available for the further reaction. The reaction mechanism is further illustrated between Fe^{3+} in $FeCl_3$ molecules and epoxy groups of ENR to form –O–Fe–O– linkages and also the chemical interaction with CNTs, as shown in a proposed reactions in Figures 6.2 and 6.3. The participation of the internal polymerization of oxirane rings of ENR molecules in the presence of CNTs is also described as the chemical reaction shown in Figure 6.4. It is noted that under the given conditions at high temperature and shear force, the oxirane rings in ENR molecules are prone to ring opening reaction with a product that are capable of forming new linkages with another ring opened ENR fragment via Fe^{3+} bridge, as previously described (Damampai *et al.*, 2021). Furthermore, the epoxy group containing molecules can even undergo an 'internal polymerization' type of reaction and yield many exchanged and complicated polymeric microstructures which can result in very strong crosslinking structures (Damampai *et al.*, 2021). Therefore, increasing trend of curing rheometric torque (Figure 6.1) and hence crosslink density based on torque difference (Table 6.1) are seen. In Figure 6.1, it is also seen that the cure curves of ENR-$FeCl_3$/CNTs nanocomposite show higher marching cured curves, indicating by a dramatically increase in torques with increasing testing time and increasing loadings of the CNTs. This reflects that the ENR-$FeCl_3$/CNTs compounds require longer time to complete the crosslinking reaction. In Table 6.1, it can be seen that incorporation of CNTs causes acceleration of the curing reaction of

ENR-FeCl$_3$ compounds by reducing of scorch time (T_{s2}) and cure time (T_{c90}) together with raising of the cure rate index (CRI). This might be due to higher thermal conductivity of FeCl$_3$ and CNTs that cause enhancing and accelerating of the curing reaction of the ENR and FeCl$_3$ together with internal polymerization of epoxide groups and hence increasing of the chemical interaction between polar functional groups in ENR and CNTs surface (Nakaramontri *et al.*, 2014). Also, incorporation of CNTs caused higher torque difference (Table 6.1) that reflects higher stiffness and also crosslinking structures and reinforcement of the ENR vulcanizates. Furthermore, increasing loading level of CNTs causes an increase in thermal conductivity of the ENR compound that may facilitate and hence accelerate the curing reaction. Also, higher possibility of the polar functional groups on the CNT surfaces can interact with the epoxide groups of ENR and their opened ring products.
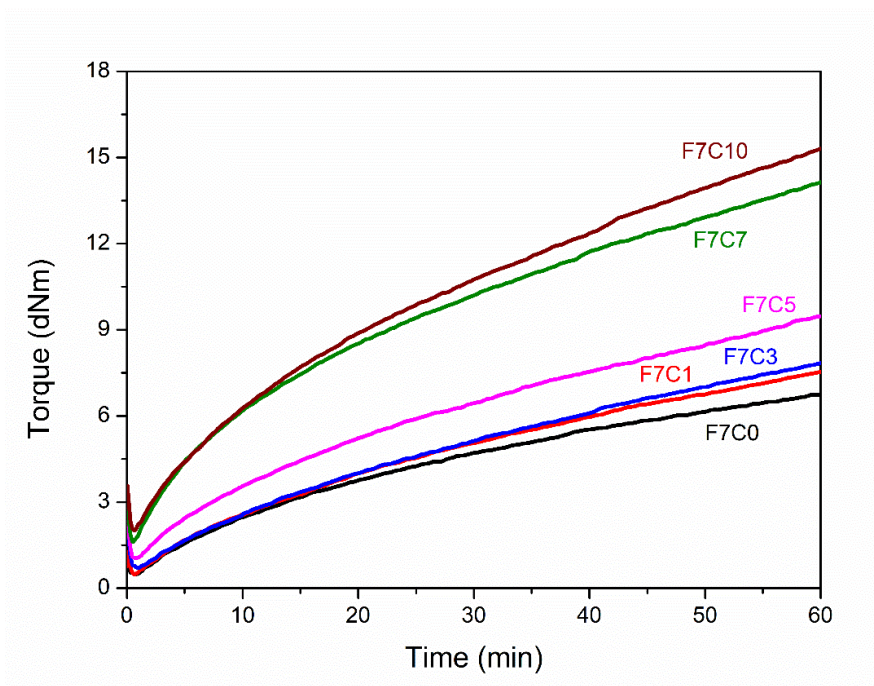
Figure 6.1 Cure curves of ENR-FeCl$_3$ compound without (F7C0) and with various CNTs loadings at 1, 3, 5, 7 and 10 phr (i.e., F7C1, F7C3, F7C5, F7C7 and F7C10).

Table 6.1 Cure characteristics in terms of minimum torque (M_L), Maximum torque (M_H), torque difference (M_H-M_L), scorch time (T_{s2}) and cure time (T_{c90}) of ENR-FeCl$_3$ without and with CNTs.

Compounds	M_L (dNm)	M_H (dNM)	M_H-M_L (dNm)	T_{s2} (min)	T_{c90} (min)	CRI
F7C0	0.48	6.75	6.27	2.20	7.40	19.23
F7C1	0.76	7.53	6.77	2.11	7.38	18.98
F7C3	0.83	7.84	7.01	2.02	6.72	21.27
F7C5	1.06	9.48	8.42	1.60	6.34	21.10
F7C7	1.62	14.15	12.53	1.32	5.91	21.78
F7C10	2.02	15.31	13.29	1.21	5.58	22.88
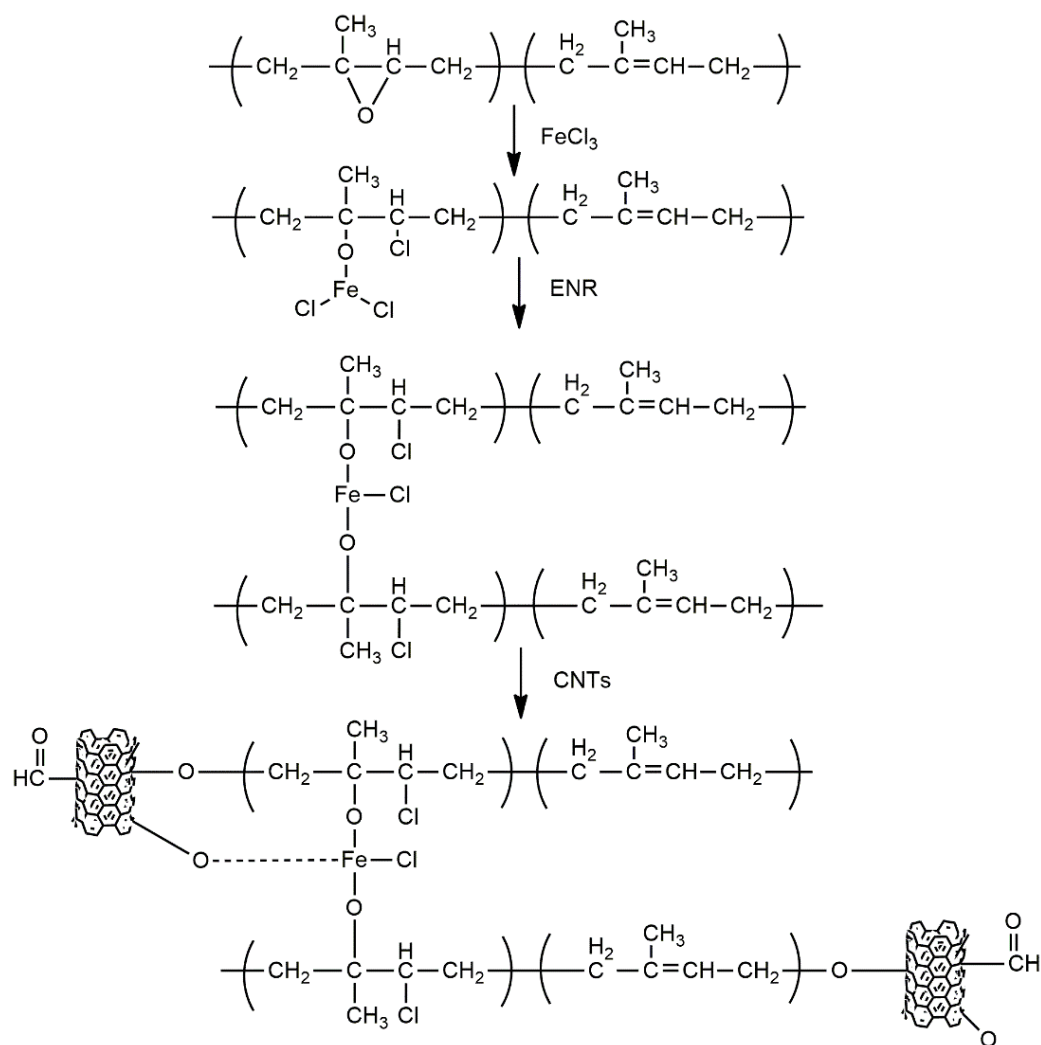
Figure 6.2 A proposed reaction mechanism among epoxidized natural rubber, ferric chloride and carbon nanotubes. The nucleophilic chloride is attached with **α** position with respect to the methyl group.
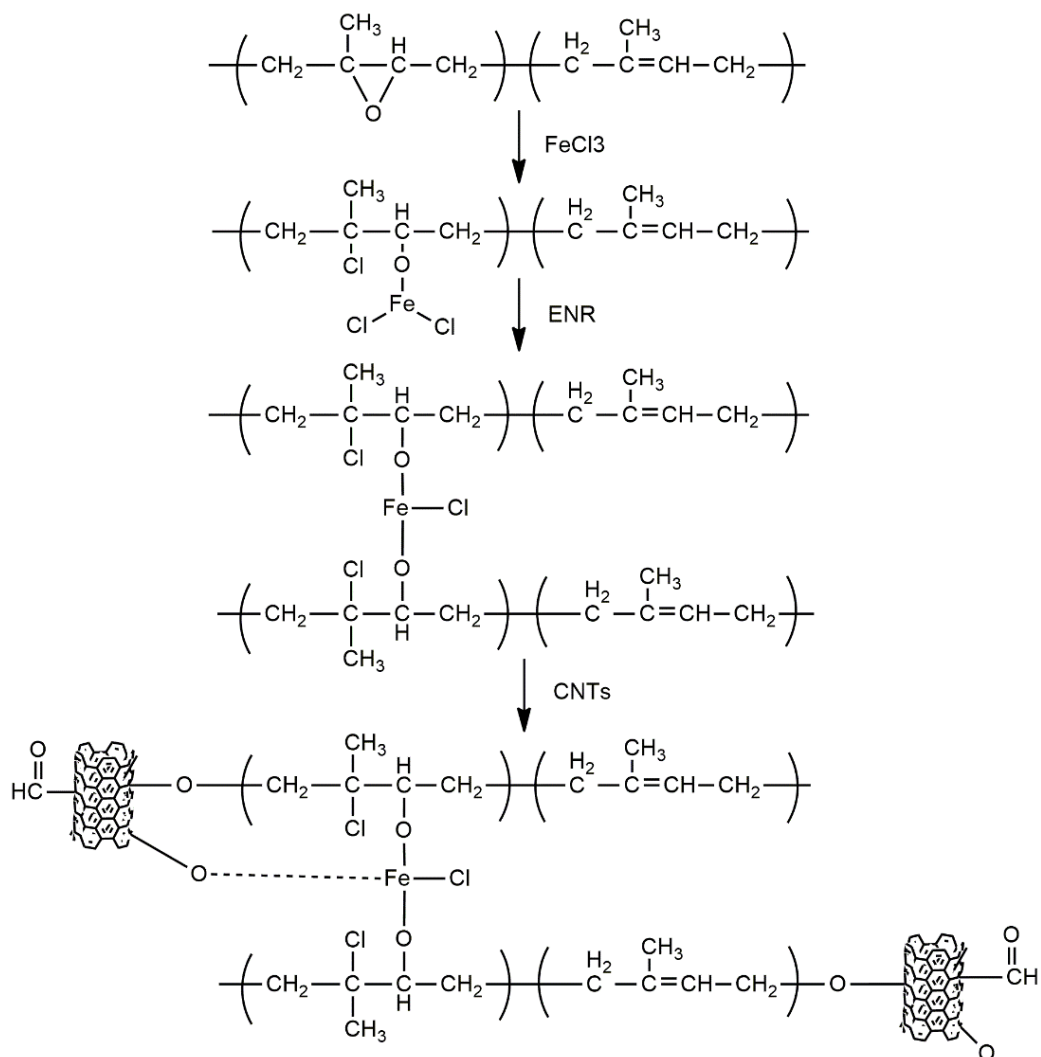
Figure 6.3 A proposed reaction mechanism among epoxidized natural rubber, ferric chloride and carbon nanotubes. The nucleophilic chloride is attached with β position with respect to the methyl group.
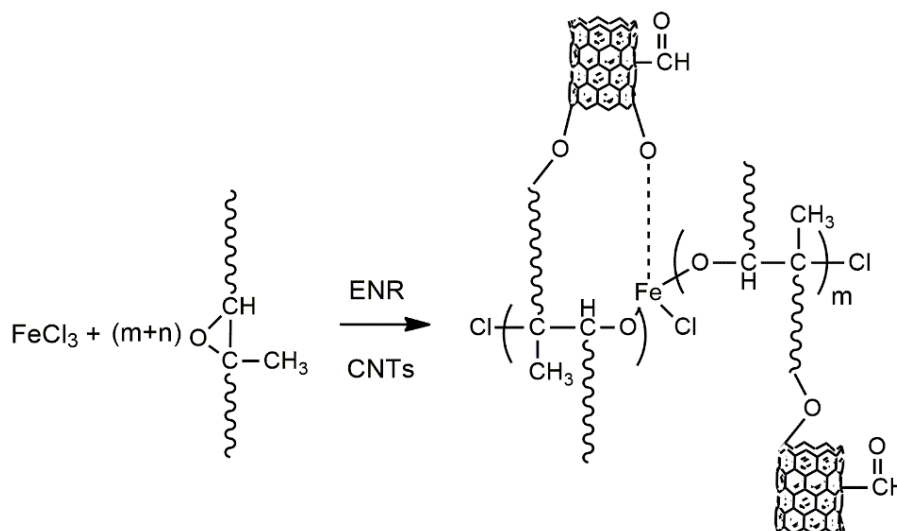
Figure 6.4 A proposed reaction mechanism of 'internal polymerization' of epoxy groups of epoxidized natural rubber with ferric chloride and carbon nanotubes.

6.3.2 Attenuated total reflection (ATR) fourier transform infrared spectrophotometry (FTIR)

The ATR-FTIR was used to identify chemical structures of ENR-FeCl$_3$ compound with 7 mmol FeCl$_3$ (F7C0) without and with 7 phr CNTs (i.e., F7C7), as the experimental procedure described in section 3.4.4. Figure 6.5 shows ATR-FTIR spectra of ENR-FeCl$_3$ compounds without and with CNTs loading at 7 phr. Also, the peak assignments for the FTIR spectra in Figure 6.5 are listed in Table 6.2. It can be seen that the absorption peaks for the characteristic of ENR molecules are seen at the wavenumbers of 1663 and 1543 cm^{-1}, which are assigned to C=C stretching and N–H bending vibrations of proteins amide II in ENR molecules, respectively (Nun‑anan *et al.*, 2019). Also, the FTIR absorption peak characteristic of ENR molecules is seen at the wavenumber of 870 cm^{-1}, which indicates the C–O stretching vibration of ENR molecules (Table 6.2). Furthermore, the absorption peaks at the wavenumbers 2825 and 2914 cm^{-1} that assign to –CH$_2$ stretching vibrations are clearly seen. In addition, the absorption peak at 2963 and 1375 cm^{-1} which are assigned to –CH$_3$ stretching vibrations and –CH$_3$ bending vibrations in the ENR molecules are also seen, respectively. In both FTIR spectra, the absorption peak at the wavenumbers of 835 cm^{-1} is also observed. It corresponds to =C–H out of plane bending in ENR molecules. Furthermore, the absorption peak at

470 cm^{-1}, which reflects the Fe–O stretching vibration in the ENR-FeCl$_3$ and Fe–O stretching vibration in the functional group on the CNTs surface are clearly seen (Biju, 2018). In Figure 6.5, it is also clear that the ENR-FeCl$_3$/CNTs nanocomposite shows significant absorption peaks at similar locations as the FTIR peaks of the ENR-FeCl$_3$ compound without CNTs but with lower peak intensities. This may be attributed to the chemical interactions of polar functional groups in ENR molecules and polar groups on the CNT surfaces. Moreover, the addition of CNTs gives rise to a new absorption peak at wavenumbers 1221 cm^{-1}, which is assigned to C–O stretching vibrations of polar functional groups on the CNTs surfaces (Coates., 2006)
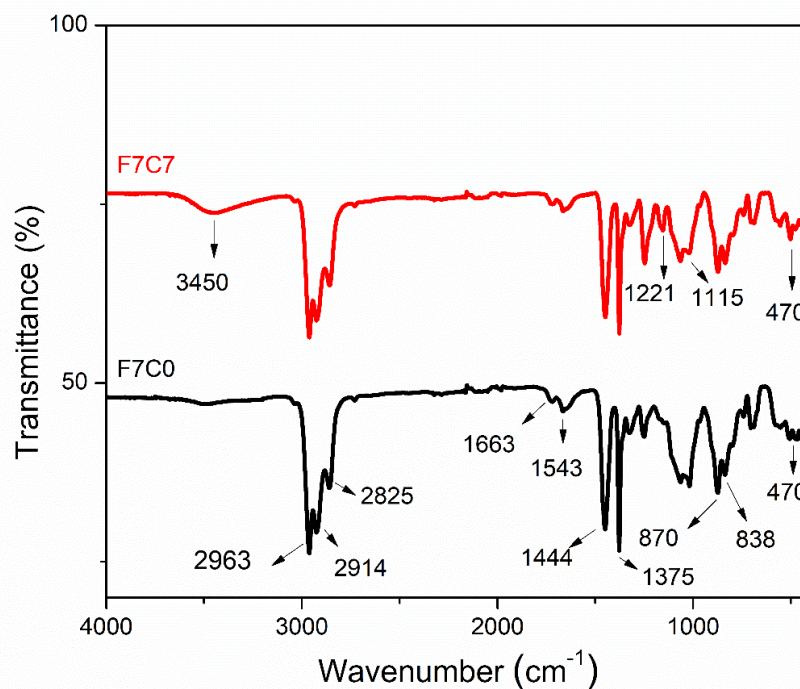
Figure 6.5 ATR-FTIR spectra of ENR-FeCl$_3$ compound with 7 mmol FeCl$_3$ (F7C0) without and with 7 phr CNTs (i.e., F7C7).

Table 6.2 Peak assignments for ENR-FeCl$_3$ compound with 7 mmol FeCl$_3$ (F7C0) without and with 7 phr CNTs (i.e., F7C7) for the FTIR spectra in Figure 6.5.

Wavenumber [cm^{-1}]	Assignment
2963	-CH$_3$ stretching vibration
2914	-CH$_2$ stretching vibration
2825	-CH$_2$ stretching vibration
1663	C=C stretching vibration
1543	N–H bending vibration of amide II
1375	-CH$_3$ bending vibration
1221	C-O stretching vibration of CNT
1115	C–O stretching vibration of CNT
870	C-O stretching vibration of ENR
835	=C-H out of plane bending
470	Fe-O stretching vibration

6.3.3 Tensile properties

Tensile properties of ENR-50 compounds were characterized as the experimental procedure described in section 3.4.2. Figure 6.6 shows stress-strain curves of ENR- FeCl$_3$ compound without CNTs (i.e., F7C0) and with various CNTs loadings at 1, 3, 5, 7 and 10 phr (i.e., F7C1, F7C3, F7C5, F7C7 and F7C10, respectively). Also, mechanical properties in terms of 100% modulus, tensile strength, elongation at break and hardness (Shore A) of various ENR-FeCl$_3$ compounds without and with CNTs are summarized in Table 6.3. It is clearly seen that the addition and increasing CNTs loadings affect the characteristic of the stress-strain behavior of ENR vulcanizates by a significant increase in Young's moduli (i.e., slope at the initial part of the curves), 100% moduli, and tensile strength as compared with the F7C0 compound without CNTs (Table 6.3). This is due to the formation of stronger three-dimensional networks based on the reaction of Fe^{3+} and oxirane rings and the internal polymerization of oxirane groups in ENR molecules. Furthermore, higher chemical interaction among the polar functional groups at the CNTs surfaces and oxirane rings in ENR molecules causes

higher reinforcement as increasing of the CNTs loadings. In Figure 6.6 and Table 6.3, it is also seen that a decrease in elongation at break is seen upon increasing of CNTs loadings. However, similar levels of moduli, tensile strength and elongation at break are seen in the ENR-FeCl$_3$/CNTs nanocomposites with CNTs loadings at 7 and 10 phr. This may be due to the re-agglomeration of CNTs owing to an excess amount of solid particulates inside the ENR matrix. In Table 6.3, it is also clear that the hardness of the ENR-FeCl$_3$/CNTs nanocomposites increases with an increase in CNTs loadings. This is attributed to an increase in the degree of crosslinks between ENR-50 molecules via –O–Fe–O– linkages, and internal polymerization of the epoxirane rings. Also, the chemical interaction among polar functional groups in ENR and CNTs, together with higher rigidity due to a higher amount of solid CNTs are other main reasons for an increase in hardness.
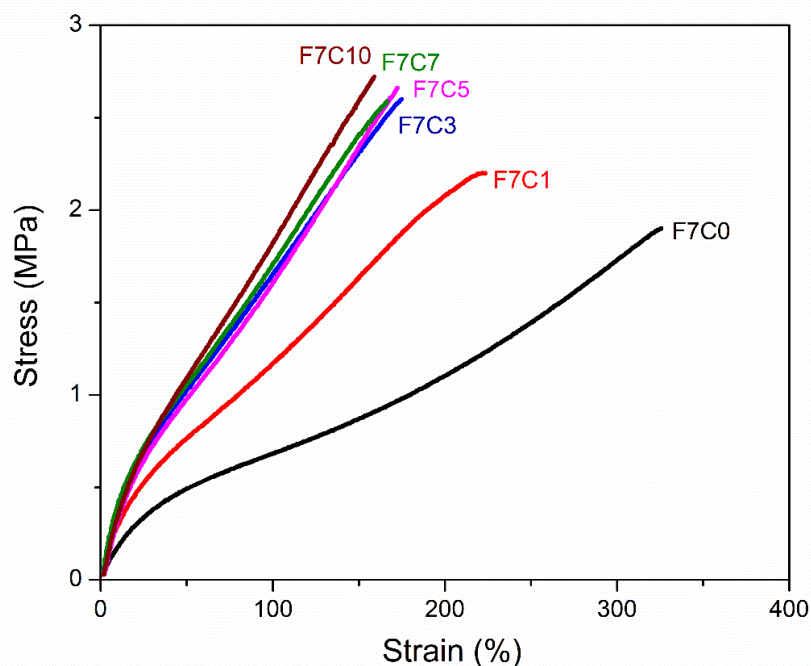
Figure 6.6 Stress-strain curves of ENR-FeCl$_3$ compound without (F7C0) and with various CNTs loadings at 1, 3, 5, 7 and 10 phr as denoted by F7C1, F7C3, F7C5, F7C7 and F7C10, respectively.

Table 6.3 Mechanical properties in terms of 100% modulus, tensile strength, elongation at break and hardness (Shore A) of ENR-FeCl$_3$ compounds without (F7C0) and with CNTs at 1, 3, 5, 7 and 10 phr (i.e., F7C1, F7C3, F7C5, F7C7 and F7C10, respectively).

Materials	100% Modulus (MPa)	Tensile Strength (MPa)	Elongation at Break (%)	Hardness (Shore A)
F7C0	0.89±0.18	1.89±0.11	325.70±20.21	44.50±1.00
F7C1	1.17±0.22	2.20±0.35	223.14±18.51	45.60±1.10
F7C3	1.65±0.15	2.60±0.23	174.88±22.23	58.30±3.10
F7C5	1.71±0.10	2.71±0.17	174.50±15.59	61.10±1.50
F7C7	1.72±0.13	2.76±0.24	166.16±17.72	73.70±1.30
F7C10	1.75±0.18	2.81±0.43	166.25±13.32	76.60±2.00

6.3.4 Payne effect

The Payne effect of ENR compounds were determined based on relationship between storage modulus as a function of strain amplitude using RPA test, as the experimental procedure described in section 3.4.7.2. Figure 6.7 shows the storage modulus (G') as a function of strain amplitude of ENR-FeCl$_3$ with 7 mmol of FeCl$_3$ (F7C0) without and with various CNTs loadings at 1, 3, 5, 7 and 10 phr. It can be seen that the F7C0 compound without CNTs exhibits the lowest storage modulus at a given strain amplitude. However, the storage modulus is increased after the incorporation of CNTs and increasing CNTs loadings. The storage moduli of all samples showed a decreasing trend as increasing strain amplitude over 10% magnitude. This may be due to the shearing forces causing breaking down of the CNTs networks or agglomerates under high temperature conditions (Das *et al*., 2009). The Payne effect has been typically used to verify the filler-filler and filler-rubber interactions in a rubber composite (Payne, 1966). It can be assessed from a decreasing trend of the storage modulus (G') as increasing the strain amplitudes.

In Figure 6.7, a slight decreasing trend of storage modulus is also seen in the F7C0 compound without CNTs. It may arise from the chain disentanglement of ENR molecules together with a breakdown of crosslinked networks under high shear stress and high heat conditions (Kołodziejczak *et al*., 2012). On the other hand, the ENR-FeCl$_3$/CNTs nanocomposites show the typical Payne effect, which indicates the breakdown of filler-filler interactions. It is clear in Figure 6.7 that the Payne effect is more prominent in the nanocomposites with higher CNTs loadings. Table 6.4 shows storage moduli at very low strain (G′0.56) and at very high strain amplitudes (G′100), as well as the storage modulus difference (ΔG′) of the ENR-FeCl$_3$ compound with 7 mmol of FeCl$_3$ (F7C0) without and with various CNT loadings at 1, 3, 5, 7 and 10 phr. It can be seen that a strong decrease in storage modulus with an increase in the Payne effect in terms of the difference in storage modulus (*ΔG′*) is clearly seen with increasing in the CNTs loadings. This implies that strong CNTs agglomeration is present in the ENR matrix with higher CNTs loadings (Subramaniam *et al*., 2013). Moreover, the lowest Payne effect was observed in the F7C0 without CNTs (*ΔG′* = 0.01). This is due to solely the breakdown of molecular chain entanglement of ENR molecules and of the linkages in ENR crosslinking networks, and also a breakdown of small FeCl$_3$ clusters that remain in the ENR matrix. Therefore, it is concluded that the higher Payne effect in ENR-FeCl$_3$/CNTs nanocomposites relates to the breakdown of strong filler-filler interactions (Fröhlich *et al.,* 2005).
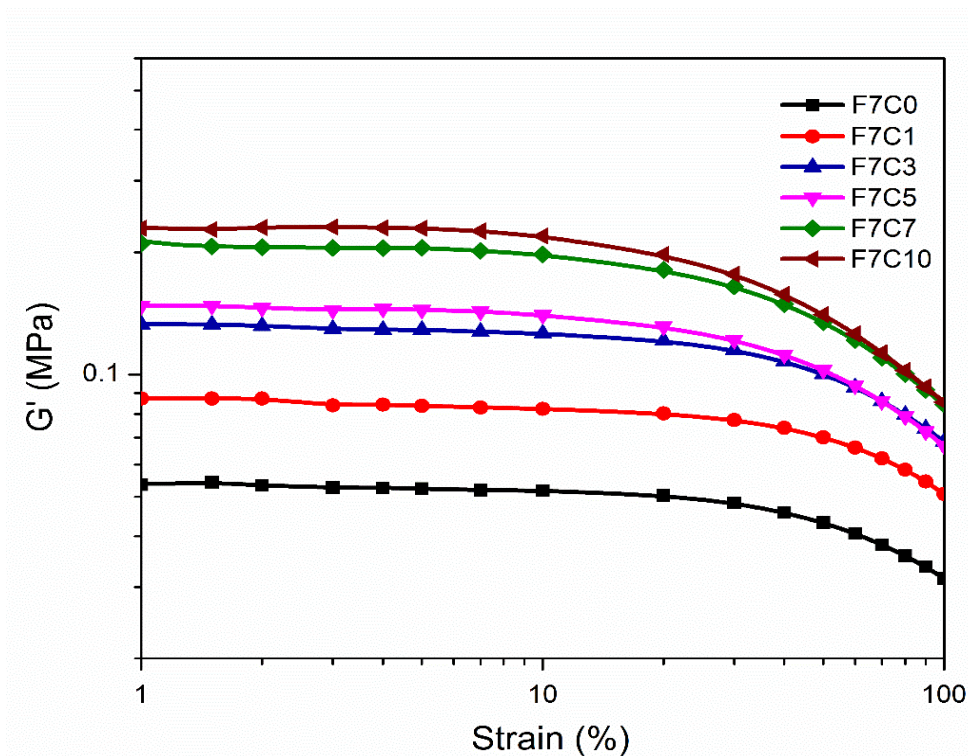
Figure 6.7 Storage modulus as a function of strain amplitude of ENR-FeCl$_3$ compound with 7 mmol of FeCl$_3$ (F7C0) without and with different CNTs loadings.

Table 6.4 Storage modulus at very low strain ($G'0.56$) and at very high strain ($G'100$), and their difference ($\Delta G'$) of ENR-FeCl$_3$ compound without and with CNTs.

Compounds	G'_0	G'_{100}	$\Delta G'$
F7C0	0.04	0.03	0.01
F7C1	0.09	0.05	0.04
F7C3	0.13	0.07	0.06
F7C5	0.17	0.07	0.10
F7C7	0.20	0.08	0.12
F7C10	0.25	0.09	0.16

6.3.5 Morphological properties

Morphological properties of ENR compounds were determined by using SEM, as the experimental procedure described in section 3.4.6. Figure 6.8 shows SEM micrographs of ENR-FeCl$_3$ compound without and with different CNTs loadings at 1, 3, 5, 7, and 10 phr. It can be seen that F7C0 without CNTs shows homogeneous dispersion of solid particles of FeCl$_3$ in the ENR matrix (Figure 6.8(a)). However, in the ENR-FeCl$_3$/CNTs nanocomposites with CNTs loadings at 1, 3, 5 and 7 phr, large agglomerates are absent rather, some small CNTs aggregates are clearly seen in Figure 6.8(b) to Figure 6.8(e). This indicates good dispersion of CNTs in ENR-FeCl$_3$ and may be good compatibility between CNTs and the ENR-FeCl$_3$ compounds. On the other hand, in Figure 6.8(f), large agglomerates are clearly seen in the ENR-FeCl$_3$ compound with 10 phr of CNTs. This is due to re-agglomeration of excess amount of CNTs in the ENR matrix, causing poorer dispersion, distribution and hence stronger CNTs agglomeration in ENR matrix.
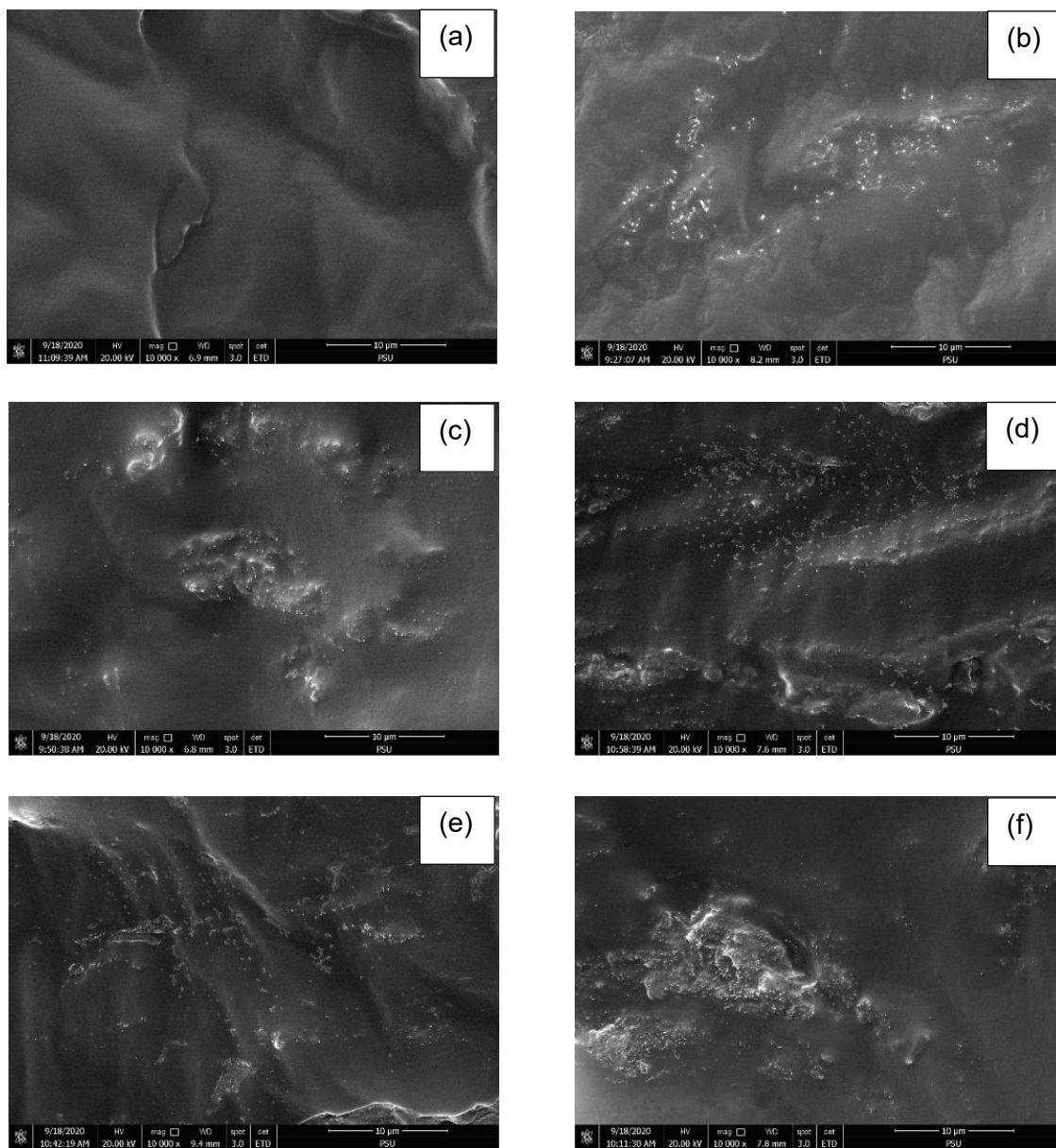
Figure 6.8 SEM micrographs of ENR-FeCl$_3$ compound with 7 mmol of FeCl (F7C0) without (a) and with various CNTs loadings at 1 phr (b), 3 phr (c), 5 phr (d), 7 phr (e), and 10 phr (f)

6.3.6 Bound rubber contents

Bound rubber contents of ENR-50 compounds were characterized as the experimental procedure described in section 3.4.9. Table 6.5 shows the bound rubber/gel content contents of ENR-FeCl$_3$ compound without and with various CNTs contents. It is found that the F7C0 sample without CNTs shows a slight gel-like content in the bound rubber experiment. In the present case, most probably, FeCl$_3$ started to react with epoxy group even at room temperature or during the shear mixing condition, resulting in a gel-like formation in the experiment. It is noted that the presence of FeCl$_3$ is also cannot be ruled out. It is clearly seen that the bound rubber content increases with an increase in CNTs loadings. This is due to an increase in filler-rubber interactions between ENR and polar functional groups at the CNTs surface. It is also seen that the ENR-FeCl$_3$ compound with CNTs showed much larger bound rubber contents than that of the ENR-FeCl$_3$ compound without CNTs, especially in the ENR nanocomposite with CNTs loadings higher than 5 phr. Also, the ENR-FeCl$_3$/CNTs nanocomposite with 7 phr of CNTs reaches the optimum bound rubber content due to the finer dispersion and distribution of CNTs in the ENR matrix are clearly seen in Figure 6.8. Increasing CNTs loading to 10 phr causes a small increase in bound rubber content due to the large agglomeration of CNTs, as shown in Figure 6.8(e)

Table 6.5 Bound rubber contents of ENR-FeCl$_3$ compound with FeCl$_3$ without and with various CNTs loadings determined by equilibrium swelling measurements.

Sample	Bound rubber contents (%)
F7C0	1.09
F7C1	18.79
F7C3	22.37
F7C5	36.17
F7C7	42.31
F7C10	42.56

6.3.7   Thermogravimetric analysis (TGA)

Thermogravimetric analysis (TGA) of ENR-50 compounds and its CNTs nanocomposites were performed, as the experimental procedure described in section 3.4.8. Figure 6.9 shows the TGA and DTG thermograms of the ENR-FeCl$_3$ compound without and with various concentrations of CNTs at 1, 3, 5, 7 and 10 phr. It is noted that two steps TGA was performed first under a nitrogen atmosphere in the temperature range 30–600°C, before switching to an oxygen atmosphere and heated until 900°C with the same heating rate at 10 °C/min. In Figure 6.9 (a), the first degradation step under N$_2$ atmosphere of various ENR compounds is seen in the temperature range of 255–265°C. This is clearly indicated by the first DTG peaks in Figure 6.9 (b) and T_{d1} in Table 6.6, which associates to the dissociation of water molecules in the crystal structure of FeCl$_3$. (Damampai *et al.*, 2021) In addition, the second DTG peaks are seen at around 420–430°C (i.e., T_{d2} in Table 6.6), due to the decomposition of the hydrocarbon in ENR molecules. It is clear that the second degradation peak height decreases with the increase of the CNTs loading. This is activated by higher thermal conductivity due to FeCl$_3$ and CNTs particles which are thoroughly dispersed in the ENR matrix.
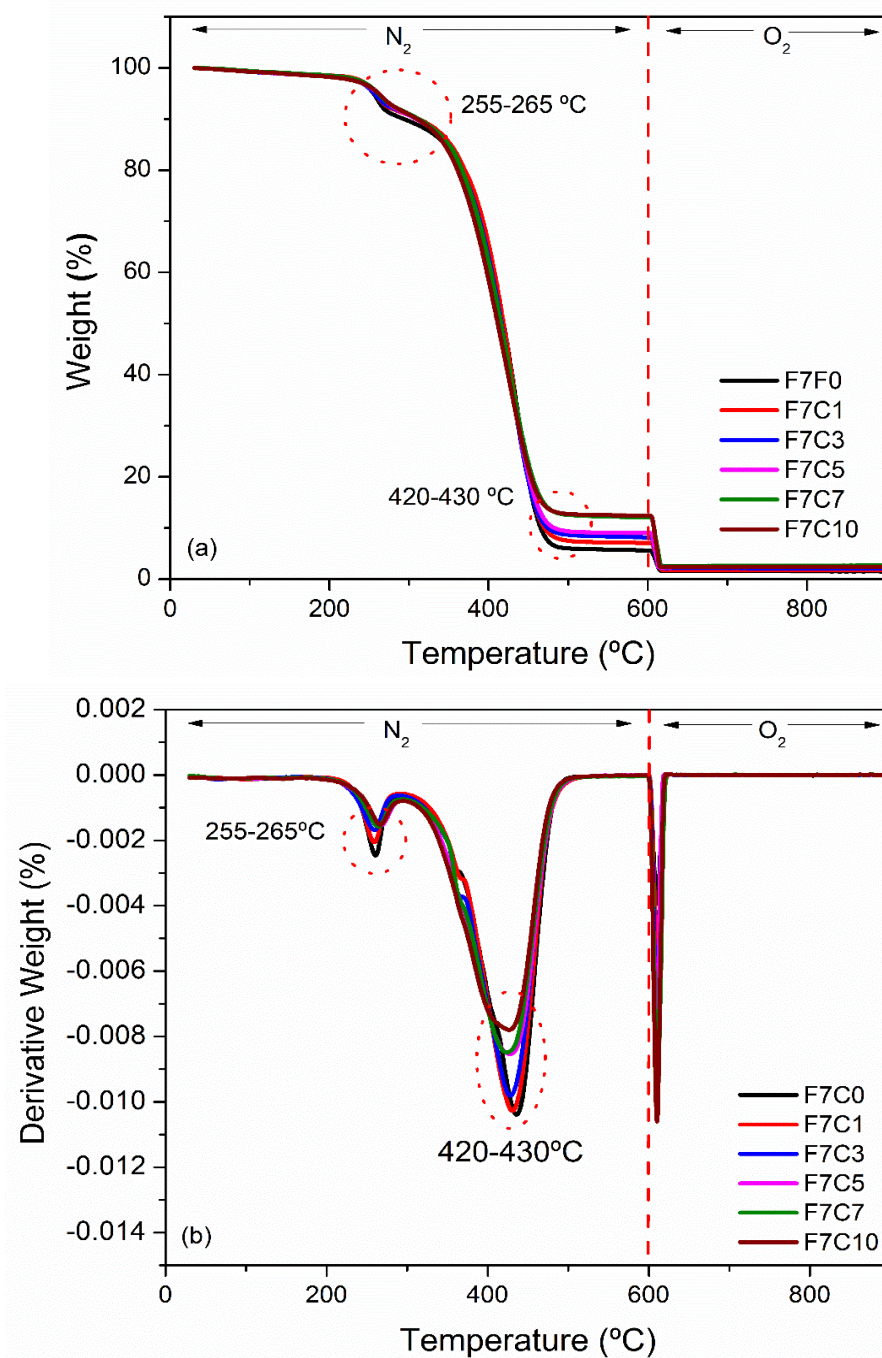
Figure 6.9 TGA (a) and DTG thermograms (a) of ENR-FeCl$_3$ compound with 7 mmol of FeCl$_3$ (F7C0) without and with different loadings of CNTs at 1, 3, 5, 7 and 10 phr.

Table 6.6 Degradation temperature (T_d) and weight losses of ENR-50 compound with 7 mmol of FeCl$_3$ (F7C0) without and with various CNTs loadings at 1, 3, 5, 7 and 10 phr.

Sample	T_{d1} (°C)	T_{d2} (°C)	weight loss (%) under the nitrogen atmosphere	weight loss (%) under the oxygen atmosphere
F7C0	258.67	430.34	90.14	1.15
F7C1	259.91	429.01	91.24	1.99
F7C3	260.11	427.78	91.37	2.03
F7C5	260.75	425.56	91.89	2.34
F7C7	261.21	424.21	91.93	2.62
F7C10	261.36	420.06	92.48	2.67

6.3.8   Dynamic mechanical analysis (DMA)

Dynamic mechanical analysis (DMA) of ENR-50 compounds were performed, as the experimental procedure described in section 3.4.7.1. Figure 6.10 shows storage modulus (E′) and loss tangent (tan **δ**) as a function of temperature for ENR-FeCl$_3$ compound without (F7C0) and with various CNTs loadings at 1, 3, 5, 7 and 10 phr. It can be seen that the storage moduli in the glassy region of ENR-FeCl$_3$/CNTs composites are higher than the F7C0 without CNTs. Also, the storage moduli increase with an increase in CNTs loadings. This may be due to higher reinforcement of ENR by CNTs particles, resulting in stronger CNTs and rubbery network Also, more solid CNTs contents in the ENR nanocomposites cause the formation of higher stiffness materials.

In Figure 6.10, it is also seen that the addition of CNTs in ENR causes shifting of the tan δ peaks (Figure 6.10(b)) and glass transition temperature (T_g) (Table 6.7) toward higher temperature ranges as compared with the F7C0 without CNTs. This is attributed to more rigid ENR molecular networks with an increase in CNTs loadings due to interaction among polar functional groups at CNTs surfaces and the polar groups in ENR molecules. Even more free volume is obvious in the ENR matrix due to CNTs agglomeration with high CNTs loadings that may cause molecular rubber chains to move more freely. However, the influence of chemical interaction on the thermal properties of the ENR-FeCl$_3$/CNTs may play a more significant role. It results in an increase in T_g of ENR-FeCl$_3$/CNTs nanocomposites with increasing of CNTs loadings.
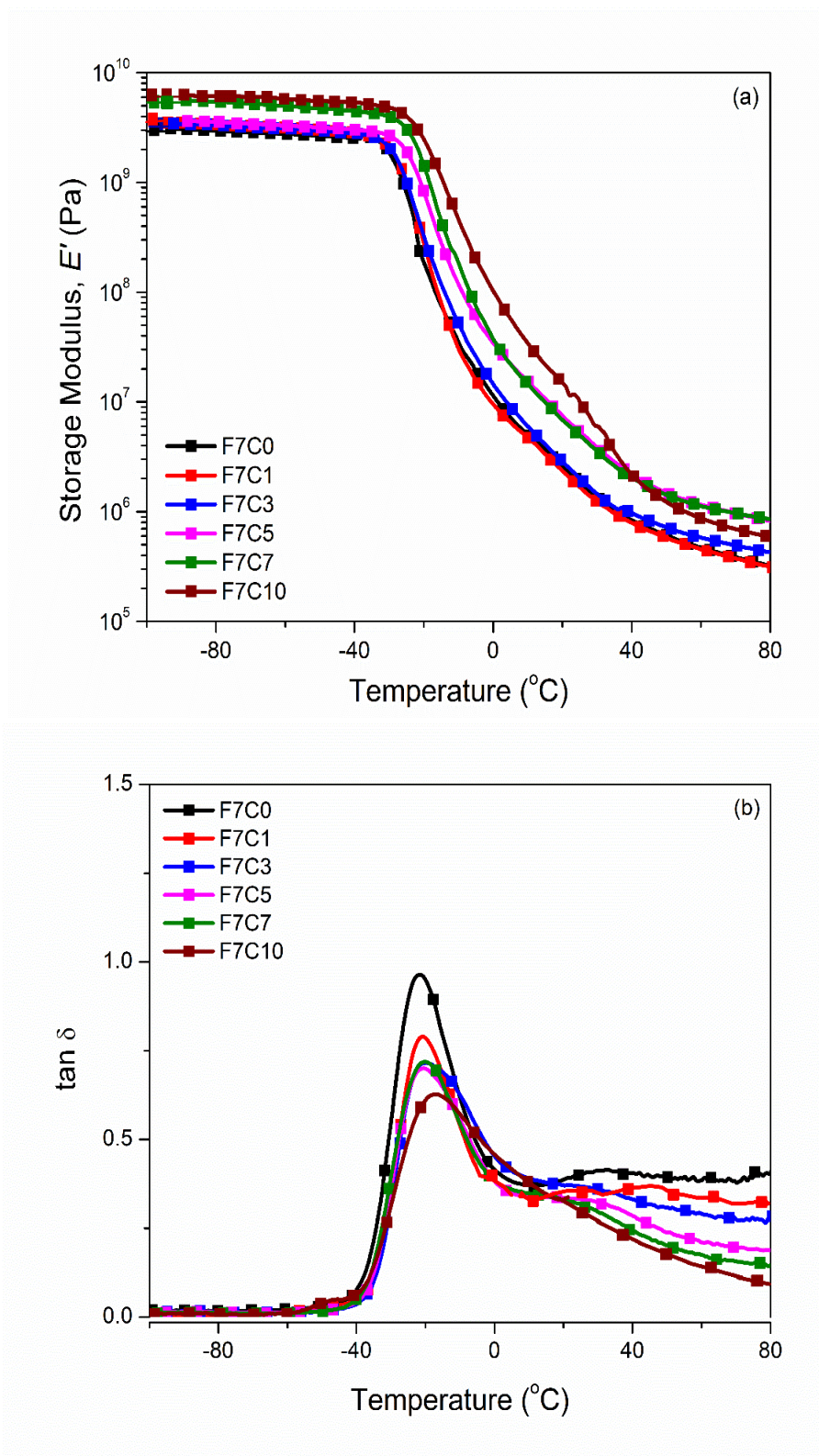
Figure 6.10 Storage modulus (a) and tan **δ** (b) as a function of the temperature of ENR-FeCl$_3$ compound with 7 mmol of FeCl$_3$ (F7C0) without and with various CNTs loadings at 1, 3, 5, 7 and 10 phr.

Table 6.7 Glass transition temperature (T_g) of ENR-50 compound with 7 mmol of $FeCl_3$ (F7C0) without and with various CNTs loadings at 1, 3, 5, 7 and 10 phr.

Samples	Glass transition temperature ($^\circ$C)
F7C0	-20.3
F7C1	-20.1
F7C3	-19.7
F7C5	-19.0
F7C7	-18.3
F7C10	-17.1

6.3.9 Electrical properties

Electrical properties of ENR-50 compounds were determined as the experimental procedure described in section 3.4.11. Figure 6.11 shows electrical conductivity as a function of the frequency of ENR-$FeCl_3$ compound with 7 mmol of $FeCl_3$ (F7C0) without and with various CNTs loadings at 1, 3, 5, 7 and 10 phr. It is seen that the electrical conductivity-frequency curves of the ENR-$FeCl_3$/CNTs nanocomposites are located above the curve of the neat ENR-50 and F7C0 without CNTs. Also, it is clearly seen that the incorporation of CNTs in ENR causes a sudden improvement of the electrical conductivity of the ENR-$FeCl_3$ compound. In addition, the electrical conductivity increases with increasing concentrations of CNTs. Figure 6.12 shows the electrical conductivity at a frequency of 50 Hz at various CNTs loadings as compared with the neat ENR-50 and F7C0 compound without CNTs. It is clearly seen that the neat ENR-50 shows very low electrical conductivity (about $1.09 \cdot 10^{-9}$ S/cm). However, an abrupt increase in electrical conductivity to about $8.75 \cdot 10^{-6}$ S/cm is seen upon the addition of $FeCl_3$ in ENR to form F7C0. This is due to the higher electrical conductivity of Fe^{3+} that is present in the ENR matrix. Furthermore, electrical conductivity is gradually increased again with the incorporation of 1 phr of CNTs in the ENR matrix. This may be due to the higher electrical conductivity of CNTs networks in the ENR matrix. In Figure 6.12, it is also seen that an increase in CNTs loadings from 1

to 5 phr, cause a marginal increase in the electrical conductivity. However, a sudden increase in electrical conductivity is seen after adding of CNTs beyond 5 phr due to the formation of conductive CNTs networks. Therefore, the CNTs networks act as the bridge to carry electron charges throughout the ENR matrix, causing powerful transfers of electrons and significantly enhancing the electrical conductivity of the composites. It is noted that the CNTs concentration that causes the formation of the fully CNTs network is called the percolation threshold concentration (PTC), which is about 7 phr of CNTs in this case (Figure 6.12). In such a case, three-dimensional CNTs networks are successfully formed in the ENR matrix. This may be attributed to strong filler-rubber interactions between oxirane rings in ENR molecules and polar functional groups on CNT surfaces. Figure 6.13 shows the dielectric constant as a function of the frequency of the neat ENR-50 and ENR-FeCl$_3$ with 7 mmol of FeCl$_3$ (F7C0) without and with various CNTs. It is seen that the neat ENR-50 shows an independent dielectric constant with frequency. This may be due to poor polarization of the ENR molecular chains (Salaeh *et al*., 2011). Moreover, the ENR-FeCl$_3$ has a higher dielectric constant than the neat ENR-50. It corresponds to the trend of electrical conductivity (Figure 6.11). In addition, the dielectric constant of the ENR-FeCl$_3$/CNTs compounds show a significantly increasing trend as the CNTs loading increases. It may be attributed to the sp^2 - hybridization in CNTs with abundant numbers of free electrons forming electric dipoles (Krainoi *et al.,* 2018).
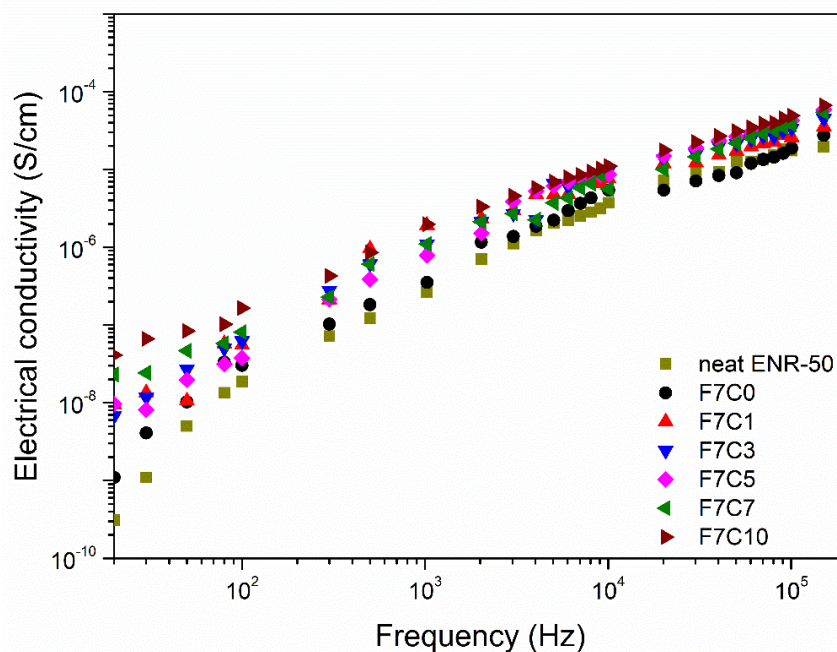
Figure 6.11 Electrical conductivity as a function of frequency of ENR-FeCl$_3$ compound with 7 mmol of FeCl$_3$ (F7C0) without and with various CNTs loadings at 1, 3, 5, 7 and 10 phr
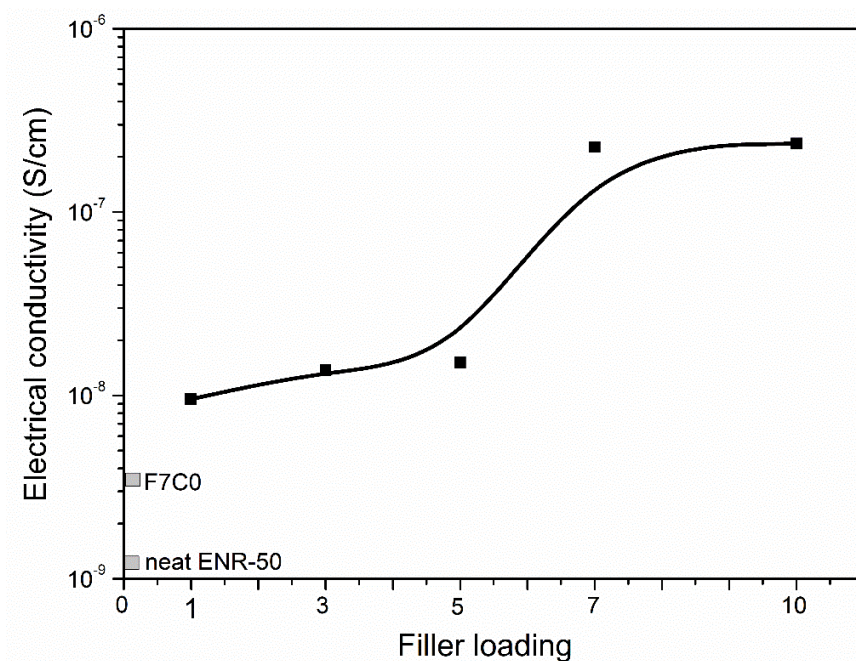
Figure 6.12 Electrical conductivity at a frequency at 50 Hz of neat ENR-50, ENR-FeCl$_3$ compound with 7 mmol of FeCl$_3$ (F7C0) with various CNTs loadings at 1, 3, 5, 7 and 10 phr.
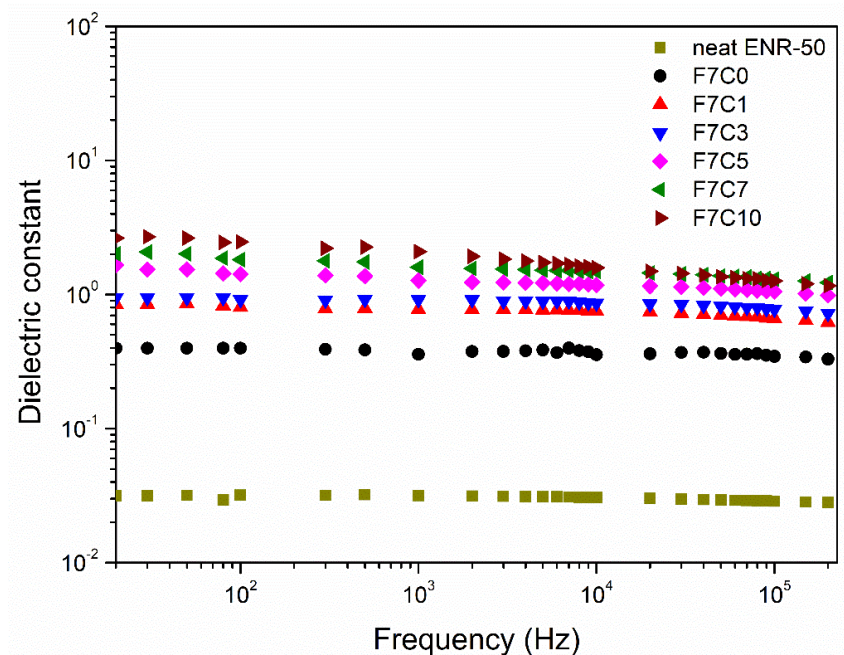
Figure 6.13 Dielectric constant as a function of the frequency of neat ENR-50, ENR-FeCl$_3$ compound with 7 mmol of FeCl$_3$ (F7C0) without and with various CNTs loading at 1, 3, 5, 7 and 10 phr.

6.4   Conclusions

ENR-50 was successfully crosslinked by Fe^{3+} ion of FeCl$_3$ to form the coordination crosslinks (–O–Fe–O– linkages) between ENR molecules and to form internal polymerized oxirane groups of ENR molecules. In addition, the incorporation of CNTs improves various properties of ENR-FeCl$_3$ compounds, including tensile strength, dynamic properties, electrical conductivity, and thermal properties. It is clearly seen that the ENR-FeCl$_3$ compounds filled with various CNTs loadings have higher torque differences and mechanical properties than the ones without CNTs. This is due to higher contents of the crosslinking structures of ENR, the three-dimensional CNTs networks, and the reinforcement effect of CNTs in the ENR matrix. SEM micrographs reveal very small CNTs aggregates in the ENR-FeCl$_3$ compounds with 5 and 7 phr of CNTs loadings, which indicate good dispersions of CNTs in the ENR matrix. However, ENR-FeCl$_3$ compound with 10 phr of CNTs shows a large agglomerate due to re-agglomerates of CNTs. According to DMA, glass transition temperature (T_g) increases

with an increase in CNTs loadings due to more restrictions on chain mobility of ENR molecules. Furthermore, the ENR-FeCl$_3$/CNTs nanocomposites show improvement of storage modulus, 100% moduli, electrical conductivity, and dielectric constant as compared with the ENR-FeCl$_3$ compound without CNTs. It was also found that the ENR-FeCl$_3$/CNTs nanocomposites have the percolation threshold concentration at about 7 phr of CNTs. It indicates the presence of the three-dimensional network, which is in agreement with the morphological properties. Also, the thermal resistance of ENR-FeCl$_3$/CNTs nanocomposites increases with an increase in CNTs loadings. This is due to the higher content of the coordination linkages of ENR-FeCl$_3$ and reinforced by CNTs.

CHAPTER   7

CROSSLINKED EPOXIDIZED NATURAL RUBBER BY FERRIC CHLORIDE FILLED WITH CARBON NANOTUBES AND CONDUCTIVE CARBON BLACK HYBRID FILLER

7.1   Introduction

Epoxidized natural rubber (ENR) has been generally reinforced by various fillers, including montmorillonite clay (Yokkhun *et al*., 2013), conductive carbon black (CCB) (Matchawet *et al*., 2015), geopolymers (Yangthong *et al*., 2019), and carbon nanotubes (CNTs) (Krainoi *et al*., 2018). Carbon nanotubes were first discovered in 1991 (Subramaniam *et al*., 2013) and it can enhance several epoxidized natural rubber composite properties, including mechanical properties, electrical conductivity and thermal stability (Krainoi *et al*., 2018). However, the mechanical properties of the developed rubber composites typically depend on the quality of the dispersion and distribution of filler in the rubber matrix. It is noted that CNTs have a high aspect ratio and strong van der Waals forces, causing strong agglomeration by bonding together in the rubber matrix and hence causes inferior mechanical properties (Subramaniam *et al*., 2013; Le *et al*., 2012; Steinhauser *et al*., 2012). Thus, incorporation of a second filler into the rubber–CNT composite system may improve the CNTs' dispersion and distribution and enhance the mechanical properties, thermal stability, electrical conductivity and other related properties (Rooj *et al*., 2015; Poikelispää *et al*., 2013; Iijima *et al*., 1991). Various types of hybrid fillers have been investigated in polymer systems containing CNT filled ENR and epoxy, including carbon black (Socher *et al*., 2011; Zhang *et al*., 2012), nano-clay (NC) (Bao *et al*., 2009), graphene nano platelets (Chen *et al*., 2019), zinc oxide (Thongkong *et al*., 2020), silver nanoparticles (AgNPs) (Krainoi *et al*., 2018) and conductive carbon black (CCB) (Nakaramontri *et al*., 2017). It was found that the secondary filler generally contributes to improve the CNTs' dispersion in the rubber matrix (Nakaramontri *et al*., 2017). Moreover, they could connect to the CNT encapsulates and form conductive CNT–CCB–CNT pathways in the ENR composites, causing significant improvement in the electrical conductivity (Nakaramontri *et al*., 2017). The novelty of the current work is that we are the first to study the influence of CNT–CCB hybrid fillers for the reinforcement of epoxidized

natural rubber (ENR) crosslinked by coordination bonds via Fe^{3+} linkages. Furthermore, CCB in the hybrid filler system provides a new filler network of CNTs by connecting the CNT bundles, promoting superior electrical and mechanical properties of ENR nanocomposites.

In this work, therefore, epoxidized natural rubber (ENR) was crosslinked after compounding with Fe^{3+} from ferric chloride ($FeCl_3$) and then reinforced with a hybrid filler system that consists of carbon nanotubes (CNTs) and conductive carbon black (CCB). The main aim was to increase filler–rubber interactions between the different filler particles and the rubber matrix in order to form a three-dimensional filler network with high electrical conductivities and tensile properties. Furthermore, cure characteristics, mechanical properties, crosslink densities, bound rubber content, temperature scanning stress relaxation (TSSR), dynamic properties and electrical conductivity were investigated.

7.2 Preparation of CNTs/CCB hybrid filler filled ENR crosslinked by ferric chloride

The ENR-$FeCl_3$ compounds filled with CNTs/CCB hybrid filler with different CCB loadings were prepared by mixing method according to the experimental procedure described in section 3.3.4.

7.3 Testing and characterization

ENR-50 compounds with a fixed amount of 7 mmol $FeCl_3$, 7 phr CNTs and mixed with various CCB hybrid filler loadings at 2.5, 5.0, 7.0, 10.0 and 15.0 phr (i.e., CNT7/CCB2.5, CNT7/CCB5.0, CNT7/CCB7.0, CNT7/CCB10.0 and CNT7/CCB15.0, respectively), according to the experimental procedure described in section 3.4

7.3.1 Cure characteristics

Curing characteristics of various ENR compounds were determined by using an MDR test, as the experimental procedure described in section 3.4.1. Figure 7.1 shows the cure curves of ENR filled with CNTs (without $FeCl_3$), ENR filled with CNT–CCB hybrid filler (without $FeCl_3$), ENR–$FeCl_3$ filled with CNTs without CCB (F7-CNT7) and with 7 phr CNTs in combination with various CCB loadings at 2.5, 5.0, 7.0, 10.0 and 15.0 phr (i.e., CNT7/CCB2.5, CNT7/CCB5.0, CNT7/CCB7.0, CNT7/CCB10.0 and CNT7/CCB15.0, respectively). It can be seen that the ENR-50 (without $FeCl_3$) filled with CNTs and CNT–CCB hybrid filler had no response in the cure curve. This is attributed to the absence of a crosslinking reaction between ENR molecules. However, a curing reaction of ENR-50 with 7 mmol $FeCl_3$ (ENR–$FeCl_3$) filled with 7 phr CNTs (F7-CNT7) is observed from increasing torque with time. This is attributed to the chemical reaction between oxirane rings in ENR molecules and Fe^{3+} ion to form rubber network structures via –O–Fe–O– coordination linkages (Damampai *et al.*, 2021). Moreover, the internal polymerization from the reaction of ENR with epoxy groups in the presence of $FeCl_3$ could take place, resulting in many complicated polymeric microstructures, a mixture of isomeric and homologous compounds (Bořkovec., 1958). This results in strong crosslinking structures in ENR molecules (Damampai *et al.*, 2021 and 2022). Furthermore, the ENR–$FeCl_3$ filled with 7 phr of CNTs and CNT–CCB hybrid fillers with various CCB loadings show increased mixing torque–time curves with increasing CCB loadings. The matching curing curves, i.e., increasing torque with time, are clearly seen in Figure 7.1. This may be because the crosslinking reaction might require a longer time to complete its reaction to approach the equilibrium state.
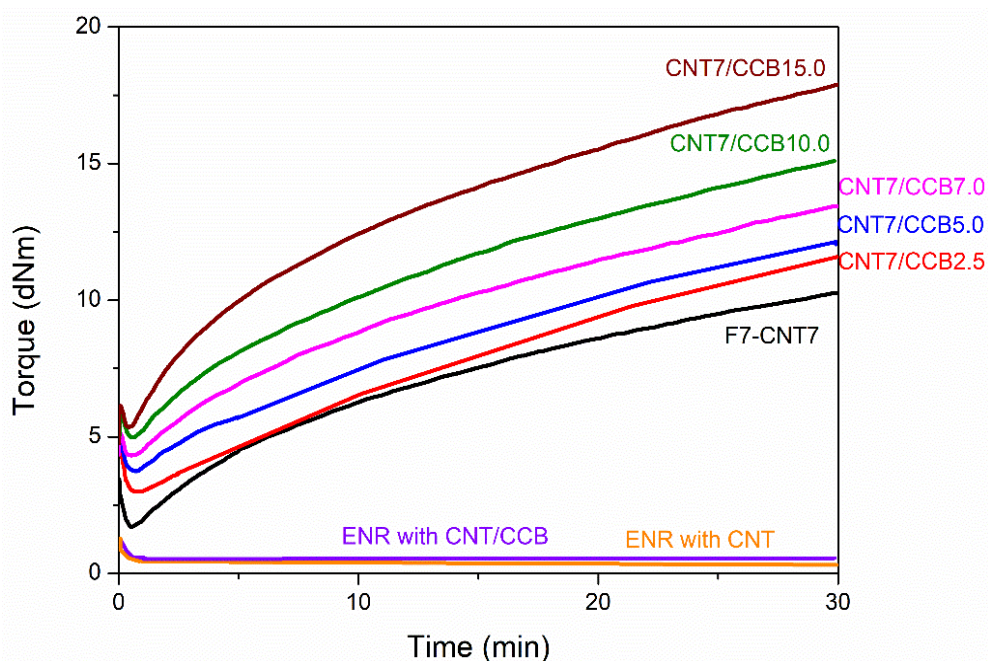
Figure 7.1 Mixing torque-time curves of ENR with CNT (without $FeCl_3$), ENR with CNT/CCB (without $FeCl_3$), ENR-$FeCl_3$ with CNT without CCB (F7-CNT7) and ENR-$FeCl_3$ with 7 phr CNT and various CCB loadings at 2.5, 5.0, 7.0, 10.0 and 15.0 (i.e., CNT7/CCB2.5, CNT7/CCB5.0, CNT7/CCB7.0, CNT7/CCB10.0 and CNT7/CCB15.0).

Table 7.1 shows the curing data of the ENR compounds. The values of minimum torque (M_L), maximum torque (M_H), torque difference (M_H-M_L), scorch time (t_{s2}) and cure time (t_{c90}) are extracted from the rheometric curing curves. A maximum torque and torque difference of the ENR–$FeCl_3$ filled with CNTs (i.e., F7-CNT7) had the lowest values, but these properties were higher with incorporating and increasing CCB loadings. This is due to a finer filler dispersion and distribution in the ENR matrix. That is, the CCB particles might hinder the CNTs' agglomeration. Therefore, the CCB secondary filler contributes to improving the CNTs' dispersion and distribution in the rubber matrix by connecting to the CNT encapsulates and forming CNT–CCB–CNT pathways in the ENR matrix, causing significant improvements in the maximum torque and torque difference (Nakaramontri *et al.*, 2017).

Table 7.1 Cure characteristics in terms of minimum torque (M_L), maximum torque (M_H), torque difference (M_H-M_L), scorch time (T_{s2}) and cure time (T_{c90}) of ENR-50 compounded with $FeCl_3$ (ENR-$FeCl_3$) and mixed with CNTs and (F7-CNT7) and CNTs/CCB hybrid fillers.

Compound	M_L (dN.m)	M_H (dN.M)	M_H-M_L (dN.m)	T_{s2} (min)	T_{c90} (min)	CRI
F7-CNT7	1.62	9.21	7.59	1.32	5.91	21.78
CNT7/CCB2.5	2.61	11.17	8.56	1.30	5.74	22.52
CNT7/CCB5.0	3.15	11.81	8.66	1.19	5.54	22.98
CNT7/CCB7.0	3.81	12.87	9.06	1.09	5.01	25.51
CNT7/CCB10.0	4.84	14.51	9.67	1.01	4.76	27.32
CNT7/CCB15.0	5.02	17.79	12.77	0.78	4.23	28.98

In Table 7.1, it is also seen that the scorch time (t_{s2}) and cure time (t_{c90}) of ENR compounds were shortened by the addition of CCB. Moreover, the t_{s2} and t_{c90} decreased with increasing CCB loadings. Furthermore, incorporating and increasing CCB loadings caused an increasing cure rate index (CRI). It is noted that the cure rate index (CRI) is a measurement of the cure rate based on the differences between the optimum cure time (t_{c90}) and incipient scorch time (t_{s2}). Therefore, the increased CRI is due to higher thermal conductivity of CCB and CNTs that cause enhancing and accelerating of the curing reaction of the ENR compounds (Zhang *et al.*, 2012). Furthermore, increasing the CCB loading causes an increase in thermal conductivity of the ENR composites that may facilitate and hence accelerate the curing reaction. This also increases the chemical interaction between polar functional groups in ENR molecules and filler surfaces (CNTs and CCB) (Nakaramontri *et al.*, 2014). Higher contents of CCB in the ENR composite also cause an acceleration of the crosslinking reaction between the Fe^{3+} and ENR molecules via oxirane groups due to higher thermal conductivity.

In Table 7.1 it is also seen that the ENR-50 with CNT–CCB hybrid filler had a higher torque difference than the ENR with only CNTs. This indicates higher reinforcement due to higher crosslink density and higher solid particulate contents. This also indicates higher chemical linkages between ENR molecules via Fe^{3+} and also stronger chemical interactions between polar functional groups in ENR molecules and CNT–CCB hybrid fillers' surfaces.

7.3.2 Tensile properties

Tensile properties of ENR-50 compounds were characterized as the experimental procedure described in section 3.4.2. Figure 7.2 shows stress–strain curves of ENR-50 with 7 mmol of $FeCl_3$ ($FeCl_3$-ENR), filled with 7 phr of CNTs (F7-CNT7) and CNT–CCB hybrid fillers with various CCB loadings at 2.5, 5.0, 7.0, 10.0 and 15.0 phr (i.e., CNT7/CCB2.5, CNT7/CCB5.0, CNT7/CCB7.0, CNT7/CCB10.0 and CNT7/CCB15.0, respectively). Tensile properties in terms of 100% modulus, tensile strength and elongation at break of various ENR compounds are also summarized in Table 7.2. It is clearly seen that adding and increasing CCB loadings affect the characteristics of the stress–strain behaviors of ENR compounds by significantly increasing the 100% modulus and tensile strength as compared with the ENR filled with only CNTs (F7-CNT7). This is due to the reinforcing efficiencies of CNT–CCB hybrid fillers because the strong CNT–CCB networks were formed in the ENR matrix. Moreover, the finer filler dispersion and distribution due to the newly formed CNT–CCB networks strongly affected the enhancement of the rubber–filler interaction.
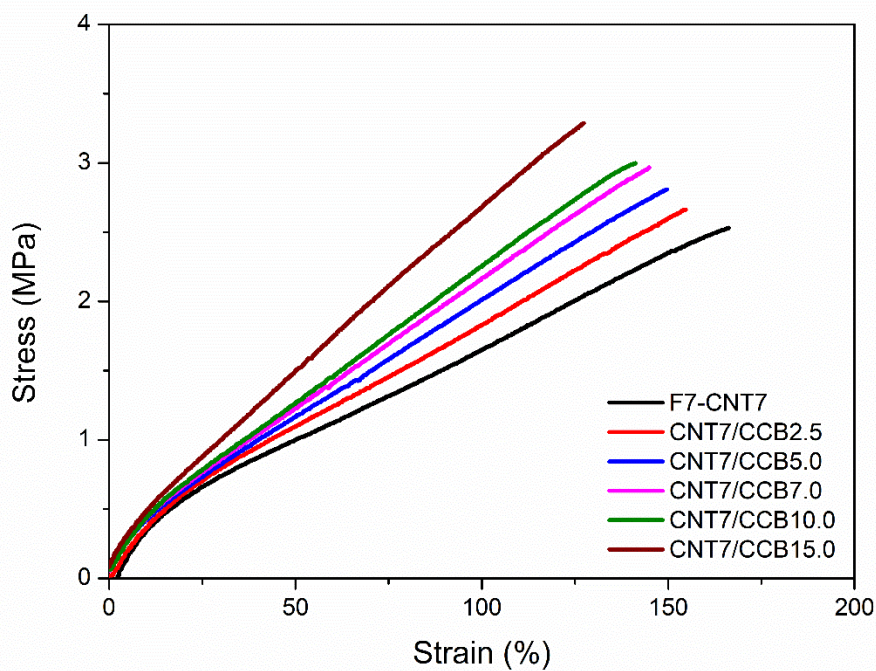
Figure 7.2 Stress-strain curves of ENR-FeCl$_3$ with CNTs (F7-CNT7) and ENR-FeCl$_3$ with CNTs/CCB and with various CCB loadings at 2.5, 5.0, 7.0, 10.0 and 15.0 phr.

In Table 7.2, increasing CCB loadings in CNT–CCB hybrid fillers also caused an increase in the 100% modulus and tensile strength. This is again due to the formation of the stronger CNT–CCB filler networks dispersed in the ENR matrix together with stronger crosslinking ENR networks via the Fe-O-Fe coordination bridges and the internal polymerization. In Figure 7.2 and Table 7.2, it is also clearly seen that the elongation at break decreased upon increasing CCB loadings. This is normally observed in rubber composites with well-dispersed reinforcing fillers that restrict the chain mobility of rubber molecules by rubber–filler interactions.

Table 7.2. Mechanical properties in terms of 100% modulus, tensile strength and elongation at break of ENR-50 compounds with $FeCl_3$ (ENR-$FeCl_3$) and mixed with CNTs (F7-CNT7) and CNTs/CCB hybrid fillers.

Materials	100% Modulus (MPa)	Tensile Strength (MPa)	Elongation at Break (%)
F7-CNT7	1.63	2.58	165.55
CNT7/CCB2.5	1.68	2.67	155.62
CNT7/CCB5.0	1.96	2.83	144.02
CNT7/CCB7.0	2.16	2.96	141.53
CNT7/CCB10.0	2.21	3.16	137.66
CNT7/CCB15.0	2.66	3.43	136.05

7.3.3 Morphological properties

Morphological properties of ENR compounds ware determined by using SEM, as the experimental procedure described in section 3.4.6. Figure 7.3 shows SEM micrographs of ENR–$FeCl_3$ filled with CNTs (F7-CNT7) and CNT–CCB hybrid filler with various CCB loadings at 0, 2.5, 5.0, 7.0, 10.0 and 15.0 phr. The F7-CNT7 shows uneven dispersion of CNT bundles with some agglomerates in the ENR matrix (Figure 7.3 (a)). Furthermore, in the ENR-50 with CNT–CCB hybrid fillers, the CCB particles are partially connected to form more dispersive CNT networks in the ENR matrix, as seen in Figure 7.3 (b)–(e). Therefore, the CCB particles and their small aggregates may act as the filler bridges at the end of the CNT bundle to form stronger and more dispersive filler networks in the ENR matrix. However, in Figure 7.3 (f), the large filler agglomerates are seen in the ENR-50 filled with CNT–CCB hybrid filler at a CCB loading of 15 phr due to the excess amount of CCB particles. Despite the large agglomerates of CCB, their dispersion and distribution in the ENR matrix still provide favorable tensile properties and other related properties of ENR composites.
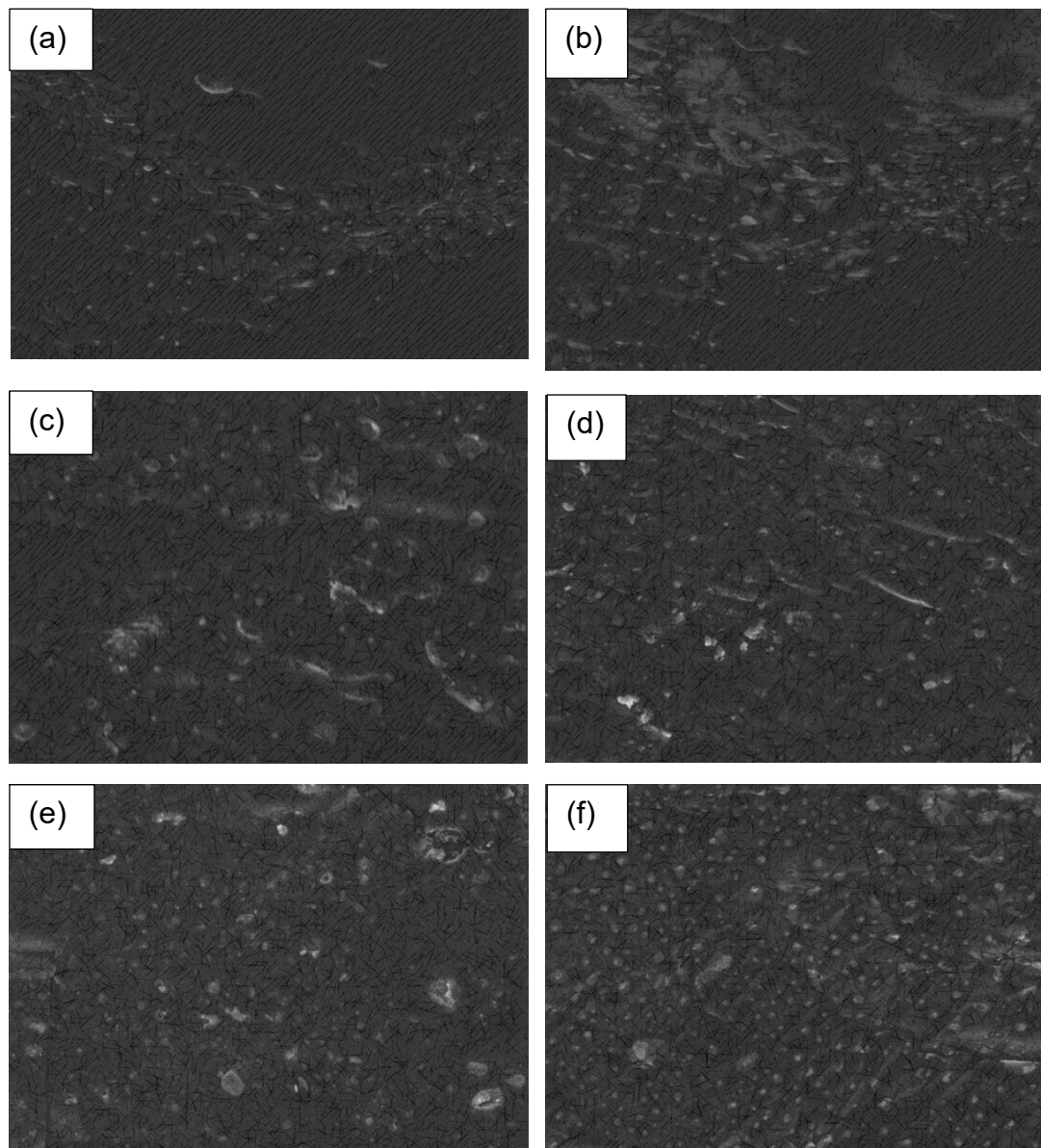
Figure 7.3 SEM micrographs of ENR-FeCl$_3$ filled with CNTs (F7-CNT7) (a) and CNTs-CCB hybrid filler with various CCB loadings at 2.5 (b), 5.0 (c), 7.0 (d), 10.0 (e) and 15.0 phr (f).

7.3.4 Payne effect

The Payne effect of ENR compounds were determined based on relationship between storage modulus as a function of strain amplitude by using RPA test, as the experimental procedure described in section 3.4.7.2. Figure 7.4 shows storage modulus as a function of strain amplitude of ENR–FeCl$_3$ filled with CNTs (F7-CNT7) and CNT–CCB hybrid fillers with various CCB loadings at 2.5, 5.0, 7.0, 10.0 and 15.0 phr. It can be clearly seen that the storage modulus of the F7-CNT7 compound shows a constant storage modulus in the low strain region (i.e., lower than 20% strain), but a slight decreasing trend is seen when the strain amplitude is higher than 20%. This may be due to the breakdown of CNT filler networks, indicating the level of the filler–filler or CNT–CNT interaction in the ENR matrix. Furthermore, the storage moduli of the ENR–FeCl$_3$ filled with CNT–CCB hybrid fillers were dramatically decreased after strain amplitudes higher than 20% due to the breakdown of the hybrid filler network structures.

Figure 7.4 Storage modulus as a function of strain amplitude of ENR-FeCl$_3$ filled with CNT (F7-CNT7) and CNTs-CCB hybrid fillers with various CCB loadings at 2.5, 5.0, 7.0, 10.0 and 15.0 phr.

Table 7.3 shows the Payne effect of ENR–FeCl$_3$ filled with CNTs (F7-CNT7) and CNT– CCB hybrid fillers with various loadings of CCB based on a calculation by equation 3.8 in section 3.4.7.2. It can lead to deformation-induced changes in the material's microstructure, i.e., to breakage and recovery of weak physical bonds linking adjacent filler clusters. Therefore, in Table 7.3, it is clearly seen that the Payne effect or filler–filler interaction increases with increasing CCB loadings. In Figure 7.4, it is also seen that the storage modulus of the ENR–FeCl$_3$ filled with CNT–CCB hybrid filler with CCB loadings higher than 7 phr showed slightly different modulus–strain curves as compared to the composites with CCB loadings lower than 5 phr. This might be attributed to the large agglomeration of fillers in the ENR matrix for the composites with CCB loadings higher than 7 phr (as SEM micrographs indicates in Figure 7.3 (e) and (f)).

Table 7.3. Payne effect of ENR-50 compounded with FeCl$_3$ (ENR-FeCl$_3$) filled with CNTs (F7-CNT7) and CNTs-CCB hybrid fillers with various loadings of CCB.

Samples	Payne effect (%)
F7-CNT7	20.12
CNT7/CCB2.5	31.35
CNT7/CCB5.0	35.12
CNT7/CCB7.0	39.51
CNT7/CCB10.0	42.07
CNT7/CCB15.0	46.41

7.3.5 Bound rubber contents

Bound rubber contents of ENR-50 compounds were characterized as the experimental procedure described in section 3.4.9. Figure 7.5 shows the bound rubber contents of ENR–FeCl$_3$ filled with 7 phr of CNTs (F7-CNT7) and CNT–CCB hybrid

fillers with various concentrations of CCB at 2.5, 5.0, 7.0, 10.0 and 15.0 phr (i.e., CNT7/CCB2.5, CNT7/CCB5.0, CNT7/CCB7.0, CNT7/CCB10.0 and CNT7/CCB15.0, respectively). In Figure 7.5, It is seen that F7-CNT7 filled with only CNTs displays the lowest bound rubber content. Moreover, the bound rubber content of the ENR filled with the CNT–CCB hybrid composite is higher than the ENR–CNT (F7-CNT7) composite, and it increases with an increase in CCB loading. This is attributed to an increase in filler–filler interaction (i.e., Payne effect in Table 7.3) and filler–rubber interactions between the polar functional groups of ENR molecules and the polar groups at the filler particle surface (i.e., CNTs and CCB). This is also due to the finer dispersion and distribution of hybrid filler networks in the ENR matrix (Figure 7.3), which caused increasing filler–rubber interactions, as indicated by the higher storage moduli in Figure 7.4.

Figure 7.5 Bound rubber contents of ENR-FeCl$_3$ filled with CNT (F7-CNT7) and CNTs-CCB hybrid filler with various CCB loadings at 2.5, 5.0, 7.0, 10.0 and 15.0 phr.

7.3.6 Temperature scanning stress relaxation (TSSR)

Temperature scanning stress relaxation of ENR-50 compounded with FeCl$_3$ and conventional sulfur vulcanization system was performed as the experimental

procedure described in section 4.4.10. The relaxation modulus of ENR–FeCl$_3$ filled with 7 phr of CNTs (F7‑CNT7) and CNT–CCB with various CCB loadings at 2.5, 5.0, 7.0, 10.0 and 15.0 phr as a function of temperature can be found from Figure 7.6. The ENR–FeCl$_3$ filled with CNT–CCB hybrid fillers showed a higher initial relaxation modulus and relaxation modulus at a given temperature than the F7‑CNT7 without CCB. Moreover, these properties increased with increasing CCB loadings. This might be due to the higher level of crosslink structures, bound rubber content (Figure 7.5), filler–filler interactions and filler–rubber interactions (Figure 7.4). This causes an enhancement of the F7‑CNT7 with CCB as compared with the F7‑CNT7 without CCB, which also correlates well to higher torque difference (Table 7.1), 100% modulus (Table 7.2) and crosslink density (Table 7.4). It is noted that the crosslink density of the ENR vulcanizates was also calculated from the maximum slope of the outset part of the stress–temperature curve (Figure 7.6), using equations (3.5) and (3.6) in section 3.4.5.2 (Nakaramontri *et al.*, 2014), as described in the following section.

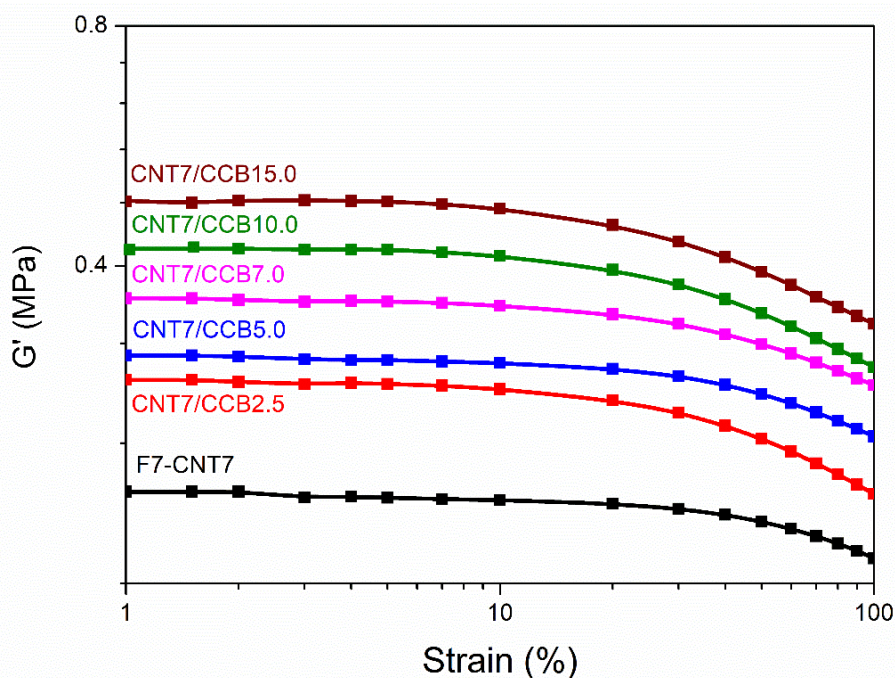**Figure 7.6** Relaxation modulus as a function of temperature of ENR-FeCl$_3$ filled with CNT (F7-CNT7) and CNTs-CCB hybrid filler with various CCB loadings at 2.5, 5.0, 7.0, 10.0 and 15.0 phr.

7.3.7 Crosslink density

Crosslink density of ENR-50 compounded with $FeCl_3$ and conventional sulfur vulcanization system was determined as the experimental procedure described in section 3.4.5. Table 7.4 shows the crosslink densities of ENR–$FeCl_3$ and its filled composite with 7 phr of CNTs (F7-CNT7) and CNT–CCB hybrid fillers with various CCB loadings at 2.5, 5.0, 7.0, 10.0 and 15.0 phr. There are two different approaches to estimate the crosslink densities of ENR vulcanizates in this work: the swelling measurement via the Flory–Rehner relation (equation (3.4) described in section 3.4.5.1) and the TSSR measurement based on the maximum slope in the initial part of the stress–temperature curve (equations (3.5) and (3.6)). In Table 7.4, it is clearly seen that the resulting crosslink densities from the TSSR evaluation and swelling measurements show large differences in magnitude but have the same trends. That is, the unfilled ENR–$FeCl_3$ compound shows the lowest crosslink density. The addition of CNTs and CNT–CCB hybrid fillers led to an increase in crosslink densities, which are in agreement with higher torque difference (M_H-M_L) (Table 7.1) and bound rubber contents (Figure 7.5) of the ENR-50 with filler and increasing CCB loadings. In Table 7.4, the highest crosslink density was observed in the ENR–$FeCl_3$ filled with the CNT–CCB hybrid filler with a CCB loading of 15 phr. This may be attributed to the highest level of chemical interaction between polar functional groups on the CNT–CCB surfaces and the ENR molecular networks that and bridged by the coordination –Fe–O–Fe– linkages.

Table 7.4 Crosslink densities of ENR-50 compounded with FeCl$_3$ and mixed CNTs (F7-CNT7) and CNTs/CCB hybrid fillers with various loadings of CCB.

Sample	Mooney-Rivlin eq.	TSSR evaluation
	Crosslink densities (mol/m^3)	Crosslink densities (mol/m^3)
ENR-FeCl$_3$	110.13 ± 2.01	66.28
F7-CNT7	167.97±2.16	71.71
CNT7/CCB2.5	171.52±8.18	76.98
CNT7/CCB5.0	184.21±1.12	85.27
CNT7/CCB7.0	193.49±1.98	87.52
CNT7/CCB10.0	215.24±10.15	91.65
CNT7/CCB15.0	217.93±10.01	96.55

7.3.8 Dynamic mechanical analysis (DMA)

Dynamic mechanical analysis (DMA) of ENR-50 compounds were performed, as the experimental procedure described in section 3.4.7.1. Figure 7.7 shows the storage modulus (E') and loss tangent (tan **δ**) as functions of temperature of ENR–FeCl$_3$ filled with 7 phr of CNTs (F7-CNT7) and CNT–CCB hybrid fillers with various CCB loadings at 2.5, 5.0, 7.0, 10.0 and 15.0 phr. It is clearly seen that the ENR–FeCl$_3$ filled with CNT–CCB hybrid fillers had higher storage moduli in the glassy region (i.e., in the temperature ranges from −60 °C to −30 °C) than the ENR filled only with CNTs (F7-CNT7). Moreover, the storage moduli increased with an increase in CCB loading. This may be due to the higher reinforcement of ENR by filler networks of CNT bundles and CCB particles, resulting in stronger CNT–CCB networks dispersed in the ENR matrix.

Additionally, more CCB solid contents in the ENR nanocomposites cause higher stiffness in materials. In Figure 7.7, it is also seen that the addition of CNT–CCB hybrid fillers caused shifts in the tan δ peaks (Figure 7.7 (b)) and hence the glass transition temperature (T_g) (Table 7.5) toward higher temperature ranges as compared with the ENR filled only with CNTs (F7-CNT7). This resulted in an increase in T_g of ENR–FeCl$_3$ filled with CNT–CCB hybrid filler with increasing CCB loadings. This is attributed to more rigidity of the ENR molecular networks with an increase in CCB loading, due to higher interaction among polar functional groups at CNT–CCB surfaces and the polar groups in ENR molecules, resulting in less chain flexibility and hence higher glass transition temperature. In Figure 7.7 (b), it can also be seen that the height and area underneath the transition peak of the ENR–FeCl$_3$ filled with CNT–CCB hybrid fillers decreased with an increase in CCB loading with an abruptly decreasing trend in the composites with CCB loadings at 10 and 15 phr. This might be due to the large filler agglomeration in the ENR matrix, as evidenced in SEM micrographs in Figure 7.3.

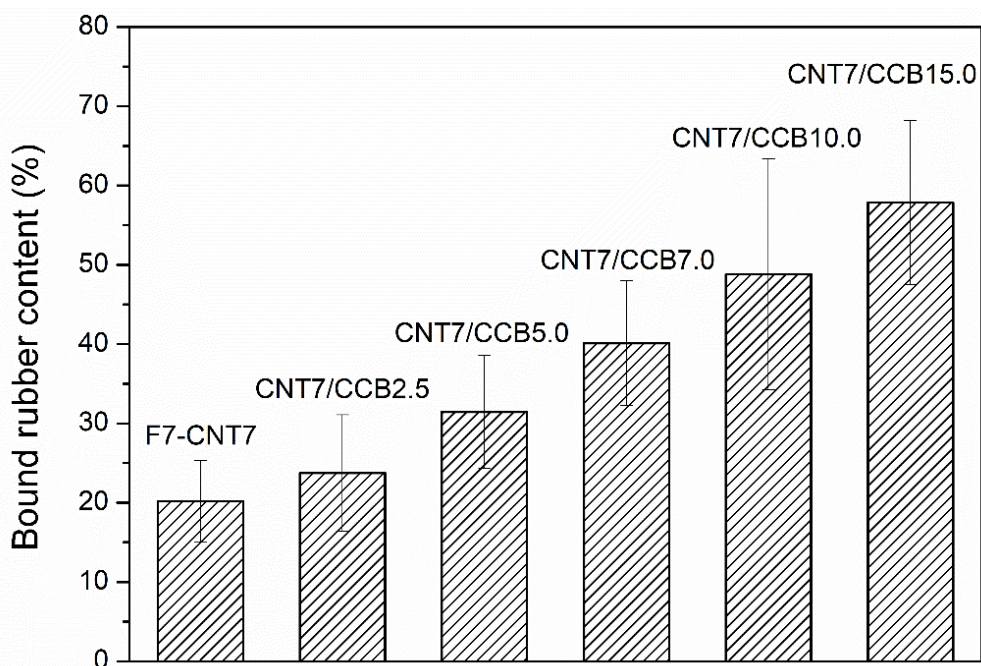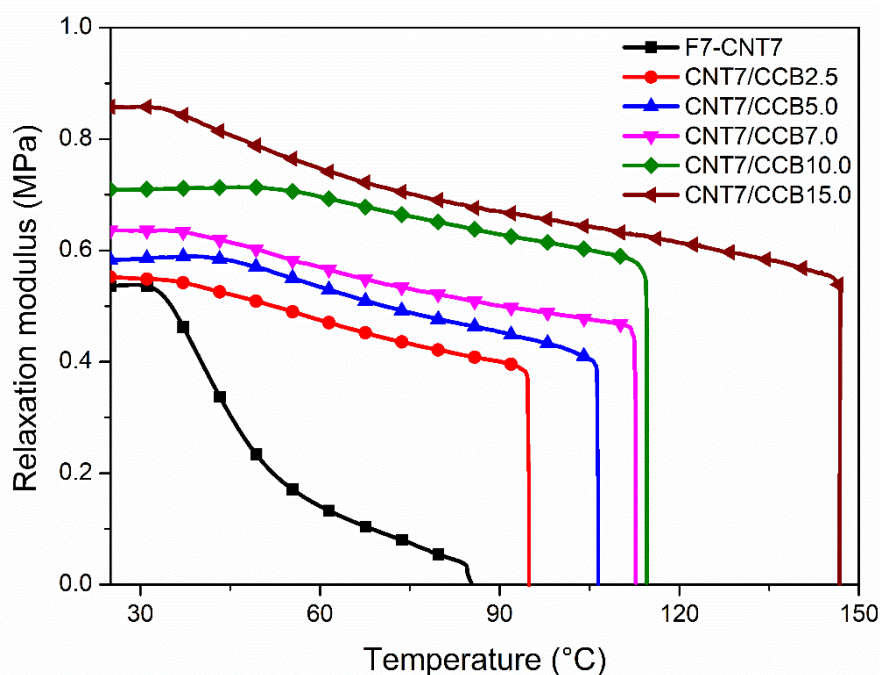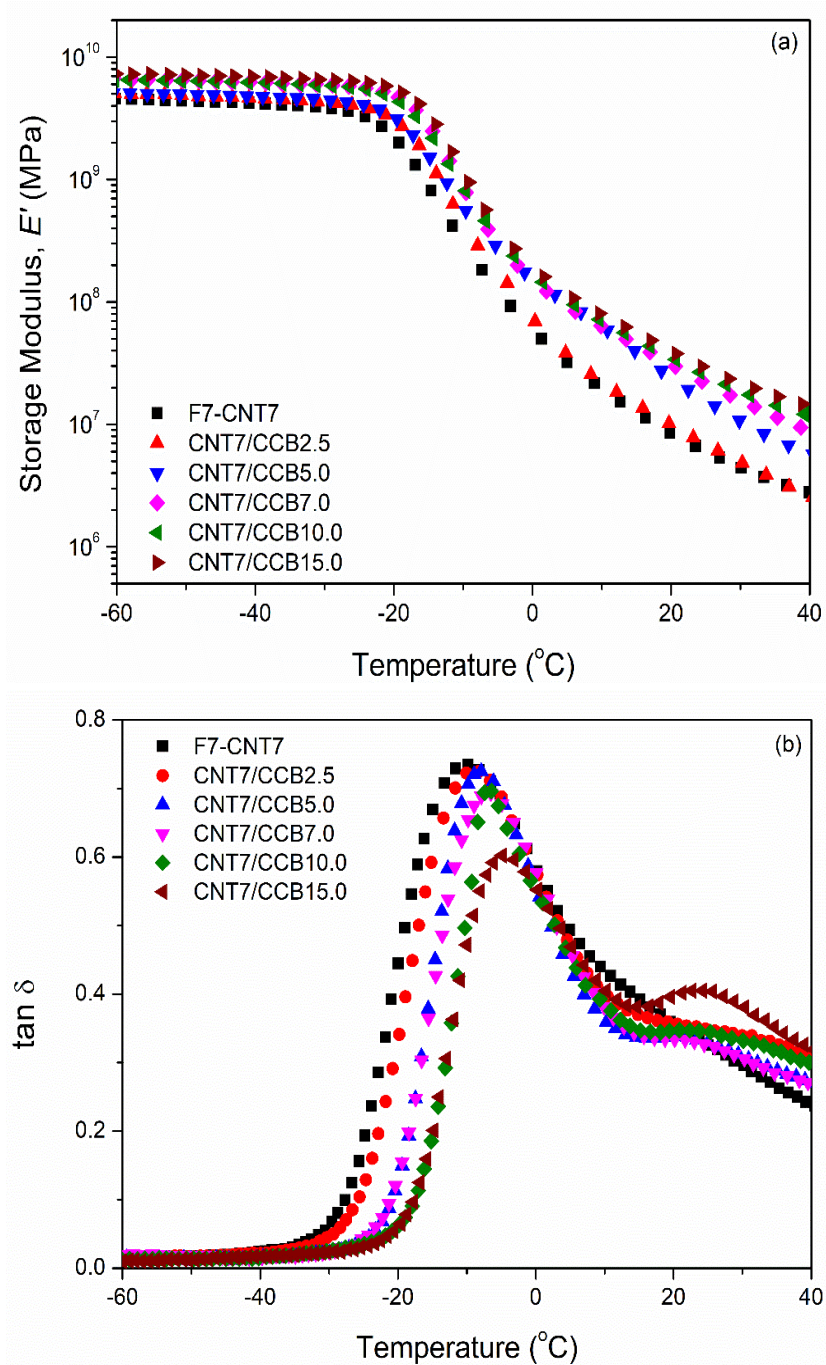**Figure 7.7** Storage modulus (a) and Tan δ (b) as a function of temperature of ENR-FeCl$_3$ filled with CNT (F7-CNT7) and CNTs-CCB hybrid fillers with various CCB loadings at 2.5, 5.0, 7.0, 10.0 and 15.0 phr.

Table 7.5. Glass transition temperature (T_g) of ENR-50 compounded with $FeCl_3$ and (ENR-$FeCl_3$) mixed with CNTs (F7-CNT7) and CNTs/CCB hybrid fillers.

Samples	Glass transition temperature (°C)
F7-CNT7	-18.30
CNT7/CCB2.5	-16.35
CNT7/CCB5.0	-11.31
CNT7/CCB7.0	-10.63
CNT7/CCB10.0	-7.77
CNT7/CCB15.0	-7.68

7.3.9 Electrical properties

Electrical properties of ENR-50 compounds were determined as the experimental procedure described in section 3.4.11. The dependence of the electrical conductivity on the frequency at room temperature of ENR–$FeCl_3$ filled with CNTs (F7-CNT7) and CNT–CCB hybrid fillers with various CCB loadings at 2.5, 5.0, 7.0, 10.0 and 15.0 phr is shown in Figure 7.8. It can be seen that the electrical conductivity of the F7-CNT7 strongly increased with increasing frequencies or frequency-dependent electrical conductivity. However, in the ENR–$FeCl_3$ filled with CNT– CCB hybrid fillers, less frequency-dependent curves are seen, with a marginal increase in electrical conductivity with increasing frequency. This may be due to more free electron movement in the ENR matrix. Furthermore, the ENR filled with CNT–CCB hybrid composites shows higher electrical conductivity than the ENR–CNT composite. In addition, the electrical conductivity at a given frequency increases with increasing CCB loadings. This is attributed to the formation of more conductive CNT–CCB networks in the ENR matrix. That is, the CCB particles or small CCB aggregates may act as the filler bridges to connect the CNT bundles to form the strong filler networks which are dispersed in the ENR matrix to facilitate the movement of free electrons. This also

causes higher filler–filler (CNT–CCB) and rubber–filler interactions between polar functional groups of hybrid fillers and the ENR matrix. This causes the formation of three-dimensional filler networks in the rubber networks with the enhancement of end-to-end electron hopping among CNT–CCB bridges, causing electron transfer and significantly enhancing the electrical conductivity of the rubber composites.
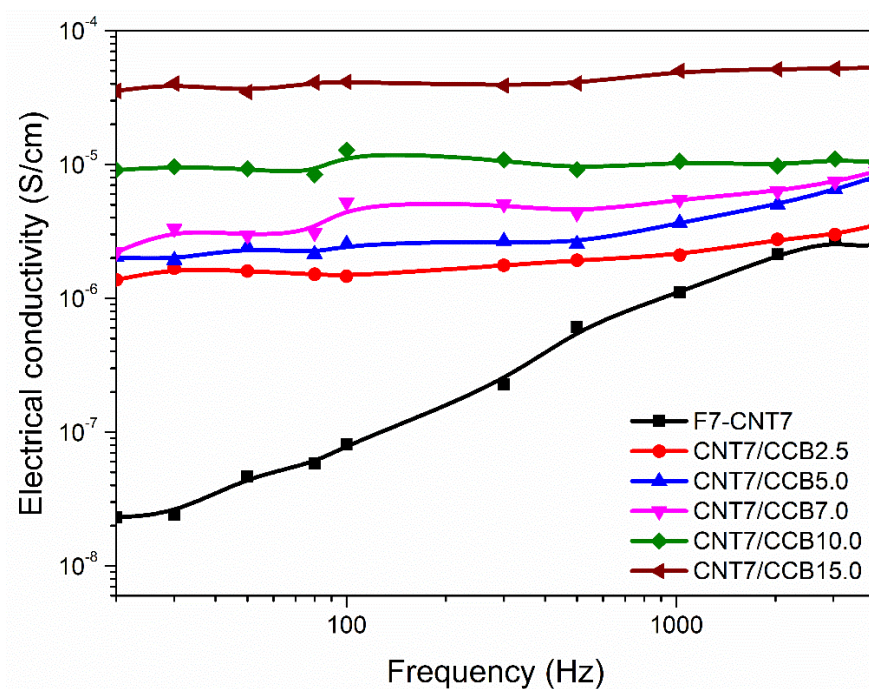
Figure 7.8 Electrical conductivity as a function of frequency of ENR-FeCl$_3$ with CNT (F7-CNT7) and ENR-FeCl$_3$ with CNTs/CCB hybrid filler with various CCB loadings at 2.5, 5.0, 7.0, 10.0 and 15.0 phr.

The formation of conductive paths of filler networks is verified by the percolation threshold concentration (CTC) based on the plots of electrical conductivity versus filler concentration, as shown in Figure 7.9. It is clearly seen that the CTC of the ENR–FeCl$_3$/CNT– CCB hybrid composites is lower than 2.5 phr of CCB, where the material turns from an insulator to the conductive rubber material.
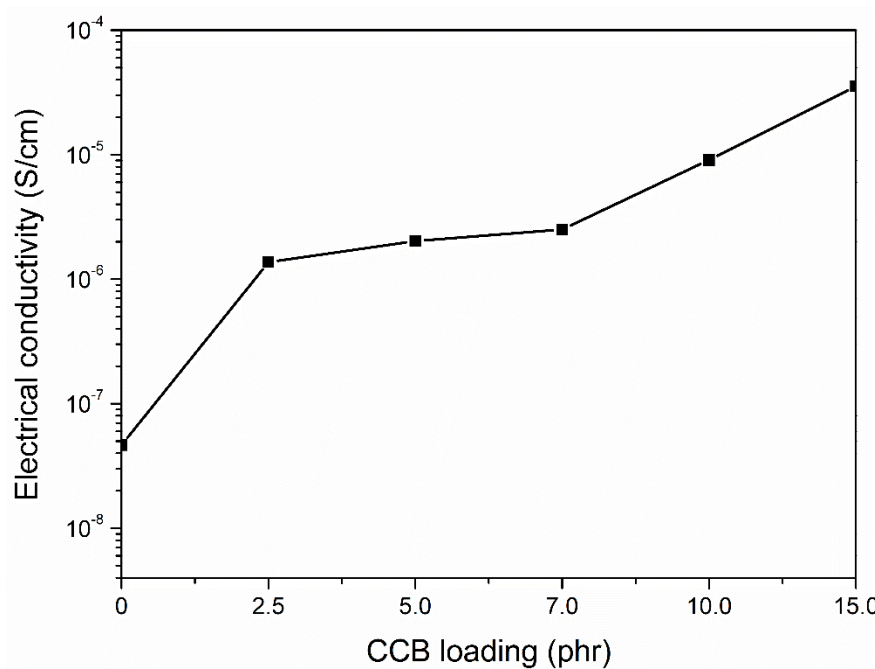
Figure 7.9 Electrical conductivity (at a frequency at 50 Hz) as a function if CCB loadings of ENR-FeCl$_3$ with CNT (0 phr) and ENR-FeCl$_3$ with CNTs/CCB hybrid fillers at various CCB loadings at 2.5, 5.0, 7.0, 10.0 and 15.0 phr.

Figure 7.10 shows dielectric constant as a function of frequency of ENR–FeCl$_3$ filled with CNTs (F7-CNT7) and CNT–CBB hybrid fillers with various CCB loadings at 2.5, 5.0, 7.0, 10.0 and 15.0 phr. It is clearly seen that the F7-CNT7 has the lowest dielectric constant, and this property is more or less independent of frequency. On the other hand, the ENR filled with CNT–CCB hybrid fillers with various CCB loadings has a higher dielectric constant than the F7-CNT7, but the frequency-dependent dielectric constant is seen. This means the electric current moves through the conductive filler pathways induced by polarization in the ENR vulcanizates (Pötschke *et al.*, 2003). It was also found that an increasing dielectric constant is seen with an increase in CCB loading, which corresponds to the trend of electrical conductivity (Figure 7.8). In addition, a significantly increasing trend of the dielectric constant of the ENR filled with CNT–CCB hybrid fillers is seen with an increase in CCB loading. This might be due to the increasing polarizability of the fillers and also to anomalous diffusion within aggregates of CNTs and CCB, together with their dispersion in the rubber matrix.
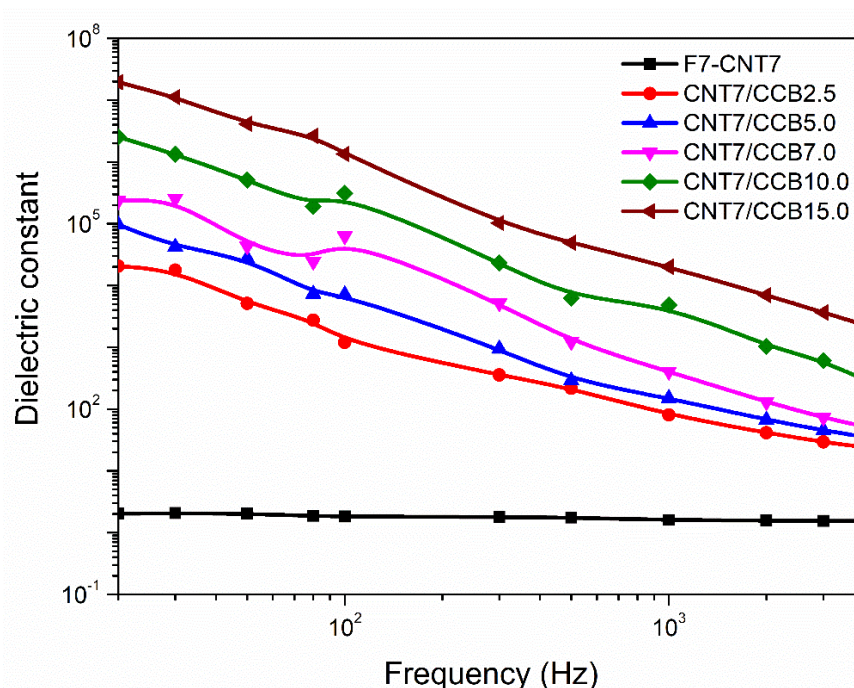
Figure 7.10 Dielectric constant as a function of frequency of ENR-FeCl$_3$ with CNT (F7-CNT7) and ENR-FeCl$_3$ with CNTs/CCB hybrid fillers with various CCB loadings at 2.5, 5.0, 7.0, 10.0 and 15.0 phr.

7.4 Conclusions

Epoxidized natural rubber with 50 mol % was successfully crosslinked by Fe^{3+} ion (7 mmol FeCl$_3$) to form the coordination linkages (–O–Fe–O–) between oxirane rings in ENR molecules and Fe^{3+} ions. This novel elastomer material was further filled with 7 phr of CNTs (F7-CNT7) and CNT–CCB hybrid fillers with various CCB loadings at 2.5, 5.0, 7.0, 10.0 and 15.0 phr. It was found the ENR–FeCl$_3$ compound filled with CNTs and the CNT–CCB hybrid filler had shorter scorch and cure times and a higher cure rate index than the ENR–FeCl$_3$ filled with only CNTs. Furthermore, the ENR/CNT–CCB hybrid composites indicated higher 100% modulus, tensile strength and crosslink density than the ENR–CNTs composite. This is attributed to a higher level of chemical interaction between polar functional groups in the CNTs, CCB surfaces and the ENR molecular networks. Furthermore, CCB secondary filler caused an improvement in the CNTs' dispersion in the ENR matrix by connecting to the CNT encapsulates, forming CNT–CCB–CNT pathways and hence strong CNT–CCB networks. This significantly

improved the mechanical properties, bound rubber, crosslink density and electrical properties, revealed by the SEM micrographs of the ENR composites with suitable dispersion and distribution of fillers in the rubber matrix. Moreover, the ENR–FeCl$_3$ filled with CNTs and the CNT–CCB hybrid filler indicated superior electrical conductivities as compared to the ENR–FeCl$_3$ filled with only CNTs. This is also attributed to the formation of stronger conductive CNTs and CCB networks in the ENR matrix. Finally, the novel ENR/CNT–CCB hybrid nanocomposites with coordination crosslinking system and adequate performance in terms of mechanical and electrical properties will encourage further research in the field of smart materials.

CHAPTER 8

CONCLUSIONS

8.1   Ferric chloride cross-linked epoxidized natural rubber with 25 mol% epoxide (ENR-25)

ENR-25 was successfully vulcanized with $FeCl_3$ by a crosslinking reaction between opened ring products of an oxirane ring in ENR and Fe^{3+} to create metal–oxygen coordination (–O-Fe-O-) cross-links. It was found that the ENR-25 compounds with $FeCl_3$ showed good tensile properties with increased curing torque, as the $FeCl_3$ concentration increased. This is attributed to chemical reaction between oxirane rings in ENR molecules and Fe^{3+} ion to form rubbery network.

8.2   Cross-linked of epoxidized natural rubber with 50 mol% epoxide (ENR-50) by ferric chloride

ENR-50 can be very efficiently crosslinked by using Fe^{3+} from $FeCl_3$. In the present case, a small amount of $FeCl_3$ was used to cure ENR. The linkages between $FeCl_3$ and oxirane ring in the ENR molecule (i.e., -O-Fe-O) was confirmed from the FTIR studies. The epoxy group can follow a ring opening type "internal polymerization" that is, increasing the network formation of ENR and $FeCl_3$ via coordination -O-Fe-O-linkages. Moreover, it was found that an increased concentration of $FeCl_3$ improved the properties of ENR-50 compounds, including maximum rheometric torque, crosslinking densities, tensile strength, dynamic properties, electrical conductivity and thermal properties. The conventional sulfur vulcanization of ENR-50 compounds and unmodified NR compounded with 7 mmol $FeCl_3$ were used for comparison and it is found that $FeCl_3$ cannot cure NR. Furthermore, the ENR-50 compounded with $FeCl_3$ at 7 and 10 mmol showed higher crosslinking densities and mechanical properties than the ENR-50 cured with conventional sulfur cured system. This might be due to higher crosslinking structures of the cured samples. Additionally, the internal polymerization of epoxy moieties with $FeCl_3$ offers very dense network structures, which are reflected in mechanical and dynamic mechanical properties. Additionally, T_g values increased

with increasing concentrations of $FeCl_3$. This is due to the increase in the crosslinking densities that restricted the mobility of ENR molecules. Furthermore, the ENR-50 compounded with $FeCl_3$ showed the highest electrical conductivity than other samples without $FeCl_3$. Additionally, thermal resistance was increased with increasing concentration of $FeCl_3$. The reaction between ENR and $FeCl_3$ could be very rapid at a higher temperature and the principle can be applied for other epoxy-based materials.

8.3   Crosslinked epoxidized natural rubber by ferric chloride filled with carbon nanotubes

ENR-50 was successfully crosslinked by Fe^{3+} ion of $FeCl_3$ to form the coordination crosslinks (–O–Fe–O– linkages) between ENR molecules and to form internal polymerized oxirane groups of ENR molecules. In addition, the incorporation of CNTs improves various properties of ENR-$FeCl_3$ compounds, including tensile strength, dynamic properties, electrical conductivity, and thermal properties. It is clearly seen that the ENR-$FeCl_3$ compounds filled with various CNTs loadings have higher torque differences and mechanical properties than the ones without CNTs. This is due to higher contents of the crosslinking structures of ENR, the three-dimensional CNTs networks, and the reinforcement effect of CNTs in the ENR matrix. SEM micrographs reveal very small CNTs aggregates in the ENR-$FeCl_3$ compounds with 5 and 7 phr of CNTs loadings, which indicate good dispersions of CNTs in the ENR matrix. However, ENR-$FeCl_3$ compound with 10 phr of CNTs shows a large agglomerate due to re-agglomerates of CNTs. According to DMA, glass transition temperature (T_g) increases with an increase in CNTs loadings due to more restrictions on chain mobility of ENR molecules. Furthermore, the ENR-$FeCl_3$/CNTs nanocomposites show improvement of storage modulus, 100% moduli, electrical conductivity, and dielectric constant as compared with the ENR-$FeCl_3$ compound without CNTs. It was also found that the ENR-$FeCl_3$/CNTs nanocomposites have the percolation threshold concentration at 7 phr of CNTs. It indicates the presence of the three-dimensional network, which is in agreement with the morphological properties. Also, the thermal resistance of ENRFeCl$_3$/CNTs nanocomposites increases with an increase in CNTs loadings. This is

due to the higher content of the coordination linkages of ENR-FeCl$_3$ and reinforced by CNTs.

8.4 Crosslinked epoxidized natural rubber by ferric chloride filled with carbon nanotubes and conductive carbon black hybrid filler

Epoxidized natural rubber with 50 mol % was successfully crosslinked by Fe^{3+} ion (7 mmol FeCl$_3$) to form the coordination linkages (–O–Fe–O–) between oxirane rings in ENR molecules and Fe^{3+} ion. This novel elastomer material was filled with 7 phr of CNTs (F7-CNT7) and CNT–CCB hybrid fillers with various CCB loadings at 2.5, 5.0, 7.0, 10.0 and 15.0 phr. It was found the ENR–FeCl$_3$ compound filled with CNTs and the CNT–CCB hybrid filler had shorter scorch and cure times and a higher cure rate index than the ENR–FeCl$_3$ filled with only CNTs. Furthermore, the ENR/CNT–CCB hybrid composites indicated higher 100% modulus, tensile strength and crosslink density than the ENR–CNTs composite. This is attributed to a higher level of chemical interaction between polar functional groups in the CNTs, CCB surfaces and the ENR molecular networks. Furthermore, CCB secondary filler caused an improvement in the CNTs' dispersion in the ENR matrix by connecting to the CNT encapsulates, forming CNT–CCB–CNT pathways and hence strong CNT–CCB networks. This significantly improved the mechanical properties, bound rubber, crosslink density and electrical properties, revealed by the SEM micrograph of the ENR composites with suitable dispersion and distribution of fillers in the rubber matrix. Moreover, the ENR–FeCl$_3$ filled with CNTs and the CNT–CCB hybrid filler indicated superior electrical conductivities as compared to the ENR–FeCl$_3$ filled with only CNTs. This is also attributed to the formation of stronger conductive CNTs and CCB networks in the ENR matrix. Finally, the novel ENR/CNT–CCB hybrid nanocomposites with coordination crosslinking system and adequate performance in terms of mechanical and electrical properties will encourage further research in the field of smart materials.

REFFERENCES

Ajayan, P. M., Schadler, L. S., Giannaris, C., Rubio, A. 2000. Single-walled carbon nanotube-polymer composites: strength and weakness. Advanced Materials, 12(10), 750–753.

Ajayan, P., Stephan, O., Colliex, C., Trauth, D. 1994. Aligned carbon nanotube arrays formed by cutting a polymer resin–nanotube composite. Science, 265, 1212–1214.

Akiba, M. 1997. Vulcanization and crosslinking in elastomers. Progress in Polymer Science, 22(3), 475–521.

Andrews, R., Jacques, D., Rao, A. 1999. Nanotube composite carbon fibers. Applied Physic Letter, 75, 1329-1331.

Angnanon, S., Prasassarakich, P., Hinchiranan, N. 2011. Styrene/acrylonitrile graft natural rubber as compatibilizer in rubber blends. Polymer-Plastics Technology and Engineering, 50(11), 1170–1178.

Asaletha, R., Kumaran, M. G., Thomas, S. 1998. Thermal behavior of natural rubber/polystyrene blends: thermogravimetric and differential scanning calorimetric analysis. Polymer Degradation and Stability, 61(3), 431–439.

Bachtold, A., Strunk, C. and Salvetat, J. 1999. Aharonov-bohm oscillations in carbon nanotubes. Nature, 397, 673-675.

Bai, J., Li, H., Shi, Z., Yin, J. 2015. An Eco-friendly scheme for the cross-linked polybutadiene elastomer via thiol–ene and diels–alder click Chemistry. Macromolecules, 48, 3539-3546.

Baker, C., Gelling, I., Samsuri, A. 1986. Epoxidised natural rubber. Journal of Natural Rubber Research, 1, 135-144.

Balandin, A. A. 2011. Thermal properties of graphene and nanostructured carbon materials. Nature Materials, 10(8), 569–581.

Bao, S. P., Liang, G. D., Tjong, S. C. 2009. Positive temperature coefficient effect of polypropylene/carbonnanotube/montmorillonite hybridnanocomposites. IEEE Transactions on Nanotechnology, 8(6), 729–736.

Biju C, S. 2018. Properties of **α**-Fe$_2$O$_3$/graphene nano hybrid synthesized by a simple hydrothermal/solution mixing method. Nano-Structures & Nano-Objects, 13, 44–50.

Bořkovec, A.B. Reaction of epoxides with ferric chloride. 1985. Journal of Organic Chemistry, 23, 828–830.

Brosse, J. C., Campistron, I., Derouet, D., El Hamdaoui, A., Houdayer, S., Reyx, D., Ritoit, G. S. 2000. Chemical modifications of polydiene elastomers: A survey and some recent results. Journal of Applied Polymer Science, 78(8), 1461–1477.

Cao, L., Gong, Z., Liu, C., Fan, J., Chen, Y. 2021. Design and fabrication of mechanically strong and self-healing rubbers via metal-ligand coordination bonds as dynamic crosslinks. Composite Science Technology, 207, 108750.

Cao, J., Zhou, C., Su, G., Zhang, X., Zhou, T., Zhou, Z., Yang, Y. 2019. Arbitrarily 3D configurable hygroscopic robots with a covalent-noncovalent interpenetrating network and self-healing ability. Advance Material, 31, e1900042.

Chao, A., Negulescu, I., Zhang, D. 2016. Dynamic Covalent polymer networks based on degenerative imine bond exchange: tuning the malleability and self-healing properties by solvent. Macromolecules, 49, 6277-6284.

Chatterjee, T., Vennemann, N., Naskar, K. 2017. Temperature scanning stress relaxation measurements: A unique perspective for evaluation of the thermomechanical behavior of shape memory polymer blends. Journal of Applied Polymer Science, 135, 45680.

Chen, J-H., An, X-P., Li, Y-D., Wang, M., Zeng, J-B. 2018. Reprocessible epoxy networks with tunable physical properties: synthesis, stress relaxation and recyclability. Journal of Polymer Scince, 36, 641-648.

Chen, W., Duan, W., Liu, Y., Wang, Q., Qi, F. 2019. Facile fabrication of multifunctional polymer composites based on three-dimensional interconnected networks of graphene and carbon nanotubes. Industrial & Engineering Chemistry Research, 58, 21531–21541.

Chen, Y., Tang, Z., Zhang, X., Liu, Y., Wu, S., Guo, B. 2018. Covalently cross-linked elastomers with self-healing and malleable abilities enabled by boronic ester bonds. ACS Applied Polymer Material, 10, 24224-24231.

Cheng, B., Lu, X., Zhou, J., Qin, R., Yang, Y. 2019. Dual cross-linked self-healing and recyclable epoxidized natural rubber based on multiple reversible effects. ACS Sustainable Chemistry Engineering, 7, 4443-4455.

Childers, M.I., Longo, J.M., Van, Zee, N.J., LaPointe, A.M., Coates, G.W. 2014. Stereoselective epoxide polymerization and copolymerization. Chemistry Review, 114, 8129–8152.

Coates, J. 2006. Interpretation of infrared spectra, A practical approach. Encyclopedia of Analytical Chemistry. 10815–10837.

Coran, A. Y. 2003. Chemistry of the vulcanization and protection of elastomers: A review of the achievements. Journal of Applied Polymer Science, 87(1), 24–30.

Cui, X., Li, J., Su, J., Jin, Q., Wang, Y., Cui, S. 2019. Effect of temperature on mechanical performance and tensoresistivity of a new sensor-enabled geosynthetic material. Journal of Materials in Civil Engineering, 31(6),

Cunneen, J. I., Russell, R. M. 1970. Occurrence and prevention of changes in the chemical structure of natural rubber tire tread vulcanizates during service. Rubber Chemistry and Technology, 43(5), 1215– 224.

Damampai, K., Pichaiyut, S., Das, A., Nakason, C. 2022. Internal polymerization of epoxy group of epoxidized natural rubber by ferric chloride filled with carbon nanotubes: Mechanical, morphological, thermal and electrical properties of rubber vulcanizates. Express Polymer Letter, 16, 812–826.

Damampai, K., Pichaiyut, S., Mandal, S., Wießner, S., Das, A., Nakason, C. 2021. Internal polymerization of epoxy group of epoxidized natural rubber by ferric chloride and formation of strong network structure. Polymers, 13, 4145.

Damampai, K., Pichaiyut, S., Stöckelhuber, K.W., Das, A., Nakason, C. 2022. Ferric ions crosslinked epoxidized natural rubber filled with carbon nanotubes and conductive carbon black hybrid fillers. Polymers, 14, 4392.

Dang, Z.M., Zhang, B., Li, J., Zha, J.W., Hu G.H. 2012. Copper particles/epoxy resin thermosetting conductive adhesive using polyamide resin as curing agent. Journal of Applied Polymer Science.

Das, A., Kasaliwal, G.R., Jurk, R., Boldt, R., Fischer, D., Stöckelhuber, K.W., Heinrich, G. 2012. Rubber composites based on graphene nanoplatelets, expanded graphite, carbon nanotubes and their combination: A comparative study. Composites Science and Technology, 72, 1961–1967.

Das, A., Stöckelhuber, K. W., Jurk, R., Fritzsche, J., Klüppel, M., Heinrich, G. 2009. Coupling activity of ionic liquids between diene elastomers and multi-walled carbon nanotubes. Carbon, 47, 3313–3321.

Demczyk, B., Wang, Y., Cumings, J. 2006. Direct mechanical measurement of the tensile strength and elasticmodulus of multiwalled carbon nanotubes. Microscopy and Microanalysis, 12, 934-935.

Derakhshandeh, B., Shojaei, A., Faghihi, M. 2008. Effects of rubber curing ingredients and phenolic-resin on mechanical, thermal, and morphological characteristics of rubber/phenolic-resin blends. Journal of Applied Polymer Science, 108(6), 3808–3821.

Dresselhaus, M., Dresselhaus, G., Saito, R. 1995. Physics of carbon nanotubes. Carbon, 33, 883-891.

Du F., Fischer J., Winey K. 2003. Coagulation method for preparing single-walled carbon nanotube/poly(methyl methacrylate) composites and their modulus, Electrical Conductivity, and Thermal Stability. Polymer Science: Part B, 41, 3333-3338.

Ebbesen T. W., Ajayan P. M. 1992. Large-scale synthesis of carbon nanotubes. Nature, 358, 220–222.

El-Wakil, A. A. 2007. Study on effect of natural rubber-graft-1, 2- phenylenediamine as antioxidant on oxidation resistance for natural rubber. Polymer-Plastics Technology and Engineering, 46(6), 661–666.

Fan, J., Huang, J., Gong, Z., Cao, L., Chen, Y. 2021. Toward robust, tough, self healable supramolecular elastomers for potential application in flexible substrates. ACS Applied Polymer Material, 13, 1135-1144.

Feng, Z., Hu, J., Yu, B., Tian, H., Zuo, H. 2019. Environmentally friendly method to prepare rhermo-reversible, self-healable biobased elastomers by one-step melt processing. ACS Applied Polymer Material, 1, 169-177.

Flory, P. J., Rehner, J. 1943. Statistical mechanics of cross‑linked polymer networks II. swelling. The Journal of Chemical Physics, 11(11), 521–526.

Frank, S., Poncharal, P., Wang, Z. and Heer, W. 1998. Carbon nanotube quantum resistors. Science. 280: 1744-1746.

Fröhlich, J., Niedermeier, W., Luginsland, H-D. 2005. The effect of filler–filler and filler–elastomer interaction on rubber reinforcement. Composites Part A: Applied Science and Manufacturing, 36, 449–460.

Gan, S.N., Ting K.F. 1993. Effect of treating latex with some metal ions on storage hardening of natural rubber. Polymer. 34.

George, N., Chandra, J., Mathiazhagan, A., Joseph, R. 2015. High performance natural rubber composites with conductive segregated network of multiwalled carbon nanotubes. Composite. Science. Technology. 11: 633-640.

Hakim, R. N., Ismail, H. 2009. Cure Characteristics, tensile properties and morphology of natural rubber/organoclay nanocomposites: Effect of maleated natural rubber. Polymer-Plastics Technology and Engineering, 48(9), 910–918.

Hamerton, I., Brendan, J., Howlin., John, R., Jones., Liu, S. and Barton J.M. 1995. Preparation of metal aromatic diamine complexes and their influence on the cure of a commercial epoxy resin. Polymer Bulletin. 36, 295-302.

Hamzah, R., Mohamad Abu, B., Khairuddean M., Mohammed, I.A., Adnan, R. 2012. A structural study of epoxidized natural rubber (ENR-50) and its cyclic dithiocarbonate derivative using NMR spectroscopy techniques. Molecules, 17, 10974-10993.

Hamzaha, R., Bakarb, M.A., 2013. The structural studies of oxirane ring opening reaction in epoxidized natural rubber (ENR-50) by $SnCl_2.2H_2O$ and the formation of ENR/Tin Complex Hybrid. Advanced Materials Engineering and Technology. 626, 727-737.

Harun, F., Chan, C.H. 2016. Electronic applications of polymer electrolytes of epoxidized natural rubber and Its composites. Polymer. Composite. Material, 37–59.

Henning, S.K. 2008. Use of coagents in the radical cure of elastomers. Wire & Cable Technology International XXXVI, 52-59.

Hernandez, M., Grande, A.M., Dierkes, W., Bijleveld, J., Zwaag, S., García, S.J. 2016. Turning vulcanized natural rubber into a self-healing polymer: Effect of the disulfide/polysulfide Ratio. ACS Sustain. Chemistry Engineering, 4, 5776.

Huang, Q., Tang, Z., Wang, D., Wu, S., Guo, B. 2021. Engineering segregated structures in a cross-linked elastomeric network enabled by dynamic cross-Link reshuffling. ACS Macromolecules Letter, 10, 231-236.

Ibarra, L., Rodresiguez, A., Barrantes I.M. 2009. Crosslinking of carboxylated nitrile rubber (XNBR) induced by coordination with anhydrous copper sulfate. Polymer International, 58, 218–226.

Idris, R., Glasse, M.D., Latham, R.J., Linford, R.G., Schlindwein, W.S. 2001. Polymer electrolytes based on modified natural rubber for use in rechargeable lithium batteries. Journal of Power Sources, 94(2), 206-211.

Iijima, S. 1991. Helical microtubules of graphitic carbon. Nature, 354, 56–58.

Imanifar, M., Ostad Movahed, S., Ahmadpour, A. 2018. Effects of peroxide and phenolic cure systems on characteristics of the filled ethylene-propylene-diene monomer rubber (EPDM). Journal of Applied Polymer Science, 135(21), 46213.

Ismail, H., Salleh, S.Z., Ahmad, Z. 2012. Fatigue and hysteresis behavior of halloysite nanotubes-filled natural rubber (SMR L and ENR 50) nanocomposites. Journal of Applied Polymer Science, 127, 3047–3052.

Kasyanenko, V.M., Lin, Z., Rubtsov, G.I., Donahue, J.P., Rubtsov I.V. 2009. Energy transport via coordination bonds. Journal of Chemistry Physic, 131, 154508.

Khairul, A. S., Mariatti, M., Azizan, A. Chee, Mang N., Tham W.T. 2011. Effect of different types of silver and epoxy systems on the properties of silver/epoxy conductive adhesives. Journal of Material Science: Mater Electron. 22, 757-764.

Kołodziejczak-Radzimska, A., Markiewicz, E., Jesionowski, T. 2012. Structural characterisation of ZnO particles obtained by the emulsion precipitation method. Journal of Nanomaterials, 656353/1–656353/9.

Krainoi, A., Kummerlöwe, C., Nakaramontri, Y., Vennemann, N., Pichaiyut, S., Wisunthorn, S., Nakason C. 2018. Influence of critical carbon nanotube loading on mechanical and electrical properties of epoxidized natural rubber nanocomposites. Polymer Testing 66, 122–136.

Krainoi, A., Kummerlöwe, C., Nakaramontri, Y., Wisunthorn, S., Vennemann, N., Pichaiyut, S., Kiatkamjornwong, S., Nakason C. 2019. Influence of carbon nanotube and ionic liquid on properties of natural rubber nanocomposites. Express Polymer Letters, 13, 327–348.

Krainoi, A., Kummerlöwe, C., Vennemann, N., Nakaramontri, Y., Pichaiyut, S., Nakason, C. 2018. Effect of carbon nanotubes decorated with silver nanoparticles as hybrid filler on properties of natural rubber nanocomposites. Journal of Applied Polymer Science, 13, 47281.

Kruželák, J., Sýkora, R., Hudec, I. 2017. Vulcanization of rubber compounds with peroxide curing systems. Rubber Chemistry and Technology, 90(1), 60–88.

Kurian, T., Mathew, N. M. 2011. Natural rubber: production, properties and applications. Biopolymers, 403–436.

Lattimer, R. P., Layer, R. W., Rhee, C. K. 1984. Mechanisms of antiozonant protection: antiozonant-rubber reactions during ozone exposure. Rubber Chemistry and Technology, 57(5), 1023–1035.

Lakshmi, B., Shivananda, K. N., Avaji, P.G., Rama, K.R.K. 2011. Synthesis of Co(II), Ni(II) and Cu(II) complexes from schiff base ligand and reactivity studies with thermosetting epoxy resin. Bulletin of the Korean Chemical Society, 32(5), 1613-1619.

Le, H., Hoang, X., Das, A., Gohs, U., Stoeckelhuber, K.-W., Boldt, R., Heinrich, G., Adhikari, R., Radusch, H.-J. 2012. Kinetics of filler wetting and dispersion in carbon nanotube/rubber composites. Carbon, 50, 4543–4556.

Lee, H., Neville, K. 1967. Handbook of Epoxy Resins. McGraw-Hill, New York, p.   5.2.

Li, J., Isayev, A. I., Wang, Q., Soucek, M. D. 2017. Sustainable plasticizer for butyl rubber cured by phenolic resin. Journal of Applied Polymer Science, 135(24), 45500.

Lin, Q., Lu, Y., Ren, W. Zhanga Y., 2015. The grafting reaction of epoxidized natural rubber with carboxyl ionic liquids and the ionic conductivity of solid electrolyte composites. Royal Society of Chemistry. 5, 90031–90040.

Ma, P.C., Liu, M.Y., Zhang, H., Wang, S.Q., Wang, R., Wang, K., Wong, Y.K., Tang, B.Z., Hong, S.H., Paik, K.W. Kim, J.K. 2009. Enhanced electrical conductivity of nanocomposites containing hybrid fillers of carbon nanotubes and carbon black. ACS Applied Materials Interfaces. 1, 1090-1096.

Ma, P.C., Siddiqui, N.A., Marom, G., Kim J.K. 2010. Dispersion and functionalization of carbon nanotubes for polymer–based nanocomposites: A review. Composites Part A. 41, 1345–1367.

Maka, H., Spychaj, T. 2012. Epoxy resin crosslinked with conventional and deep eutectic ionic liquids. Polimery. 57. nr 6.

Mallon, P. E., McGill, W. J., Shillington, D. P. 1995. A DSC study of the crosslinking of polychloroprene with ZnO and MgO. Journal of Applied Polymer Science, 55(5), 705–721.

Manchado, M., Herrero, B. Arroyo, M. 2004. Organoclay-natural rubber nanocomposites synthesized by mechanical and solution mixing methods. Polymer International, 53, 1766-1772.

Mandal, S., Simon, F., Banerjee, S. S., Tunnicliffe, L. B., Nakason, C., Das, C., Das, A. 2021. Controlled release of metal ion cross-linkers and development of self-healable epoxidized natural rubber. ACS Applied Polymer Materials, 3(2), 1190–1202.

Marzocca, A.J.; Mansilla, M.A. 2006. Vulcanization kinetic of styrene–butadiene rubber by sulfur/TBBS. Journal of Applied Polymer Science, 101, 35–41.

Matchawet, S., Kaesaman, A., Bomlai, P., Nakason, C. 2015. Effects of multi-walled carbon nanotubes and conductive carbon black on electrical, dielectric and mechanical properties of epoxidized natural rubber composites. Polymer Composites, 38, 1031–1042.

Matchawet, S., Kaesaman, A., Bomlai, P., Nakason, C. 2016. Electrical, dielectric, and dynamic mechanical properties of conductive carbon black/epoxidized natural rubber composites. Journal of Composite Materials, 50, 2191-2202.

Matchawet, S., Kaesaman, A., Vennemann, N., KumerlӦwe, C., Nakason, C. 2017. Effects of imidazolium ionic liquid on cure characteristics, electrical conductivity and other related properties of epoxidized natural rubber vulcanizates. European Polymer Journal, 87, 344–359.

Matos, C. F., Galembeck, F., Zarbin, A.J.G. 2014. Multifunctional and environmentally friendly nanocomposites between natural rubber and graphene or graphene oxide. Carbon, 78, 469- 479.

Mensah, B., Kim, H.G., Lee, J.H., Arepalli, S., Nah, C. 2015. Carbon nanotube-reinforced elastomeric nanocomposites: a review. International Journal of Smart and Nano Materials, 6, 211–238.

Mohamad, N., Muchtar, A., Ghazali, M., Mohd, D. and Azhari C. 2008. Correlation of filler loading and silane coupling agent on the physical characteristics of epoxidized natural rubber-alumina nanoparticles composites. European Journal of Scientific Research. 4, 538-547.

Mou, H., Xue, P., Shi, Q., Guo, W., Wu, C and Fu, X. 2012. A direct method for the vulcanization of acrylate rubber through in situ coordination crosslinking. Polymer Journal, 44, 1064–1069.

Nakaramontri, Y., Kummerlöwe, C., Nakason, C., Vennemann, N. 2014. Effect of modified natural rubber and functionalization of carbon nanotubes on properties of natural rubber composites. Advanced Materials Research, 844, 301-304.

Nakaramontri, Y., Kummerlöwe, C., Nakason, C., Vennemann, N. 2014. The effect of surface functionalization of carbon nanotubes on properties of natural rubber/carbon nanotube composites. Polymer Composites, 36, 2113–2122.

Nakaramontri, Y., Kummerlöwe, C., Vennemann, N., Wisunthorn, S., Pichaiyut, S., Nakason C. 2018. Effect of bis(triethoxysilylpropyl) tetrasulfide (TESPT) on properties of carbon nanotubes and conductive carbon black hybrid filler filled natural rubber nanocomposites. Express Polymer Letters, 12, 867–884.

Nakaramontri, Y., Nakason, C., Kummerlöwe, C., Vennemann, N. 2015. Effects of in-situ functionalization of carbon nanotubes with bis(triethoxysilylpropyl) tetrasulfide (TESPT) and 3-aminopropyltriethoxysilane (APTES) on properties of epoxidized natural rubber–carbon nanotube composites. Polymer Engineering & Science. 55, 2500-2510.

Nakaramontri, Y., Nakason, C., Kummerlöwe, C., Vennemann, N. 2015. Influence of modified natural rubber on properties of natural rubber-carbon nanotube composites. Rubber Chemistry and Technology, 88, 199-218.

Nakaramontri, Y., Pichaiyut, S., Wisunthorn, S., and Nakason, C. 2017. Hybrid carbon nanotubes and conductive carbon black in natural rubber composites to enhance electrical conductivity by reducing gaps separating carbon nanotube encapsulates. European Polymer Journal, 90, 467–484.

Nakason, C., Kaesman, A., Homsin, S., Kiatkamjornwong, S. 2001. Rheological and curing behavior of reactive blending. I. Maleated natural rubber-cassava starch. Journal of Applied Polymer Science, 81(11), 2803–2813.

Nakason, C., Kaesaman, A., Supasanthitikul, P. 2004. The grafting of maleic anhydride onto natural rubber. Polymer Testing, 23(1), 35–41.

Nakason, C., Saiwari, S., Kaesaman, A. 2006. Rheological properties of maleated natural rubber/polypropylene blends with phenolic modified polypropylene and polypropylene-g-maleic anhydride compatibilizers. Polymer Testing, 25(3), 413–423.

Negri, V., Pacheco-Torres, J., Calle, D., López-Larrubia, P. 2020. Carbon nanotubes in biomedicine. topics in Current Chemistry, 378(1).

Nun-anan, P., Wisunthorn, S., Pichaiyut, S., Nathaworn, C. D., Nakason, C. 2019. Influence of nonrubber components on properties of unvulcanized natural rubber. Polymers for Advanced Technologies.

Nun-anan, P., Wisunthorn, S., Pichaiyut, S., Vennemann, N., Kummerlöwe, C., Nakason, C. 2020. Influence of alkaline treatment and acetone extraction of natural rubber matrix on properties of carbon black filled natural rubber vulcanizates. Polymer Testing, 89, 106623.

Odom, T., Huang, J., Kim, P. and Lieber, C.M. 1998. Atomic structure and electronic properties of single–walled carbon nanotubes. Nature. 391, 62–64.

Okieimen, F. E., Urhoghide, I. N. 1996. Studies on miscibility of poly(vinyl chloride) with natural rubber-graft-polyacrylonitrile and natural rubber-graft-poly(methyl methacrylate). Journal of Applied Polymer Science, 59(11), 1803-808.

Olejnik, A., Smejda-Krzewicka, A., Strzelec, K., Szynkowska, M. I. 2018. Curing and properties of chloroprene and butadiene rubber (CR/BR) blends cross-linked with copper(I) oxide or copper(II) oxide. International Journal of Polymer Analysis and Characterization, 1–14.

Omrani, A., Ghaemy, M. and Rostami, A. 2006. Curing behavior of epoxy resin using controllable curing agents based on nickel complexes. Macromolecules Material and Engineering, 291, 181–193.

Ostrowska, S., Markiewicz, B., Wasikowska, K., Baczek, N., Pernak, J., Strzelec, K. 2013. Epoxy resins cured with ionic liquids as novel supports for metal complex catalysts. Comptes Rendus Chimie. 16. 752-760.

Payne, A. R. 1966. Effect of dispersion on the dynamic properties of filler-loaded rubbers. Rubber Chemistry and Technology, 39, 365–374.

Payne, A. R., Whittaker R. E. 1971. Low strain dynamic properties of filled rubber. Rubber Chemistry and Technology, 44, 440–478.

Petriuk, I.P., Mikhailiuk, A.E., Novakov, I.A. and Kablov, V.F. 2011. Use of highly-disperse metal particles in elastomer composites. International Polymer Science and Technology, 38, 27–32.

Pham, G. 2008. Characterization and modeling of piezo-Resistive properties of carbon nanotube-based conductive polymer composites. Industrial & Manufacturing Engineering Department, College of Engineering, Florida State University, Tallahassee, USA.

Poikelispää, M., Das, A., Dierkes, W., Vuorinen, J. 2013.The effect of partial replacement of carbon black by carbon nanotubes on the properties of natural rubber/butadiene rubber compound. Journal Applied Polymer Science, 130, 3153–3160.

Pötschke, P., Dudkin, S.M., Alig, I. 2003. Dielectric spectroscopy on melt processed polycarbonate-Multiwalled carbon nanotube composites. Polymers, 44, 5023-5030.

Qian, L., Xie, Y., Zhang, S., Zhang, J. 2020. Band engineering of carbon nanotubes for device applications. Matter, 3(3), 664–695.

Qing-xiu, J., You-ping, W., Ping, X., Xin, Y., Yi-qing, W., Li-qun Zhang. 2005. Combined effect of nano-clay and nano-carbon black on properties of NR nanocomposites. Polymers and Polymer Composites, 13(7), 709–719.

Rahman, A., Penco, M., Peroni, I., Ramorino, G., Grande, A.M. Landro, L.D. 2011. Self-repairing systems based on ionomers and epoxidized natural rubber blends. ACS Applied Material Interfaces. 3, 4865–4874.

Ram, R., Rahaman, M., Aldalbahi, A., Khastgir, D. 2016. Determination of percolation threshold and electrical conductivity of polyvinylidene fluoride (PVDF)/short carbon fiber (SCF) composites: effect of SCF aspect ratio. Polymer International, 66(4), 573–582.

Rattanasom, N., Saowapark, T., Deeprasertkul, C. 2007. Reinforcement of natural rubber with silica/carbon black hybrid filler. Polymer Testing, 26(3), 369–377.

Rippel, M. M., Paula Leite, C. A. and Galembeck, F. 2002. Elemental mapping in natural rubber latex films by electron energy loss spectroscopy associated with transmission electron microscopy. Analytical Chemistry, 74(11), 2541–2546.

Roberts, A. D. 1988. Natural Rubber Science and Technology. Oxford University Press: New York.

Rodrıgues, J.F., Oliveira, F.C., Ricardo, N.M.P.S., Lima, M.C.P. 1998. Effect of Divalent metal ions on the viscosity of natural rubber from Manihot glaziovii. Journal Rubber Research, 1, 240-252.

Rooj, S., Das, A., Stöckelhuber, K.W., Wießner, S., Fischer, D., Reuter, U., Heinrich, G. 2015. Expanded organoclay assisted dispersion and simultaneous structural alteration of multiwall carbon nanotube (MWCNT) clusters in natural rubber. Composite Science Technology, 107, 36-43.

Ruksakulpiwat, C., Nuasaen, S., Poonsawat, C., Khansawai, P. 2008. Synthesis and modification of epoxidized natural rubber from natural rubber latex. Advanced Materials Research, 47-50, 734–737.

Sahakaro, K., Beraheng, S. 2008. Reinforcement of maleated natural rubber by precipitated silica. Journal of Applied Polymer Science, 109, 3839–3848.

Saito, R., Dresselhaus, G. Dresselhaus, M. 1998. Physical properties of carbon nanotubes. Physical Review, 59, 678-680.

Salaeh, S., Boiteux, G., Cassagnau, P., Nakason, C. 2015. Flexible 0-3 ceramic-polymer composites of barium titanate and epoxidized natural rubber. International Journal of Applied Ceramic Technology, 12, 106–115.

Salaeh, S., Das, A., Wießner, S., Stapor, M. 2021. Vitrimer-like material based on a biorenewable elastomer crosslinked with a dimeric fatty acid. European Polymer Journal, 151, 110452.

Salaeh, S., Muensit, N., Bomlai, P., Nakason, C. 2011. Ceramic/natural rubber composites: influence types of rubber and ceramic materials on curing, mechanical, morphological, and dielectric properties. Journal of Material Sciences, 46, 1723–1731.

Salaeh, S., Nakason, C. 2012. Influence of modified natural rubber and structure of carbon black on properties of natural rubber compounds. Polymer Composites, 33(4), 489–500.

Salim, Y.S., Zainudin, N., Chan, C.H., Chan, K. 2014. Correlation between the storage time of the NRL and the efficiency of PMMA grafting to NR. Key Elements in Polymers for Engineers and Chemists. 371-383.

Saramolee, P., Lopattananon, N., Sahakaro, K. 2014. Preparation and some properties of modified natural rubber bearing grafted poly(methyl methacrylate) and epoxide groups. European Polymer Journal, 56, 1-10.

Shanmugharaj, A. M., Ryu, S.H. 2013. Influence of aminosilane-functionalized carbon nanotubes on the rheometric, mechanical, electrical and thermal degradation properties of epoxidized natural rubber nanocomposites. Polymer International, 62, 1433–1441.

Shen, F., Yuan, X.F., Guo, W.H., Wu, C.F. 2007. Coordination crosslinking of nitrile rubber filled with copper sulfate particles. Chin Journal of Polymer Science ,25, 447–459.

Shen, F., Yuan, X.F., Wu, C.F. 2008. Effects of SC-CO_2 treatment on the properties of NBR/$CuSO_4$ composites. Journal of Macromolecules Science B. 47:250–259.

Shen, Q., Wu, M., Xu, C., Wang, Y., Wang, Q., Liu, W. 2021. Sodium alginate crosslinked oxidized natural rubber supramolecular network with rapid self-healing at room temperature and improved mechanical properties. Composite Part A Applied Science Manuf, 150, 106601.

Smejda-Krzewicka, A., Olejnik, A., Strzelec, K. 2019. The effect of metal oxide on the cure, morphology, thermal and mechanical characteristics of chloroprene and butadiene rubber blends. Polymer Bulletin, 77(8), 4131–4146.

Smith, J.D.B. 1981. Metal acetylacetonates as latent accelerators for anhydride-cured epoxy resins. Journal of Applied Polymer Science. 26, 979-986.

Socher, R., Krause, B., Hermasch, S., Wursche, R., Pötschke, P. 2011. Electrical and thermal properties of polyamide 12 composites with hybrid fillers systems of multiwalled carbon nanotubes and carbon black. Composite Science Technology, 71, 1053–1059.

Sookyung, U., Nakason, C., Thaijaroen, W., Vennemann, N. 2014. Effect of organoclay loading level on mechanical properties, thermomechanical behavior, and heat build-up of natural rubber/organoclay nanocomposites. Polymer Composite, 37.

Soto, M., Boyer, T. A., Biradar, S., Ge, L., Vajtai, R., Elías-Zúñiga, A., Ajayan, P.M., Barrera, E. V. 2015. Effect of interwall interaction on the electronic structure of double-walled carbon nanotubes. Nanotechnology, 26(16), 165201.

Steinhauser, D., Subramaniam, K., Das, A., Heinrich, G., Klueppel, M. 2012. Influence of ionic liquids on the dielectric relaxation behavior of CNT based elastomer nanocomposites. Express Polymer Letter, 6, 927–936.

Subramaniam, K., Das, A. and Heinrich, G. 2011. Development of conducting polychloroprene rubber using imidazolium based ionic liquid modified multi-walled carbon nanotubes. Composite Science Technology, 71, 1441-1449.

Subramaniam, K., Das, A., Stöckelhuber, K.W., Heinrich, G. 2013. Elastomer composites based on carbon nanotubes and ionic liquid. Rubber Chemistry Technology, 86, 367–400.

Sumfleth, J., Adroher, X.C. Schulte, K. 2009. Synergistic effects in network formation and electrical properties of hybrid epoxy nanocomposites containing multiwall carbon nanotubes and carbon black. Journal of Materials Sciences. 44, 3241–3247.

Szeluga, U., Kumanek. B.E. and Pusz S. 2015. Hybrid epoxy composites with carbon nanotubes and graphene nanoplatelets. Composites: Part A. 73, 204–231.

Tan, W.L., Bakar, M.A. 2014. The effects of magnetite particles and lithium triflate on the thermal behavior and degradation of epoxidized natural rubber (ENR-50). American-Eurasian Journal of Sustainable Agriculture, 8, 111–122.

Tang, Z.H., Huang, J., Guo, B., Zhang, L., Liu, F. 2016. Bioinspired engineering of sacrificial metal–ligand bonds into elastomers with supra-mechanical performance and adaptive recovery. Macromolecules, 49, 1781.

Teh, P. L., Mohd Ishak, Z. A., Hashim, A. S., Karger-Kocsis, J., & Ishiaku, U. S. 2004. Effects of epoxidized natural rubber as a compatibilizer in melt compounded natural rubber–organoclay nanocomposites. European Polymer Journal, 40(11), 2513–2521.

Thongkong, N., Wisunthorn, S., Pichaiyut, S., Nakason, C., Kiatkamjornwong, S. 2020. Natural rubber nanocomposites based on hybrid filler of zinc nanoparticles and carbon nanotubes: Electrical conductivity and other related properties. Express Polymer Letters, 14(12), 1137–1154.

Thostenson, E. T., Ren, Z., Chou, T.W. 2001. Advances in the science and technology of carbon nanotubes and their composites: a review. Composites Science and Technology, 61(13), 1899–1912.

Tingaev, M. I., Belenkov, E. A. 2017. Hybrid sp^2+sp^3 carbon phases created from carbon nanotubes. Journal of Physics: Conference Series, 917, 032013.

Utara, S., Saengsila P. 2015. Effect of divalent metal ions on curing characteristics and dynamic mechanical properties of natural rubber. Macromolecular Symposia, 354, 287–293.

Vennemann, N.; Bökamp, K.; Bröker, D. 2006. Crosslink density of peroxide cured TPV. Macromolecular Symposia, 245–246, 641–650.

Vennemann, N., Schwarze, C., Kummerlöwe, C. 2014. Determination of crosslink density and network structure of NR vulcanizates by means of TSSR. Advance Material Research, 844, 482–485.

Vidu, R., Rahman, M., Mahmoudi, M., Enachescu, M., Poteca, T. D., Opris, I. 2014. Nanostructures: a platform for brain repair and augmentation. Frontiers in Systems Neuroscience, 8.

Vinod, V.S., Varghese, S., Kuriakose, B. 2002. Degradation behavior of natural rubber–aluminium powder composites: effect of heat, ozone and high energy radiation. Polymer Degradation and Stability 75, 405–412.

Wang, X.Z., Xie, D.M., Zhao, X.L., Li, Y.D., Zeng, J.B. 2022. Sustainable, malleable, and recyclable castor oil-derived poly(urethane urea) networks with tunable mechanical properties and shape memory performance based on dynamic piperazine–urea bonds. Macromolecules, 55, 2243-2251.

Wei, K.K., Leng, T. P., Keat, Y. C., Osman, H., Ying, L. B. 2019. Enhancing compatibility in epoxy/vulcanized natural rubber (VNR)/Graphene nano-platelets (GNP) system using epoxidized natural rubber (ENR-50). Composites Part B: Engineering, 174, 107058.

Wolff, S., Wang, M.J., Tan, E.H. 1993. Filler-elastomer interactions. Part VII. Study on bound rubber. Rubber Chemistry and Technology, 66(2), 163–177.

Wu, M., Heinz, M., Vennemann, N. 2013. Investigation of un-vulcanized natural rubber by means of temperature scanning stress relaxation measurements. Advanced Materials Research, 718-720, 117–123.

Wu, M., Yang, L., Shen, Q., Zheng, Z., Xu, C. 2021. Endeavour to balance mechanical properties and self-healing of nature rubber by increasing covalent crosslinks via a controlled vulcanization. European Polymer Journal, 161, 110823.

Xiang, H., Yin, J., Lin, G., Liu, X., Rong, M., Zhang, M. 2019. Photo-crosslinkable, self healable and reprocessable rubbers. Chemistry Engineering Journal, 358, 878-890.

Xu, C., Huang, X., Li, C., Chen, Y., Lin, B., Liang, X. 2016. Design of "Zn^{2+}salt-bondings" cross-Linked carboxylated styrene butadiene rubber with reprocessing and recycling ability via rearrangements of ionic cross-linkings. ACS Sustainable Chemistry Engineering, 4, 6981-6990.

Xu, C., Nie, J., Wu, W., Fu, L., Lin, B. 2019. Design of self-healable supramolecular hybrid network based on carboxylated styrene butadiene rubber and nano-chitosan. Carbohydrate Polymers, 205, 410-419.

Yakobson, B. Avouris, P. 2001. Mechanical properties of carbon nanotubes. Journal Applied Physic, 80, 287-300.

Yangthong, H., Pichaiyut, S., Jumrat, S., Wisunthorn, S., Nakason, C. 2018. Novel natural rubber composites with geopolymer filler. Advance Polymer Technology, 37, 2651– 2662.

Yangthong, H., Wisunthorn, S., Pichaiyut, S., Nakason, C. 2019. Novel epoxidized natural rubber composites with geopolymers from fly ash waste. Waste Management, 87, 148–160.

Yokkhun, P., Thongnuanchan, B., Nakason, C. 2013. Influence of epoxide levels in epoxidized natural rubber (ENR) molecules on cure characteristics, dynamic properties and mechanical properties of ENR/montmorillonite clay nanocomposites. Advance Material Research, 844, 247–250.

Zainal, N., Mohamed, N.S. Idris R. 2013. Properties of ENR-50 based electrolyte system. Sains Malaysiana, 42, 481–485.

Zhang, S. M., Lin, L., Deng, H., Gao, X., Bilotti, E., Peijs, T., Zhang, Q., Fu, Q. 2012. Synergistic effect in conductive networks constructed with carbon nanofillers in different dimensions. Express Polymer Letters, 6(2), 159– 168.

Zhang, X., Liu, J., Zhang, Z., Wu, S., Tang, Z., Guo, B., Zhang, L. 2018. Toughening elastomers using a mussel-inspired multiphase design. ACS Applied Materials & Interfaces, 10(28), 23485–23489.

Zhang, X., Tang, Z., Guo, B., Zhang, L. 2016. Enabling design of advanced elastomer with bioinspired metal-oxygen coordination. ACS Applied Material Interfaces, 8, 32520–32527.

Zhang, H.; Zhong, X.; Xu, J.J.; Chen, H.Y. 2008. Fe3O4/Polypyrrole/Au nanocomposites with core/shell/shell structure: synthesis, characterization, and their electrochemical properties. Chemistry Material, 24, 13748–13752.

Zhao, F., Guana, J., Baib, W., Guc, T., Liud, H., Liaoe S. 2018. Role of divalent metal ions on the basic properties and molecular chains of natural rubber. Materials Science and Engineering, 452.

APPENDICES

APPENDICES I

Published Article in Polymers, 2021, 13, 4145.

APPENDICES II

Published Article in Express Polymer Letter, 2022, 16, 812–826.

APPENDICES III

Published Article in Polymers, 2022, 14, 4392.

APPENDICES IV

Published Article in The 17th national and the 7th international sripatum

university online conference (SPUCON2022).

CURRICULUM VITAE

Name   Mr. Kriengsak Damampai

Student ID   5940330104

Educational Attainment

Degree	Name of Institution	Year of Graduation
B. Sc. (Rubber Industry Technology)	Prince of Songkla University	2016

Scholarship Awards during Enrolment

1. Thailand Research Fund and National Research Council of Thailand for providing a Royal Golden Jubilee Ph.D. Program (Grant No. PHD/0121/2560).

2. The Graduates School, Prince of Songkla University, Surat Thani campus, Thailand.

List of Publications and Communications

Publications:

1. Damampai K., Pichaiyut S., Mandal S., Wießner S., Das A., Nakason C. (2021). Internal polymerization of epoxy group of epoxidized natural rubber by ferric chloride and formation of strong network structure, Polymers, **13**, 4145.

2. Damampai, K., Pichaiyut, S., Das, A., Nakason C. (2022). Internal polymerization of epoxy group of epoxidized natural rubber by ferric chloride filled with carbon nanotubes: Mechanical, morphological, thermal and electrical properties of rubber vulcanizates. Express Polymer Letters, **16**, 812–826.

3. Damampai, K., Pichaiyut, S., Das, A., Nakason C. (2022). Ferric ions crosslinked epoxidized natural rubber filled with carbon nanotubes and conductive carbon black hybrid fillers**.** Polymers, **14**, 4392.

4. Damampai, K., Pichaiyut, S., Das, A., Nakason C. (2022). Ferric chloride cross-linked epoxidized natural rubber. The 17th national and the 7th international sripatum university online conference (SPUCON2022).

Communications

1. Damampai K., Nakaramontri Y., Pichaiyut S., Nakason C. "Effect of carbon black and carbon nanotubes hybrid filler filled natural rubber composites: influence of types of natural rubber'' The Third Asia Pacific Rubber Conference (APRC 2017), 16-17 November 2017, Surat Thani, Thailand. (Poster presented)

2. Damampai, K., Pichaiyut, S., Das, A., Nakason C. "Metal ion cross-linking of epoxidized natural rubber" The 2021 National RGJ and RRI conferences, 14 June 2021. (Poster presented)

3. Damampai, K., Pichaiyut, S., Das, A., Nakason C. "Ferric chloride cross-linked epoxidized natural rubber'' The 17th National and 7th international Sripatum university conference research and innovations to sustainable development, 27 October 2022. (Oral presented)